

UC Merced

UC Merced Electronic Theses and Dissertations

Title

Towards the Fabrication of Three-Dimensional Cardiac Tissue Derived from Stem Cells

Permalink

<https://escholarship.org/uc/item/4ch6v1q0>

Author

Hatano, Rachel

Publication Date

2019

Peer reviewed|Thesis/dissertation

UNIVERSITY OF CALIFORNIA, MERCED

Towards the Fabrication of Three-Dimensional Cardiac Tissue Derived from Stem Cells

A dissertation submitted in partial satisfaction of the requirements for the degree of
Doctor of Philosophy

in

Biological Engineering and Small-scale Technologies

by

Rachel Hatano

Committee in charge:

Professor Kara McCloskey, Primary Advisor and Committee Chair

Professor Chelsey Simmons

Professor Nipavan Chiamvimonvat

2019

Towards the Fabrication of Three-Dimensional Cardiac Tissue Derived from Stem Cells

Copyright
Rachel Hatano, 2019
All rights reserved

The Dissertation of Rachel Hatano is approved, and it is acceptable in quality and form for publication on microfilm and electronically

Professor Kara McCloskey, Primary Advisor

Professor Chelsey Simmons

Professor Nipavan Chiamvimonvat

University of California, Merced
2019

ACKNOWLEDGEMENTS

First, I would like to acknowledge my funding sources: the National Science Foundation (NSF) Grant #0965918 IGERT: Cellular and Molecular Mechanics and BioNanotechnology fellowship, and the NSF Emergent Behaviors of Integrated Cellular Systems trainee program. I would also like to thank UC Merced for awarding me travel and summer fellowships.

I want to thank my committee members Prof. Chelsey Simmons and Prof. Nipavan Chiamvimonvat, for their encouragement, feedback, and knowledge shared.

Thank you to my supervisor, Dr. Kara E. McCloskey. Her mentorship taught me to be ambitious when choosing avenues of scientific exploration. As a leader, she taught me the value expressing myself authentically, independent of expectations.

I would also like to thank the entire McCloskey lab family: Dr. Drew E. Glaser—my first research mentor, who taught me the foundational skills needed to undergo my subsequent research project; my fellow graduate students Anley Tefera, Edwin Shen, Jose Zamora, Nicole Madfis, and Lian Wong; and undergraduate research mentees including Alejandra Preciado, Bitá Behizi, Greg Girardi, and Ariell Smith.

Throughout my educational journey, I had the good fortune of meeting numerous other mentors and collaborators. I want to thank Dr. Joo Young and Prof. Beth Pruitt at Stanford University; Dr. Luis Chia at C.S. Laboratory Technologies; Dr. Ritu Raman and Prof. Rashid Bashir at the University of Illinois; Urbana Champagne, Dr. Vincent Chan and Prof. Harry Asada at MIT; Prof. Michelle Khine and Prof. Elliot Botvinick at UC Irvine; and Dr. Tom Chen at Regeneron Pharmaceuticals.

Finally, I would like to thank all my family and friends for continually supporting my educational and personal growth.

CURRIVULUM VITAE

EDUCATION

Ph.D. Biological Engineering and Small-scale Technologies 2019

University of California, Merced

Research: Designing a novel microfluidic device to affect cardiac cell fate and produce functional engineered heart tissue from human induced pluripotent stem cells

Advisor: Kara E. McCloskey

B.S. Biological Sciences 2012

University of California, Merced

Research: Studying endothelial cells derived from stem cells' response to topographical surface patterns

- Immunology and Microbiology emphasis, Philosophy minor

AWARDS & HONORS

Fellowships

NSF IGERT Cellular and Molecular Mechanics and Bio Nanotechnology (CMMB) Fellow; University of Illinois, Urbana-Champaign. Advisor: Kara E. McCloskey
Jan. 2014- Dec. 2015

NSF Emerging Frontiers in Research and Innovation (EFRI), Multicellular and Inter-
Kingdom Signaling; Stanford University. Advisor: Beth Pruitt summer 2012

Entrepreneurship

NSF I-Corps Jan. 2018 – March 2018

Modularized Bioprinter for High Throughput Pharmaceutical Development \$50,000

PI: Kara McCloskey, UC Merced Role: Entrepreneurial Lead

First Place: Technology Conceptualization Plan Competition, NSF EBICS 2017

- *Oral Presentation* ModiPrint: A Modular, Multi-Printhead Bioprinter

Selected Finalist: UC Bioengineering Symposium Shark Tank, UC Santa Cruz 2015

- *Oral Presentation* Cardiac Chameleon

First Place Ruiz Prize in Entrepreneurship: Pitchfest, UC Merced 2015

- *Oral Presentation* Heart Patch

Presentations

Semi-Finalist: GradSLAM!, University of California, Merced; 2017

Cardiac Construction

Honorable Mention: Nanotechnology Symposium, University of Illinois, Urbana-Champaign; 2015

Cardiomyocytes from Human Pluripotent Stem Cells: Towards the Fabrication of a Cardiac Patch

Best Poster: BioNanotechnology Summer Institute, University of Illinois, Urbana Champaign; 2014

Dynamic Micro-Patterned System for Studying Vascularization through a Derived Cardiac Tissue

Research & Travel

- UC Merced BEST Bobcat Travel Award: 2016, 2017 (\$500, \$1,2000)
- GEM GradLab Invited Panelist, 2016 (\$200)
- UC Merced Summer Research BEST Bobcat Award: 2016, 2018 (\$6,000)
- Office of the President CARE UC Student Peer Education, 2016 (\$120)
- NSF EBICS MIT Research Exchange, 2015 (\$2,000)
- UC Merced School of Engineering Dean's travel award, 2015 (\$1,250)
- UC Merced Graduate Division Travel Grant: 2013, 2014 (\$500, \$500)
- NSF IGERT UIUC Bionanotechnology Summer Institute (\$3,500)
- UC System-wide Bioengineering Diversity Travel Award, 2014 (\$300)
- NSF Emerging Frontiers in Research and Innovation, REM travel grant (\$1,500)

PUBLICATIONS

1. Rachel Hatano, Ariell Smith, Kara McCloskey, Development of Gravity-Guided 3D Muscle Formation: A High Throughput Tissue Engineering Technique. (in progress)
2. Rachel Hatano, Gregory Girardi, Vincent Chan, Harry Asada, Kara E. McCloskey, Microfluidic Platform Enables Generation of Multi-Layered Scaffold-Free Muscle with Endothelialized Lumens. (in progress)
3. Rachel Hatano, Bitu Behizi, Jose Zamora, Lian Wong, Kara E. McCloskey, Compartmenting tissue engineering techniques for cardiac tissue fabrication. (in progress)
4. *Invited:* Rachel Hatano and Kara E. McCloskey. Tissue Engineering Approaches for Building Cardiac Tissue. In: *Frontiers in Stem Cell and Regenerative Medicine Research*, Atta-ur- Rahman and Shazia Anjum (ed), 2017: , Vol 7, 121-162, Betham Science, ISBN: 978-1-68108-553-1
5. Drew E. Glaser, Andrew Burns, Rachel Hatano, Magdalena Medrzycki, Yuhonog Fan, and Kara E. McCloskey Mouse Embryonic Stem Cells for Studying Vascular Development. *Stem Cells Cloning*, 2014. 7: p.79-88
6. Rachel Hatano, Jesus Luna, Drew Glaser, Kevin Mercurio, Valerie Leppert, and Kara E. McCloskey Endothelial Cells Derived from Embryonic Stem Cells Respond to Cues from Topographical Surface Patterns. *Journal of Biological Engineering*, 2013. 7:p.18

EXPERIENCE

Entrepreneurial Lead, ModiPrint

2017 – 2018

Merced, CA

Commercialization project: a modularized bioprinter for high throughput pharmaceutical development

- Lead over 100 customer discovery interviews to evaluate the product's value proposition.

- Developed a business model by identifying key partners, modeling cost structure and revenue streams, and investigating means of customer relationships and distribution channels.

Bioassay, Molecular Bio., & Protein Dev. PhD Intern, Regeneron Pharmaceuticals summer, 2017

Tarrytown, NY

- Investigated five molecular-based release assays for a cardiometabolic target
- Designed a mechanotransduction-based bioassay to measure cell-to-cell adhesion for screening
- Presented findings to the bioassay development team

Project Manager, UC Merced School of Engineering

2016 – 2017

Merced, CA

UC Merced course projects: Nerve damage diagnostic tool, crop monitoring drone, healthcare translation app, advanced accuracy syringe cap, youth recidivism assessment, laboratory animal pollutant monitor

AWARDED: UC Merced Innovate to Grow 2017 (*first place*) and 2016 (*second place*)

- Managed multi-disciplinary teams through four-month periods (17 teams, 145 students total).
- Delivered weekly feedback on engineering concepts, team organization, and commercialization.
- Provided guidance, from prototype design and analysis to product presentation to stakeholders.

Business Development Associate, C.S. Laboratory Technologies

2013

San Francisco, CA

Seed-funded start-up: a dynamic cell culture platform to mimic physiological mechanics in vitro

- Collaborated in bi-weekly meetings to discuss competitive strategy and goals.
- Executed marketing plan: published targeted white papers and crafted advertisements.
- Facilitated summer research fellowships to enhance publicity and customer relationships.
- Supported sales by scouting contact information of over 1500 potential customers.

Teaching

Intern, Center for Engaged Teaching and Learning

2014 – 2016

University of California, Merced

Lead pedagogy workshops for fellow UC Merced educators: *Surviving the Classroom with First Generation College Students*, *Developing Teaching Strategies*, and *Improving Teaching by Assessing Learning*. Selected panelist presenter for incoming engineering graduate students.

Teaching Assistant, University of California, Merced

Lead weekly classes by preparing lectures, writing exam questions, and grading reports.

BIO 001: Introduction to Biology Lab (98 students total)

fall 2013 & fall 2018

BIO 001: Introduction to Biology Discussion (60 students total) spring 2018
BIO 002: Introduction to Molecular Biology Discussion (90 students total) spring 2016

Guest Lecturer, University of California, Merced

BIO 002: Introduction to Molecular Biology: *Control of Gene Expression*
spring 2016

BIOE 114: Tissue Engineering: *Directing Stem Cell Fate, and Gene Editing* fall 2015

RESEARCH

NSF-Funded Development and Collaborations

Trainee, NSF Emergent Behaviors of Integrated Cellular Systems (EBICS) Science and Tech. Center, Multi-institutional Aug. 2014 –

Projects and initiatives driven towards creating a new scientific discipline for building living, multi-cellular machines that solve real-world problems.

- Contributed to collaborations with UIUC (Prof. Rashid Bashir) and MIT (Prof. Harry Asada) by testing microfluidic devices with human induced pluripotent stem cell-derived cardiomyocytes.
- Presented findings to internal and industry advisory boards, as well as NSF representatives, at annual meetings.

First-Author Select Presentations

Engineering the Mechanical Microenvironment: Fabrication of a Functional Human Pluripotent Stem Cell-Derived Cardiac Patch

- Biomedical Engineering Society (BMES) Annual Meeting; Phoenix, AZ *poster* 2017
- Emergent Behaviors of Integrated Cellular Systems, Annual Retreat; Chicago, IL *poster* 2016
- Emergent Behaviors of Integrated Cellular Systems, NSF Site Visit; Cambridge, MA *poster* 2015
- Biomedical Engineering Society (BMES) Annual Meeting; Tampa, FL *poster* 2015
- UC Systemwide Bioengineering Symposium; Irvine, CA *selected finalist, oral presentation* 2015
- IGERT Annual Symposium; Champaign, IL *Honorable Mention, poster* 2015
- Emergent Behaviors of Integrated Cellular Systems Annual Retreat; Atlanta, GA *poster* 2015
- 13th Annual Gene Therapy Symposium for Heart, Lung, and Blood Diseases; Sonoma, CA *oral and poster presentation* 2014
- IGERT Annual Symposium; Champaign, IL *awarded Best Poster, poster* 2014

Cell-Cell Junction's Tension Modulated by Different Substrate Stiffness Using Cadherin Sensors

- Emerging Frontiers in Research and Innovation-Research Experience and Mentoring (EFRI-REM); Washington DC *poster* 2013

Mouse Embryonic Stem-Cell Derived Endothelial Cells Respond to Topographical Surface Patterns

- UC-Systemwide Bioengineering Symposium; Berkeley, CA *oral presentation* 2012
- BMES Annual Meeting Atlanta, GA *invited speaker *Prof. McCloskey presents, and poster* 2012
- BMES Annual Meeting Hartford, CT *poster* 2011

Mentorship

Managed, trained, and mentored student researchers

- PhD student Bashrat Jahan: Biological Engineering and Small Scale Technologies; 2018
- PhD student Jose Zamora: NSF Center for Cellular and Biomolecular Machines CREST; 2017
- B.S. Ariell Smith: UC Leadership Excellence through Advanced Degrees (LEADS) Scholar; 2018
- B.S. Julia Young: Women in STEM; 2017 - 2018
- B.S. Greg Girardi: Emergent Behaviors of Integrated Cellular Systems (EBICS); 2016 – 2018
- B.S. Bitu Behziz: Applications in Modern Materials (AiMM) NSF REU; summer 2016
- B.S. Alejandra Preciado: Maximizing Access to Research Careers (MARC) USTAR; 2015 - 2016

Techniques

Cell Culture: mouse embryonic stem cell (R1), human embryonic stem cell (HES2, H7, H9), human induced pluripotent stem cell (hiPSC DF19-9-7T), endothelial (HUVEC), smooth muscle (RAOSMC), mouse myoblast (C2C12), hiPSC cardiomyocyte differentiation (EB and Matrigel™).

Assays: Ca²⁺ transient (Fluro4), cell viability (live/dead stain, propidium iodide), qPCR, immunostaining, Luciferase, Förster Resonance Energy Transfer.

Instrumentation: Microscopy (scanning & transmission electron, confocal, fluorescent), class 10,000 clean room (microfluidics), fluorescence activated cell sorting.

Murine Handling and Primary Cell Isolation: Mouse injections (sub-cutaneous, intraperitoneal), sacrifice (cervical dislocation, decapitation), primary cell isolation (rat neonatal cardiomyocyte, mouse arterial endothelial cells, mouse blastocysts for embryonic stem cell collection).

SERVICE & OUTREACH

Elected Graduate Delegate Assembly

- Reviewed grants; voted on policy changes; voiced constituent views; 2017 – 2018

NSF CMMB IGERT & NSF EBICS & Student Leadership

- Collaborated with multi-institutional partners to assess program efficacy; 2015, 2017 – 2018

Diversity, Inclusion, and Outreach

USA Science and & Engineering Festival; presenter: BIOBOTS Building with Biology; 2018

Graduate Dean’s Advisory Council on Diversity; appointed graduate student rep.; 2015 – 2018

GEM GradLab; invited speaker: Voices from the Field: Real Life Research Experience; 2016

Women in STEM

The Chancellor’s Advisory Committee on the Status of Women; appointed graduate student rep.; 2016

University of California Woman’s Caucus; appointed graduate student rep.; 2016

AAUW; invited speaker: *Girls in STEM: Why so Few and What We Can Do*; 2015

University of California Office of the President Research Policy

- Sole graduate student appointee for all universities in the UC system (representing >54k grad students). Contributed perspective on research policy and procedures, funding opportunities, and multi-institutional research facilities. Reviewed grants worth up to eight million dollars. 2015 – 2016

Campus Advocacy Resources Education Advisory Council

- Appointed grad. student rep. contributed to quarterly board meetings. Lead educational discussions relating to domestic violence and abuse. Invited speaker to incoming graduate students regarding institutional response and advocacy resources. 2014 – 2016

ABSTRACT

Towards the Fabrication of Three-Dimensional Cardiac Tissue Derived from Stem Cells

by

Rachel Hatano

in

Biological Engineering and Small-scale Technologies

UNIVERSITY OF CALIFORNIA, MERCED

Committee in charge:

Professor Kara McCloskey, Primary Advisor and Committee Chair

Professor Chelsey Simmons

Professor Nipavan Chiamvimonvat

2019

According to the American Heart Association, one in three adults currently suffer from cardiovascular disease, with coronary heart disease being the most common. This chronic ailment commonly requires clinical intervention in order to prevent congestive heart failure, including daily medications, pacemakers, and surgical treatments. Cell therapy can potentially improve heart function after myocardial infarction (MI), but cell injection alone does not provide sufficient environmental support for the injected cells to survive [2]. Engineered cardiovascular tissue, if carefully designed, could replace the damaged heart tissue, reducing the need of many patients to undergo a whole heart transplant. Furthermore, designing human cardiac tissue in vitro could serve as an exciting model for both efficacy and toxicity pharmaceutical testing. Notable obstacles to achieving this ambitious goal include generating a cardiac cell source, patterning three-dimensional tissue to mirror its native architecture, and vascularizing the tissue to provide sufficient oxygen support. This study addresses each of these three obstacles: First, prevailing human pluripotent stem cell-derived cardiomyocyte (hPSC CM) differentiation protocols were compared for cell purity and efficiency. Second, the hPSC CMs were patterned using three distinct tissue engineering methods and analyzed for cell alignment and elongation. Third, a novel microfluidic device was designed for a perfusable endothelialized lumen through engineered cardiac tissue.

TABLE OF CONTENTS

ACKNOWLEDGEMENTS	iv
CURRICULUM VITA	v
ABSTRACT	x
LIST OF FIGURES AND TABLES.....	xiii
Chapter 1: Introduction.....	1
1.1 Background.....	1
1.1.1 Societal Impact of Cardiovascular Disease	1
1.1.2 Cardiovascular Physiology	1
1.1.3 History of Coronary Heart Disease	2
1.1.4 Remodeling Consequences Following an MI.....	2
1.1.5 Lasting Impact of MI.....	3
1.2 Current Treatment Strategies Following MI	3
1.2.1 Diagnosis	4
1.2.2 Surgical Intervention	4
1.2.3 Left Ventricular Restraint.....	4
1.2.4 Pharmaceuticals.....	5
1.3 Tissue Engineering.....	5
1.3.1 Extracellular Matrix Composition in Vivo.....	6
1.3.2 Biomaterials Used for Cardiac Patch Design	7
1.3.3 ECM in Cardiac Tissue Engineering.....	10
1.3.4 Linking ECM to Hydrophobic Materials.....	10
1.3.5 Cell Sheet Technology	10
1.3.6 Cell Patterning.....	11
1.3.7 Role for Mechanical Signaling	11
1.3.8 Current Tissue Stretching Devices.....	12
1.3.9 Whole Heart Bioengineering	13
1.4 Goals and Overview.....	13
Aim 1. Generation of human pluripotent stem cell derived cardiomyocytes.....	13
Aim 2. Fabrication of cardiac muscle tissue: a methods comparison.....	14
Aim 3. Generation of multi-layered muscle with endothelialized lumens.....	14
Chapter 2: Human Pluripotent Stem Cell Derived Cardiomyocyte Protocol Comparison	16
2.1 Introduction	16
2.1.1 Cardiovascular Engineering.....	16
2.1.2 Adult Stem Cells	16
2.1.3 Human Pluripotent Stem Cells.....	19
2.1.4 Therapeutic Use of Human Pluripotent Stem Cell Derived Cardiomyocytes	19
2.1.5 Derivation of Cardiomyocytes from Human Pluripotent Stem Cells	20
2.1.6 Guiding Stem Cell Differentiation Through Extracellular Interactions....	21
2.1.7 Characterization of hPSC-derived CM.....	22
2.1.8 hPSC CM Maturation.....	23

2.1.9 Purification of hPSC-derived CM.....	24
2.1.10 Goals.....	24
2.2 Methods.....	24
2.2.1 Cell Source.....	24
2.2.2 Maintenance of human ESC cells.....	25
2.2.3 Maintenance of human iPS cells.....	25
2.2.4 Fabrication of Honeycomb Microwells.....	25
2.2.5 Growth Factor CM Induction Protocol.....	25
2.2.6 Inhibitor CM Induction Protocol.....	26
2.2.7 Purification of CM.....	27
2.2.8 Immunostaining for Fluorescence Microscopy.....	27
2.2.9 Immunostaining for Fluorescence Activated Cell Sorting.....	28
2.2.10 Beating Cardiomyocytes.....	29
2.2.11 Calcium Transience.....	29
2.3 Results.....	29
2.3.1 hPSC characterization.....	29
2.3.2 Stem Cell Derived Cardiomyocyte Differentiation Protocol Comparison.....	30
2.3.3 hiPSC CM Characterization.....	30
2.3.4 Protocol Reproducibility.....	33
2.4 Discussion & Conclusion.....	33
Chapter 3: Fabrication of Cardiac Muscle Tissue: A Methods Comparison.....	34
3.1 Introduction.....	34
3.1.1 Cell Patterning Functional Consequence.....	34
3.1.2 Guiding Cell Shape in Vitro.....	34
3.1.3 2D Surface Topography.....	34
3.1.4 3D Technology for Cell Patterning.....	35
3.1.5 Goals.....	35
3.2 Methods.....	35
3.2.1 Maintenance of human iPS cells.....	35
3.2.2 Cardiomyocyte differentiation.....	35
3.2.3 Fabricating Economical Wrinkles for hiPSC CM Alignment.....	36
3.2.4 “Wrinkled” Topography on Polyacrylamide.....	37
3.2.5 Hanging Tissue Disk.....	37
3.2.6 Microfluidic Device Fabrication.....	37
3.2.7 Sacrificial Hydrogel-based Cardiac Tissue.....	37
3.2.8 3D Printed Ring Mold.....	38
3.2.9 3D Ring-based Cardiac Tissue.....	38
3.2.10 3D Quantifying Cell Alignment and Elongation.....	39
3.2.11 Immunostaining for Fluorescence Microscopy.....	39
3.2.12 3D Statistical.....	40
3.3 Results.....	40
3.3.1 Seeding stem cell-derived CMs onto wrinkles.....	40

3.3.2 Alignment of cardiomyocytes on topography.....	41
3.3.3 Tissue engineering protocol rational.....	41
3.3.4 Alignment of cardiomyocytes in 3D culture.....	42
3.4 Discussion & Conclusion.....	43
Chapter 4: Microfluidic platform enables generation of multi-layered scaffold-free muscle with an endothelialized lumen	45
4.1 Introduction	45
4.1.1 Loss of Productivity in Pharmaceutical Discovery.....	45
4.1.2 Research and Development Bioassay Design.....	45
4.1.3 Vascular Engineering in Drug Testing Applications	46
4.1.5 Endothelial Cell Patterning.....	46
4.1.4 Microvascular Engineering.....	46
4.1.6 Promoting in Vitro Angiogenesis and Vasculogenesis	46
4.1.7 Goals.....	47
4.2 Methods.....	47
4.2.1 Device Fabrication	47
3.2.1 Maintenance of human iPS cells.....	49
3.2.2 Cardiomyocyte differentiation.....	49
4.2.3 Cell line maintenance	50
4.2.3 Scaffold-free tissue construction.....	50
4.2.3 Silk processing.....	52
4.2.3 Electrospinning	52
4.2.4 Culture Conditions under Flow.....	53
4.2.5 Cell Staining.....	53
4.3 Results.....	53
4.3.1 Design Criteria and Iterations.....	53
4.3.2 Muscle and endothelial cells form tubes using the concentric needle protocol.....	54
4.3.2 Formation of the endothelialized lumen through muscle tissue	56
4.4 DISCUSSION/CONCLUSION.....	57
Chapter 5: Conclusion	59
References.....	62

LIST OF FIGURES

Figure 1: Scar Tissue Formation.....	3
Figure 2: Cardiovascular Tissue Engineering Overview.....	6
Figure 3: Cardiac Patch Construction and Delivery.....	8
Figure 4: Nano Topography Guided Cell Alignment.....	12
Figure 5: Dissertation Outline.....	15
Figure 6: hPSC CM differentiation.....	21
Figure 7: Human hPSC CM and adult CM phenotypic comparison.....	22
Figure 8: Embryoid body and high density monolayer human pluripotent stem cell derived cardiomyocyte differentiation protocol.....	27
Figure 9: Characterization of the puromycin resistant α -myosin heavy chain DF19-9-7T hiPSCs.....	30
Figure 10: Morphological differences between the BMP4 Activin A hESC CMs, and the Wnt Inhibited hiPSC CMs.....	31
Figure 11: Replated hiPSC CMs differentiated with the inhibition method.....	32
Figure 12: hiPSC CM contraction and calcium transience profile.....	33
Figure 13: Wrinkle chip fabrication.....	36
Figure 14: Muscle strip microfluidic device.....	38
Figure 15: Muscle ring formation.....	39
Figure 16: Early seeding of hPSC CM lose alignment on wrinkles over time.....	40
Figure 17: Topographical signals align human iPSC CM.....	41
Figure 18: Sacrificial hydrogels generate ring muscle tissue.....	42
Figure 19: Tension on 3D tissue provides minimal alignment to hiPSC CM.....	43
Figure 20: PDMS device fabrication.....	48
Figure 21: Dimensions for the 3D-printed mold and completed microfluidic device.....	49
Figure 22: Endothelialized muscle tissue construction.....	51
Figure 23: Silk processing and fiber diameter.....	52
Figure 5: Biology-inspired tissue assembly device design.....	54
Figure 25: Single layer perfusable tissue tube.....	55
Figure 26: Endothelial tubes within muscle tissue.....	56
Table 1: Summary of clinical trials using autologous cells isolated from the patients' heart tissue.....	16
Table 2: Clinical trials utilizing bone marrow-derived mononuclear cell derivatives.....	17
Table 3: Mesenchymal stem cell based-therapies in clinical have reached phase II.....	18
Table 4 Time points used in current clinical studies stem cell-therapy intervention [186].	18
.....	18
Table 5 Differences between hPSC CM and adult CM.....	23
Table 6: Growth factor protocol for deriving HES2 hESC CMs.....	28
Table 7: Inhibitor protocol for deriving H9 hESC CMs and hiPSC CMs.....	28
Table 8: Comparison of growth factor and inhibitor hPSC CM differentiation efficiency.....	32
Table 9: Needle dimensions provided by Sigma.....	55

Chapter 1: Introduction

1.1 Background

1.1.1 Societal Impact of Cardiovascular Disease

Cardiovascular disease is the leading source of mortality in the westernized world playing a role in 25-30% of all deaths [1]. According to the American Heart Association, one in three adults has some form of cardiovascular disease, and despite recent education efforts in public health, these rates have remained relatively stable for the past 10 years [2]. In addition to high mortality, many affected individuals survive with lasting chronic conditions. The years of health a patient has lost due to this ailment is often quantified by disability-adjusted life years (DALY). Data suggests that 18% of DALY stems from coronary heart disease alone [3]. This leads to a cumulative expense of physician time, hospital services, medication, and lost productivity. In economic terms, this is estimated to cost about \$315.4 billion per year in the US [1, 4]. The most common form of heart disease is coronary heart disease, accounting for 43% of all global cardiovascular disease-related deaths [3]. These events, along with other coronary heart disease ailments, costs the US \$108.9 billion a year in both medical expenses, as well as lost productivity. With our aging population, these costs are expected to increase by roughly 200% over the next twenty years [5].

1.1.2 Cardiovascular Physiology

The devastating consequences of coronary heart disease stem from the vital role of a heart pump in a normal functioning cardiovascular system. The dynamic network of blood vessels (totaling about 60,000 miles in length [6]) is responsible for transferring oxygen, nutrients, and waste through the body. Deoxygenated blood passes through the vena cava into the heart's right atria and ventricles, and out through the pulmonary artery. As the blood flows through the lungs, blood is oxygenated and returns back to the heart through pulmonary veins. The oxygenated blood is pumped through the left atrium and ventricle, and out to the rest of the body through the aorta. This pumping mechanism is controlled by pacemaker cells initiating the electrical conductivity through heart muscle.

As the sinoatrial (SA) node of pacemaker cells fire an electrical signal (the action potential is known as a P wave when recorded by an electrocardiograph or ECG) across the atria, subsequent depolarization causes the cardiomyocytes to contract. During this phase, called atrial systole, blood is past from the right or left atria through the tricuspid (right) or mitral (left) valves, and into the right or left ventricle respectively. Electrical signal passing through the atrioventricular (AV) node, located in the interatrial septum, helps to prevent the ventricles from contracting before filling with blood. After passing the AV node, the electrical signal proceeds to the bundle of His (Q wave), down to the apex of the heart, and into Purkinje fibers running up each ventricle (R and S waves). Depolarized left ventricles send blood through the ventricular (right) or aortic (left) valves and into the arteries. Repolarization of the ventricles, called ventricular diastole (T wave) causes the cardiomyocytes to relax, blood flows back into the chambers, and the cycle repeats [7].

1.1.3 History of Coronary Heart Disease

The first detailed clinical record for diagnosing and treating acute myocardial infarct (MI) is credited to Dr. James Hendrick in 1912 [8]. During the time of Dr. James Hendrick's practice, an MI could only be definitively diagnosed on the autopsy table. Therefore, it was difficult for clinicians to distinguish between an uncomplicated angina and a MI. By the 1930s, coronary thrombosis had become widely diagnosed across America and Europe [9]. Before the electrocardiogram (EKG) monitoring technology, nurses were trained to detect arrhythmias by auscultation. Treatments for acute myocardial infarction from the 1920s to 1950s included hospitalization (up to one month), prescribed medication for relief of pain, anticoagulants (heparin and warfarin), and coronary vasodilation [8]. However, death rates following a MI remained high. In 1961, with the introduction of the coronary care unit, early death via myocardial infarct fell from 30% to 15%. In these specialized facilities, patients could be continually monitored using electrocardiographs. Staff trained in closed chest resuscitation and external defibrillation would respond immediately should a serious arrhythmia occur. The 1970s brought further improvement by implementing new drug treatment strategies for patients experiencing failure of the left ventricle following acute MI.

1.1.4 Remodeling Consequences Following an MI

The most common of categories of heart disease ailments include hypertension (high blood pressure), atherosclerosis, and coronary heart disease. In atherosclerosis, macrophages accumulate near the lumen of the artery, cholesterol form in intermediate lesions, and calcification of the outer mass occurs in more advanced lesions. Disease often manifests when lumen stenosis leads to ischemia (reduction in oxygen supply to tissue) in downstream tissue. More serious complications occur when the soft plaque ruptures, forming a thrombus that blocks an artery completely. Loss of oxygen to the surrounding tissue of the coronary artery causes the ischemic event.

Once the coronary artery is blocked the cardiac physiology responds to the acute ischemia within minutes, triggering an ischemic cascade; the heart cells in region lacking oxygen die and do not regenerate. A collagen scar forms in the region with matrix decreasing type III collagen, and increasing type I [10-14] while also reducing the total collagen content in the infarcted area by 50% [15]. Matrix-associated glycoproteins, elastin, and microfibrillaments are broken down, degraded, subsequently losing organization and structure [16].

In the necrotic phase (**Figure 1**), inflammation and necrosis that occurs after the infarct begins to stiffen (within 4 to 6 hours of artery occlusion). A loss of collagen, both inter and extracellular, lead to regional dilation and thinning of the infarct zone [17]. Four to five days after the onset of coronary artery occlusion, immune cells remove dead muscle from the scarring area. As necrotic phase ends around day 7, collagen production rapidly increases [18, 19].

Cardiac remodeling during a fibrosis phase results from the damaged myocardium's compensatory mechanisms attempting to reestablish homeostasis in muscle contraction

and fluid pumping. Gene expression change in molecular and cellular mediators lead to increases in the size of the heart and changes in global shape. The magnitude of remodeling relates roughly to infarct size, where, large infarcts are associated with more dilation and greater increases in systolic and diastolic stress. In progressive postinfarction dilation, the end-systolic volume index increases progressively and ejection fraction declines, correlating with mortality.

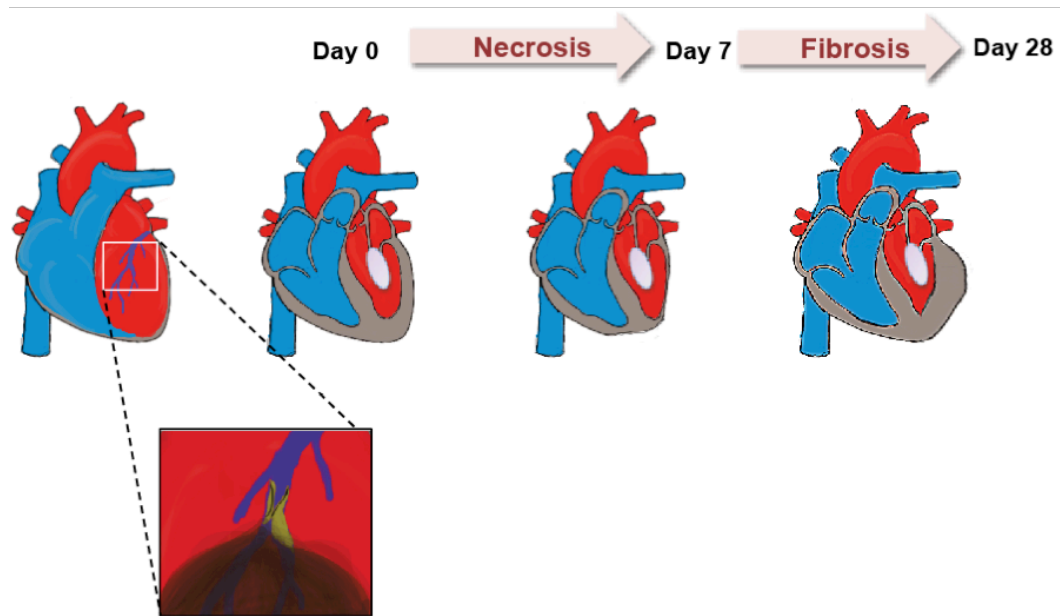


Figure 1: Scar Tissue Formation.

Duration of stages in human MI scar tissue formation [11].

1.1.5 Lasting Impact of MI

The blocked coronary artery can cause heart failure by killing 25% of the left ventricle, approximately 1 billion cells, with only a couple of hours of blocked blood flow prior to reperfusion [20]. This is in addition to the slow death of cardiomyocytes through hypertension [21], or the 38 million and 14 million myocyte nuclei/year in the left and right ventricle that are lost through aging [22]. In order to maintain the structural integrity of the heart, myofibroblasts produce an abundance of collagen type I in the new scar tissue [12]. Although the exact number of regenerating cardiomyocytes is hard to quantify, one study used the pulse of C14 during the cold war to show that 55% of cardiomyocytes are terminally differentiated, and the remaining 45% will renew only once over the adult's lifetime (or about 1% per year) [23]. Therefore, once the cardiomyocytes have died, they cannot regenerate and the subsequent scar tissue forms is permanent.

1.2 Current Treatment Strategies Following MI

1.2.1 Diagnosis

Due to the constant advances in clinical diagnostic sensitivity, the specific criteria to diagnose an acute MI is in its third iteration [24]. Currently, diagnostic techniques include a blood screening for elevated cardiac biomarkers (cardiac troponin T or I), significant ST-segment-T wave changes or pathological Q waves on an electrocardiogram (EKG), and images (nuclear with coronary perfusion, magnetic resonance imaging, single photon emission computed tomography, or echocardiogram) showing a blocked coronary artery or damaged ventricle muscle. Current treatments for an acute MI aims to lower the work-level required by the heart as well as attempt to prevent future clots from forming.

1.2.2 Surgical Intervention

Another strategy for reducing additional cardiac events is to open the coronary artery. In 1976, this strategy was first implemented by lysing coronary thrombi with infused streptokinase. In 1989, Eugene Braunwald proposed what is now called the “open-artery” hypothesis[25]. In this publication, he noticed that using percutaneous transluminal coronary angioplasty (invented by Andreas Gruentzig in 1977[26]) was beneficial even after the infarcted area had formed a scar. A number of clinical trials for late reperfusion therapy have been explored (reviewed in [27]). One of the most promising is the drug-eluting stent introduced to decrease the restenosis that occurred within one year in 30-40% of all coronary angioplasty procedures.

The field of Cardiology has progressed substantially since its origin in 1912. However, treatment strategies for more severe cardiac infarctions require further development. Medical devices that aid in filling this need include pacemakers and vascular assist devices. Pacemakers are small electrical-pulse producing medical devices surgically implanted under the skin by the left collarbone. They can be modified to each patient’s needs, and can include a defibrillator to revive a sudden cardiac arrest. Unfortunately, the convenience of modifying the pacemakers wirelessly has allowed them to be hacked and reprogrammed by unauthorized third parties. Vascular assist devices are blood pumps designed to decrease the heart’s workload. These devices are placed in the abdomen, pericardial space, or extracorporeally [28], but are usually temporary to assist surgeries or a patient up to two years.

Bypass surgery involves moving vasculature from one area of the body (usually the internal thoracic artery), to circumvent the occluded coronary artery. Both this procedure and whole heart transplants involve invasive open-heart surgeries. A whole heart transplant is the only procedure that replaces the damaged heart’s scar tissue. In addition to the aggressive surgery, complications like sepsis, graft vs. host, or organ rejection may occur even with the immunosuppressive therapy.

1.2.3 Left Ventricular Restraint

After coronary artery occlusion, the LV undergoes an extensive remodeling phase, weakening the cardiac wall. To avoid rupture of the LV and aid in the repair process, researchers are investigating restraining the LV wall using commercially available medical products. Early application of polypropylene (Marlex mesh that is currently used for hernia

repair) after MI in a sheep (ovine) model has shown to significantly improve LV remodeling in both anteroapical and posterobasal infarctions [29]. Polyester (Acorn cardiac support device currently used to treat hypertrophy in heart failure) placed on an ovine model one week post-MI showed a decrease in MI expansion and improvement in border-zone function [30]. Nitinol (Paracor HeartNet device currently moving towards clinical trial for heart-failure treatment [31]) has similarly been used for MI in dog and sheep models [32, 33].

1.2.4 Pharmaceuticals

The most common methods for lowering work demand to the heart include pharmaceutical intervention. Beta-adrenergic blockers (β -blockers) reduce the rate of heart contraction, thereby mitigating the progression of acute MI injury [34]. It should be noted that β -blockers have wide clinical application. Once activated, catecholamines, hormones responsible for the flight-or-fight response, are released from the sympathetic nervous system and bind to adrenergic receptors on the heart, blood vessels, and lungs. By blocking these adrenergic receptors, the body no longer responds to catecholamine production by increasing heart rate and heart muscle contraction, and relaxing the smooth muscle cells found in bronchial tubes [35]. Angiotensin-converting enzyme inhibitors (ACE inhibitors) are another class of medications that inhibit the enzyme converting angiotensin I to angiotensin II, allowing blood vessels to relax, which lowers blood pressure and decreases the oxygen demand from the heart. Although these drugs can extend the lifetime of the patient by reducing cardiac load, none of these approaches are reparative.

1.3 Tissue Engineering

Cell therapy can lead to moderate improvement in global heart function [36], but improvement is limited to 5% increase in ejection fraction if using mesenchymal stem cells (MSC) [37] and even less from bone marrow cell (BMC) [37-39]. Strategies for building 3D tissues that could “replace” the damage myocardial tissue hold more promise. Cardiovascular engineering is a regenerative approach to repairing the infarcted scar of the heart. Many design strategies are currently under investigation including: promoting angiogenesis, mitigating apoptosis, attempts to activate endogenous cells by promoting the differentiation of the existing cardiac progenitor cells [40], injection of stem cell derived-cardiovascular cells, biomaterials, or in vitro stem cell-derived tissue.

Although the term “Tissue Engineering” is credited to members of the NSF in 1987 [41], the first proof of concept manifested back in the 1950s [42]. In this publication, chick cardiac myocytes aggregated in spontaneously beating spheroids when gently gyrated in an Erlenmeyer flask. Since this time the field has rapidly advanced to include multiple derived cell types (**Figure 2**) as well as a broad range of biomaterials and techniques to produce more tunable systems. These include cell sheet layering, cell delivery of injectable hydrogels (reviewed in [43]), acellularization of natural materials [44, 45], or a combination therapeutic [46].

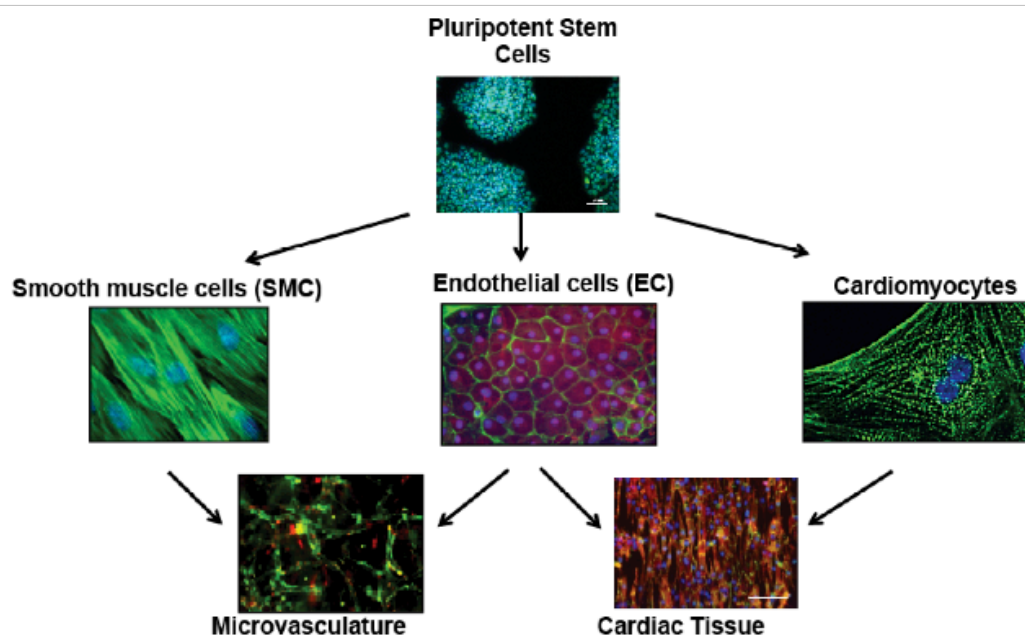


Figure 2: Cardiovascular Tissue Engineering Overview.

Embryonic stem cells (upper left) are generated by retrieving the inner cell mass of a discarded blastocyst after in vitro fertilization. Induced pluripotent stem cells (upper right) are reprogrammed by adding transcription factors to adult somatic cells. Both methods produce pluripotent stem cells can then be differentiated into three of the most common cardiovascular cells (smooth muscle, endothelial, and cardiomyocytes). Vascular and cardiac engineering strategies may bring together multiple cell types to build three dimensional tissues.

1.3.1 Extracellular Matrix Composition in Vivo

ECM production and degradation during development is a highly dynamic and controlled process (**Figure 1**[47]) [48]. What's more, although researchers have studied the up and down regulation of ECM genes, the exact make-up of ECM at different stages in development is poorly understood [49]. Due to ethical constraints, studying the ECM composition of a developing human heart is nearly impossible. Therefore the majority of information surrounding the role of ECM proteins in heart development is gained through gene knockout studies in mice and zebrafish (reviewed by Lockhard et al. [49]). Perhaps most notably, a fibronectin knockout failed to form a heart tube, and was lethal between ED 8.5 to 10.5 of mouse development [50]. Defects to perlecan, a basement membrane protein that binds together laminin and is a major component to the cardiac jelly, caused defects in the thin myocardium phenotype, and was fatal at ED 10.5 to 12 [51].

In vitro studies of cardiomyocytes have repeatedly shown both laminin and fibronectin most effectively enhance cell attachment and viability [52]. Laminin was also shown to be the most effective means of cell attachment in primary human adult cardiomyocytes (obtained via patients undergoing cardiac surgery), with little variation between atrial and ventricular cardiomyocytes [53]. Although a laminin/fibronectin optimization has been

performed for human embryonic stem cell lines [54], it has not yet been applied to human induced pluripotent stem cells. Further studies on the effect of ECM on hPSC CM maturation have yet to be explored. However, this should be done independently from the addition of mechanical cues.

Another ECM consideration includes preparing the hPSC CMs for implantation into the MI model. The ECM following MI is drastically different than a healthy heart. Once the coronary artery is blocked the cardiac physiology responds to the acute ischemia within minutes, triggering an ischemic cascade; the heart cells in region lacking oxygen die and do regenerate. A collagen scar forms in the region with matrix changes from type I collagen to type III collagen [10], while also reducing the total collagen content in the infarcted area by 50% [15]. Matrix-associated glycoproteins, elastin, and microfilaments are broken down, degraded, subsequently losing organization and structure [16]. In the necrotic phase, inflammation and necrosis that occurs after the infarct begins to stiffen (within 4 to 6 hours of artery occlusion). A loss of collagen, both inter and extracellular, lead to infarct expansion [17]. Four to five days after the onset of coronary artery occlusion, immune cells remove dead muscle from the scarring area. As necrotic phase ends around day 7, collagen production rapidly increases [18, 19].

1.3.2 Biomaterials Used for Cardiac Patch Design

Numerous biomaterials can be used in hydrogels or scaffolds, and delivered over a MI, or injected through the vasculature (**Figure 3**). Natural extracellular matrices includes hydrogels (gelatin [55], collagen gels [56, 57], fibrin [58-60], and alginate [61]), dry scaffolds (collagen or gelatin medical mesh [62, 63], lyophilized alginate [55, 61, 64], and silk [65]), or decellularized tissue ECM (native porcine small intestine [66], porcine urinary bladder matrix (UBM) [46], and both porcine [67] and human [68] heart tissue). Moreover, additional modifications are often made to these materials to optimize cell adhesion, porosity, and protein delivery [69]. Highlights of these biomaterials will be presented in this chapter with full reviews provided in the literature [70, 71]. Comprehensive tables comparing biomaterials used in cardiovascular tissue engineering (including ventricular restraints) with their intrinsic properties and fabrication methods can be found here [72]. Biomaterials used in vitro as well as in vivo models is reviewed both here [41], as well as here [73].

Hydrogels are advantageous for promoting cell-to-cell adhesions, forming anchor points with surrounding material, and flexibility to compress and stretch, allowing the tissue more adequately respond when exposed to mechanical stimulation (discussed later). Hydrogels can be made from a number of different materials including gelatin, a denatured form of collagen type-I. The ability for higher concentrations of gelatin to dissolve after a temperature increase has been used to mold both vasculature [74] and rat neonatal CM muscle strip templates [75]. Collagen type-I is most prevalent extracellular matrix in the heart, and thus an obvious choice for engineered heart tissue, however the low tensile strength and stiffness [73] mitigates its ability to physically support the diseased tissue [73, 76]. Fibrin, a mixture of fibrinogen and thrombin proteins found in blood plasma, is a critical component in wound healing and also has attractive mechanical properties for

tissue engineering with its non-linear elasticity [77], ability to covalently bind to growth factors [78], and controllable degradation via the fibrinolytic system [79]. A review of fibrin gel applications across the medical field can be found here [80]. Although hydrogels are a valuable tool for in vivo injection, their liquid-like properties make special-temporal control a continuing challenge [81].

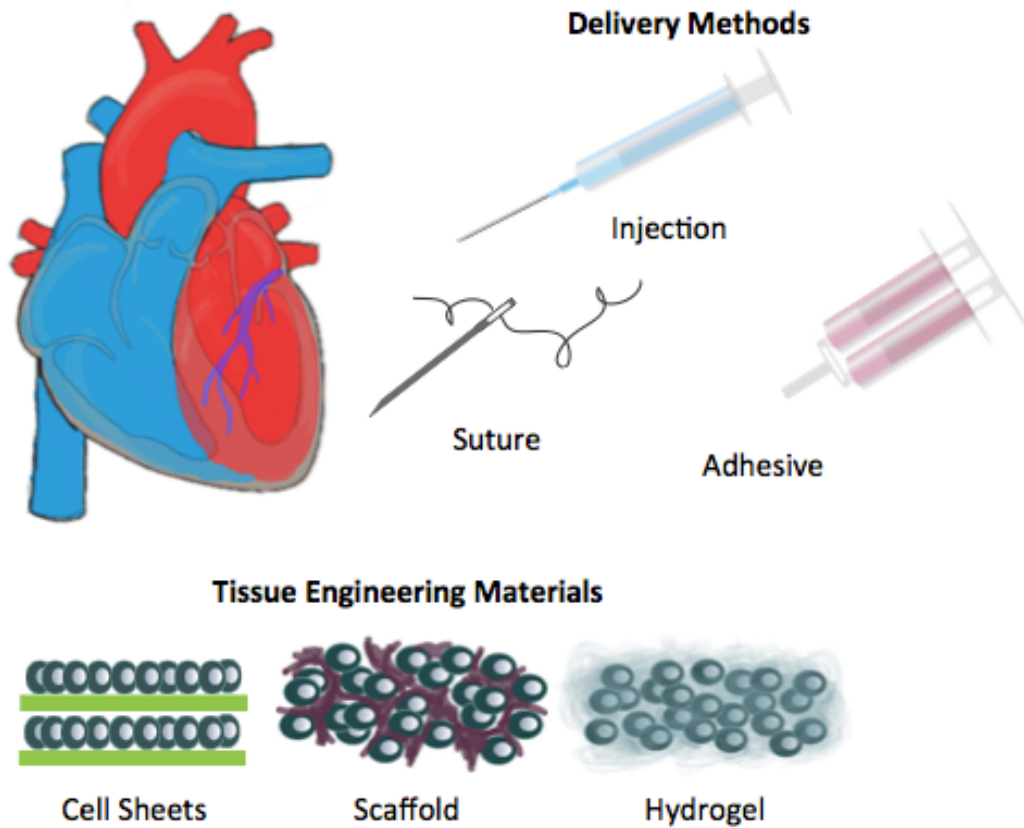


Figure 3: Cardiac Patch Construction and Delivery.

Therapies in single-cell suspension are directly injected into the muscle, or vasculature. Tissues formed by incorporating cells with injectable hydrogels are injected into the scar-tissue region. Layered cell sheets, as well as cells seeded onto scaffolds can be sutured or fibrin glued over or under the scar tissue region.

Seeding cells into pre-formed polymers aid cell adhesion, examples include: commercially available medical mesh, alginate, and silk. Alginate is a polysaccharide polymer naturally found in marine brown algae, and has been extensively studied for tissue engineering applications [82]. Modifications have been included to increase the polymer's cross-linking (thus increasing its mechanical strength and stiffness) [83], molecular weight of components (for controlling degradation rate) [84], and cell adhesion monomers [85]. Rat neonatal CM resuspended onto alginate scaffolds have been shown to improve cardiac function in rat infarct models [55, 64]. The silk produced by silkworms, spiders, and

scorpions is notoriously strong and elastic. What's more, minor processing can produce a product that is biocompatible [86], degradable [87], and capable of functionalization for drug-delivery purposes [88]. Although silk in the cardiovascular domain has been primarily used for vascularization studies [89, 90], initial reports show rat neonatal CM are capable of forming 3D contractile patches on silk [65].

Acellular xenogeneic ECM has been used successfully as a scaffold for repair and replacement of numerous tissue and organs [91, 92]. Cardiac tissue decellularization is achieved using an extended Langendorff perfusion [93], in which SDS and Triton X-100 are pumped through the ascending aorta. The acellularization processing method [94] retains the natural composition of matrix molecules such as collagen (Types I, III, IV, VII), glycosaminoglycans, proteoglycans, and glycoproteins, which are known to have important roles in host tissue repair and remodeling. Studies using acellularized matrix on infarcted left ventricular wall indicate suitable surgical handling, and facilitation of cardiac repair, through infiltration of CM, smooth muscle and endothelial cells, and generation of bioactive molecules during bioresorption [44, 45], while providing enhanced mechanical support compared with a current nonresorbable patch [44].

When using synthetic materials, extra precaution must be taken to ensure biocompatibility, as well as a non-toxic exit pathway for degradation, or limited side effects in non-degradable systems. However, the benefits of synthetic material's tunable properties, as well as their often-superior mechanical strength compared to natural biomaterials, is a promising addition to cardiac patch design [73]. Those most commonly utilize include either polyglycolic acid (PGA) [95], polyL-lactic acid (PLA) [96], and/or poly(glycerol-co-sebacate) (PGS) [97]. One of the most appealing aspects to these synthetic matrices is their ability to hold a molded form, and thus be used as building blocks to stack micro-tissues. This not only enables larger 3D constructs, but can also guide cell behavior to promote vascularization [98].

Unfortunately, the poor conductivity in many of these materials prevents cardiac tissue from robust synchronous contraction [99]. Methodologies to improve the electrical propagation include the addition of gold nanowires. Bridging the non-conducting porous walls of alginate with gold improved both the tissue contraction, and increased the expression of electro-mechanical coupling proteins [100]. It is important to note that although gold nanoparticles have been used in a variety of medical applications [101, 102], unlike the materials listed above, they are not biodegradable. Long-term effects have yet to be studied from this emerging field of nano-medicine.

The engineered tissue can package and deliver spatially patterned cells at high densities leading to increased retention of cells and host integration [5-8]. The optimal materials being explored in engineering cardiac tissue are vast, however, we expect that the decellularization of slices of native heart tissue [68] or whole hearts [67] will be critical players in engineered cardiac tissue repair. This is predominantly due to their ability to retain native ECM proteins and fibrous architecture with comparable mechanical strength to native hearts [103], as well as, potential maintenance of the perfusable vasculature.

1.3.3 ECM in Cardiac Tissue Engineering

Of the many biomaterials for CM tissue engineering purposes, none mimic a post-MI scar tissue ECM. It is possible the hPSC CMs grown on laminin, fibronectin, matragel, and ultimately the ECM that the cells endogenously produce. For the purpose of MI therapy, a CM capable of binding to the stiff, highly collagenous scar may be preferential to a CM conditioned to mimic healthy human heart tissue. Publications studying the effect of varying ECM on hPSC CMs have primarily focused on cellular adhesion, viability, and cardiac specific marker expression levels. Although a fibronectin/laminin blend may be the most efficient way for generating and culturing a high quantity of CMs, the cells must ultimately bind to the scar tissue.

1.3.4 Linking ECM to Hydrophobic Materials

After establishing the ideal ECM composition for cardiac patch construction, the next challenge includes linking the substrate to its appropriate platform. The hydrophobicity of PDMS or silicone is often determined by measuring the contact angle of water to the materials' surface. An increase in water contact angle (decrease in hydrophobicity) has been shown to be directly proportional to cell spreading [104]. Preparing the surfaces for biological application requires either chemical modification, boiling water, O₂ plasma treatment, or UV radiation [105]. Further stability can be achieved by adding additional cross-linking factors to the treated surface. Traditional proteins used included peptide sequence RGD (a section of the fibronectin protein), poly-L-lysine, heparin, and heparin sulfate. However, bonding between these cross-linkers to the treated surface is accomplished through weak non-covalent interactions (electrostatic, van der Waals), which increases the chances of protein diffusing into media [106].

Covalent bonding strategies include the following: glutaraldehyde with amino-silane((3-aminopropyl)triethoxy silane) or APTES [106-110], and organosilanes 3-glycidoxypropyltrimethoxysilane (GPTMS) [107]. In the context of measuring CM contraction, APTES was found to increase CM contractility over time, compared to GPTMS which decreased [107]. However, it should be noted that this experiment was conducted over the course of two days. Ideally, hPSC CMs would be cultured on the mechanical stimulation platforms for up to a week. Another factor contributing to cell dissociation is that long-term cell culture will lead to the replacement of plated substrate with ECM produced by the cells. The addition of mechanical loading has been shown to substantially influence ECM production [111]. The importance of these cues, along with the complexity of ECM production makes the inhibition of ECM producing gene expression a nonviable option.

1.3.5 Cell Sheet Technology

Cell sheet engineering uses the temperature sensitive polyper (poly-(N-isopropylacrlaide)), PNIPAM, to exclude the addition of a scaffold. Using this technique to increase the cell-cell connections [112] has shown promising results for engraftment potential (up to one year post-implantation) [113]. Automated systems to scale-up this technology are currently

in development to circumvent the difficulty associated with manually layering each sheets [114]. Limits of oxygen diffusion through tissues over 500 microns thick may cause potential complications in these efforts to scale-up.

1.3.6 Cell Patterning

Current cell sheet engineering protocols do not produce tissue with aligned and elongated CMs. This has lead researchers to begin using topography (**Figure 4**) to induce alignment of primary neonatal cardiomyocytes, and ECM [115], derived endothelial cells [116], as well as hPSC CMs [117]. Aligning single cell hPSC CMs with micropatterning has already been shown to enhance the maturation of β -Adrenoreceptor signaling [118], force generation [119, 120], and calcium cycling [119, 121]. What's more, mathematical models of collagen alignment in the heart indicate a positive correlation with increased left ventricular stroke volume alignment [122].

1.3.7 Role for Mechanical Signaling

After the human heart fills with blood in diastole, CMs actively contract in systole to pump this blood throughout the body. In order to precondition stem cell-derived CMs for their host environment in which they must mechanically couple with native tissue, the stem cell-derived CMs are being cyclically stretched in bioreactors. This mechanical loading also has a dramatic effect on the CMs' production of extra cellular matrix [111], increases intracellular protein content [123], as well as cytoskeletal organization, alignment, and proliferation [57]. Studies using rat neonatal cardiomyocytes (RNCM) on Col I hydrogels found that stretch of engineered heart tissue increased mitochondrial density and hypertrophy of the cells (thus promoting a more mature phenotype) [124], improved systolic and diastolic function in a rat infarct model [125]. Therefore, a variety of bioreactors have been designed mimic in vivo strain fields [126, 127] to stretch cardiac cells uniaxially, biaxially, and in three dimensionally (reviewed in [128]). Moreover, these stretching devices can also overcome the discrepancy between murine models (600 beats per min), and normal human physiology that is much lower (70 beats/min) [129].

Developmental biology has already shown examples of how the developing heart adapts to changes in mechanical load. In the fetal sheep heart, hemodynamic overloading caused changes in connexins 40, 43, and 45 [130], and these changes in connexin organization is associated with ischemic heart disease [131]. Increases in the mechanical loading in in chick embryos [132, 133], as well as neonatal rats [134], lead to myocyte hyperplasia. Specifically, the N-cadherin mechanotransducer, which localizes beta-catenin [135] and is involved in Wnt signaling [136], is expressed during the time of gastrulation [137] and is required for proper heart tube development [138]. When strain is applied to immature stem cell-derived CMs, the cells exhibited elevated expression of cardiac-specific markers, and the stretched cells also formed less scar tissue, exhibited lower apoptotic activity, higher VEGF expression, and more angiogenic activity in vivo [139]. Mechanical loading also increased mature cardiac function in three dimensional cultures of both ESC-derived CMs [140] and iPS cell-derived CMs [57].

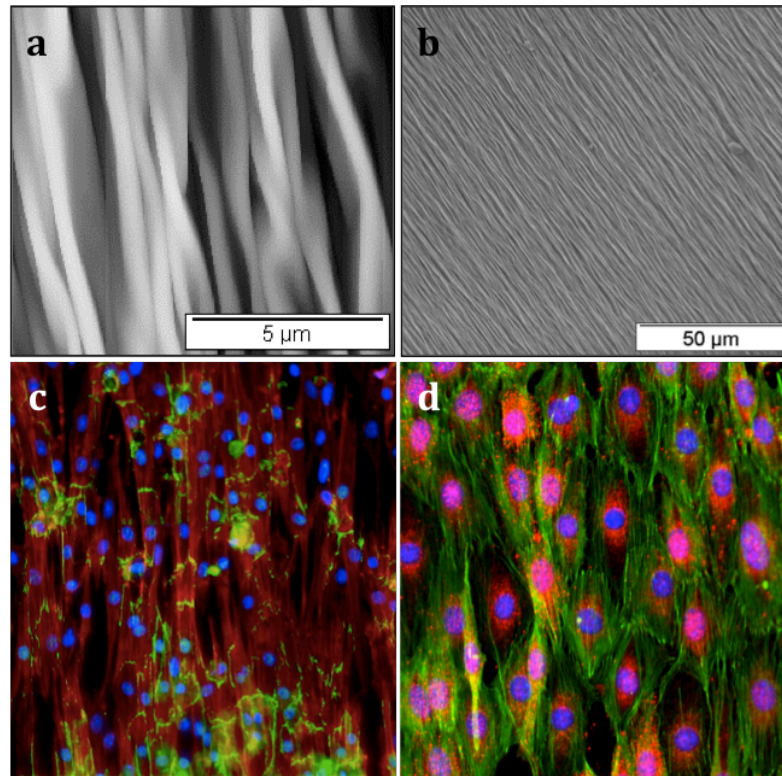


Figure 4: Nano Topography Guided Cell Alignment

a) Atomic Force Microscopy images and b) Scanning Electron Microscopy images of the wrinkle topography formed by shrinking pre-stressed polystyrene uniaxially. c) Mouse neonatal CM aligned via wrinkle topography and stained with N-cadherin (green), actin (red), and dapi (blue). d) mouse ESC-derived endothelial cells aligned via wrinkle topography and stained with F-actin (green), PECAM-1 (red), and dapi (blue).

1.3.8 Current Tissue Stretching Devices

Attempting to mimic the strain field a dynamic organ like the heart is complicated due to the various distinct regions in the heart. Moreover, the heart tissue is designed such that the CM response to strain and strain rate depends up on the magnitude and frequency of strain. To date, stretching devices have yielded data from strain magnitude (2.5 – 25%) and frequency (0.05 – 2.75 Hz) [141] with 10% and 1 Hz thought to be the most appropriate physiological values for magnitude and frequency, respectively [142, 143]. Over a dozen cell/tissue mechanical stimulating systems have been designed for in vitro studies. Advantages and limitations of various systems from earlier days have been described (review [144]). Types of strain fields induced can be used to categorized devices that are being utilized today. Devices that exert uniaxial strain are desired due to design simplicity, uniform strain, and consistent strain fields over high strain values. However, they are low throughput (on direction at a time), and generate anisotropic strain fields. On the other hand, biaxial strain devices are more desirable for their high throughput, and more uniform anisotropic/isotropic strain fields, but lack the design simplicity of uniaxial devices [145].

1.3.9 Whole Heart Bioengineering

Some patients suffering congenital heart defects or heart failure may benefit from receiving a whole heart transplant. Building the whole organ provides additional unique engineering challenges [146]. In 2008, researchers successfully decellularized a rat heart to ECM, and subsequently re-cellularized with neonatal cardiomyocytes. The electrically paced engineered heart miraculously showed sustained contraction [67]. Studies have since compared different decellularization protocols followed by quantification of final ECM protein composition, ECM mechanical properties, and recellularization potential [147] [103]. The most prominent method to date involves decellularizing a donor heart with detergents (triton x-100, sodium dodecyl sulphate), and/or a hypotonic solution with sodium deoxycholate [148]. Decellularized murine hearts have also been used as been successfully used as templates for reseeded hiPSC cardiovascular progenitor cells [149]. Most recently, a decellularized cadaver heart has been partially seeded with iPSC cell-derived CMs, perfused, and analyzed for electrical conductivity [150] with promising results. Though the decellularization process has been successfully applied to the porcine heart [151, 152], recellularizing on such a large scale is a continuing challenge. Another significant challenge with the whole heart approach includes maintaining the valve stability necessary to prevent ventricular to atria, or artery to ventricular backflow during contraction.

1.4 Goals and Overview

Coronary artery disease is a rising pandemic that has claimed the lives of millions worldwide. [3] What's more, those that survive an ischemic heart event, or myocardial infarction (MI), are left with permanent scar tissue and no options for repairing the damage. Over the past twenty years, the field of cardiovascular tissue engineering has made substantial progress towards healing this crippling ailment. However, despite a relative abundance of research manpower and funding towards a stem cell-based therapy solution, a cost effective and robust protocol for replacing post-cardiac infarct scar tissue is far from patient use. Some of the key challenges facing cardiovascular tissue engineering include: a) generating an abundant cell source, b) guiding differentiation towards an elongated phenotype, capable of in vivo integration, and c) packaging these cells in the high concentration required for replacing scar tissue while maintaining cell survival. Because mature cardiomyocytes (CM) exhibit only limited proliferative capabilities, derivation from stem cells is crucial. One significant component of heart tissue is the micro and nano extracellular architecture. Mimicking unique topographical signals induces alignment of both CM [1] and endothelial cells (EC) [2], facilitating a more uniform electrical propagation and subsequent mechanical contraction of the heart cells. Therefore, this proposal will derive PSC-CM and integrate extracellular matrix patterning, for CM alignment. We will also mimic in vitro the strain these cells normally experience in vivo to promote elongation and alignment. These cells will then be built into a 3D cardiac patch for potential use in MI repair (**Figure 5**).

Aim 1. Generation of human pluripotent stem cell derived cardiomyocytes

Generation of 3D cardiac cell tissue hinges on access to an abundance of cardiomyocytes. For the past fifteen years, researchers have developed numerous methods for deriving cardiomyocytes from human pluripotent stem cells. Of these, major techniques claimed to

reach a purity of over 80%. A protocol first published by Gordon Keller used growth factors BMP4, activin A, bFGF, DKK1, and VEGF to guide the biphasic stages of Wnt signaling [153] was then optimized for our human stem cells lines [154, 155] and further optimized to include matrix signaling [54]. The second protocol by the Palecek group targets this same pathway using small molecule inhibitors [156]. In this aim, examined the two protocols for reproducibility, cell yield, and cardiomyocyte purity.

Aim 2. Fabrication of cardiac muscle tissue: a methods comparison

Recent attempts to directly inject hPSC-derived CMs into animals have shown a low rate of cell retention following treatment. Pre-patterning cardiac tissue has already shown to guide the cells towards a more physiological phenotype. Here, we explore and compare several cost-effective methods for alignment of muscle cells. These include using surface guidance features generated on wrinkled PDMS [116] and poly-acrylamide [157] materials. We also compare three distinct methods for forming 3D tissue. These are formed using either a hanging drop, sacrificial gelatin template [158], or 3D printed ring mold [159] and examined for cell survival, as well as cell elongation and alignment.

Aim 3. Generation of multi-layered muscle with endothelialized lumens

Although previous studies have tested hPSC-derived CM's potential as a potential therapy for myocardial infarction, results have consistently underperformed with limited left ventricular ejection fraction improvement. Here, microfluidic device was constructed to enable endothelialization of the cardiac muscle strips. This design was tested for cell survival, endothelial cell adhesion and confluence, as well as hook-up to tubing and perfusability.

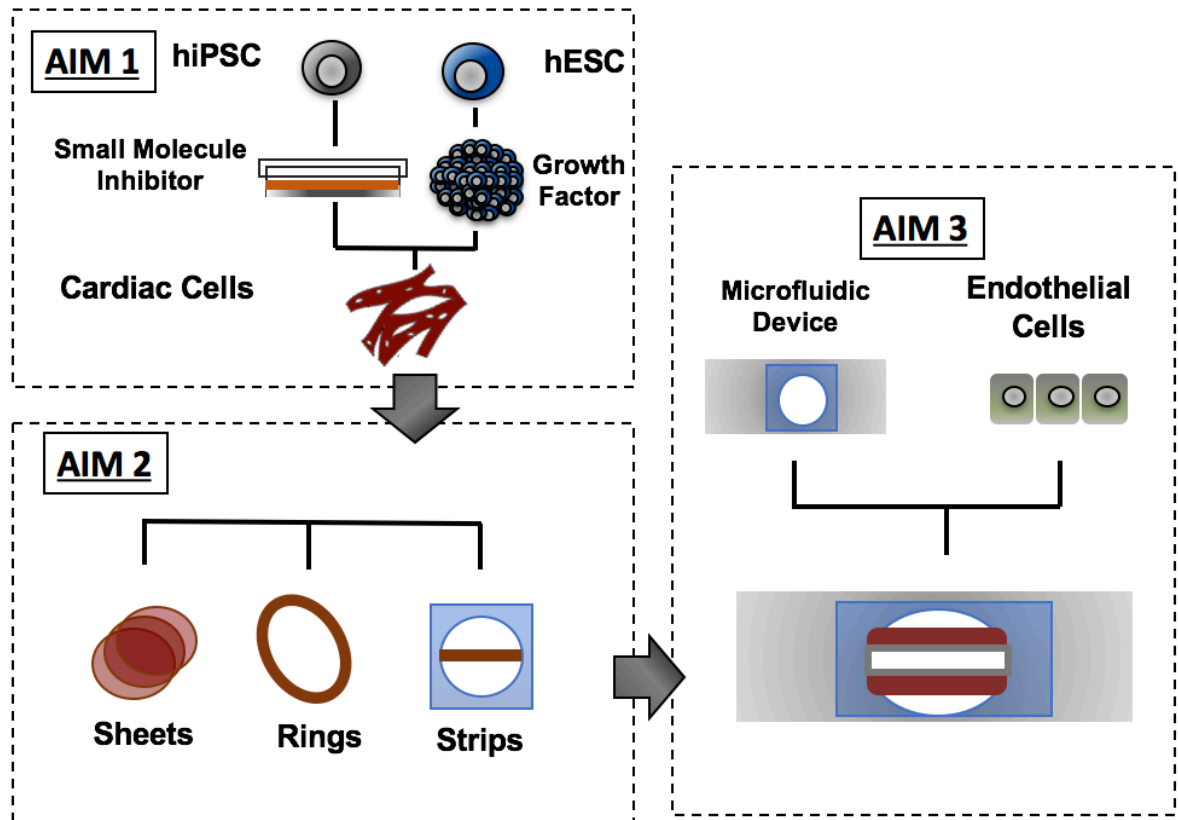


Figure 5: Dissertation Outline

A schematic showing the progression of the project from comparing hiPSC CM differentiation protocols, to using the favored protocol in 3D tissue, and finally endothelializing the 3D tissue in a novel microfluidic device.

Chapter 2: Human Pluripotent Stem Cell Derived Cardiomyocyte Protocol Comparison

2.1 Introduction

2.1.1 Cardiovascular Engineering

Cardiovascular engineering is a regenerative approach to repairing the infarcted scar of the heart with laboratory-generated derived tissue or biomaterials. Many design strategies are currently under investigation including: promoting angiogenesis, mitigating apoptosis, attempts to activate endogenous cells by promoting the differentiation of the existing cardiac progenitor cells [40], injection of stem cell derived-cardiovascular cells, biomaterials, or in vitro stem cell-derived tissue. However, one of the challenges currently facing tissue engineering is generating an abundant and pure cell source. Because mature cardiomyocytes have limited regenerative potential, deriving cells from a stem cell source will be a critical component to a potential treatment.

2.1.2 Adult Stem Cells

The current stem cell-based treatment strategies aimed towards repairing ischemic heart tissue all utilize patient-derived adult stem cells including: mesenchymal stem cells, bone marrow-derived mononuclear cell derivatives, as well as, putative cardiac progenitor cells [160]. Because all of these cells are patient-derived, the risk of rejection is minimal, however, none of these stem cell derivatives have been shown to generate the functionally mature cardiac cell numbers required for regeneration of the damaged heart tissue.

Cardiac progenitor cells (CPCs) are defined by their ability to form multicellular spheroids, express c-KIT [161] or SCA-1 [162] stem cell markers, and increase in number following heart injury [163]. These cardiac-derived cells are included in the most recent stem cell therapies approved for human clinical trials, but are also the most controversial. The three most prominent clinical trials using cardiac-derived cells are SCIPIO [164], CADUCEUS [165], and ALCADIA [166] (*Table 1*, reviewed by Yacoub et al [167]). All trials have reached Phase I in patients less than 33 with left ventricular ejection fractions (LVEF) below 45%. In the SCIPIO trial, patients had an average LVEF of 27.5%, putting them at risk for life threatening irregular heartbeats. It should also be noted that although the data from this trial is the most promising, it is also currently under an ongoing investigation regarding previously published work [168], and process results from c-KIT+ CPC treatment have not been clearly linked to in vivo differentiation and could include mast cells that are not only found throughout solid tissue, but would also accumulate following a myocardial infarct [169]. These trials also consistently deliver the cell therapy past the remodeling phase of the wound-healing process.

Table 1: Summary of clinical trials using autologous cells isolated from the patients' heart tissue.

	Clinical Trials	Patients	Cells from Biopsy	Result

Cardiac-Derived Cells	SCIPO [164]	33	c-kit+ from atrial tissue	12.3% LV EF at 12 months. (data integrity in question)
	CADUCEUS [165]	17	MSC from endomyocardium	No significant change in EF, reduced infarct size
	ALCADIA [166]	6 (no controls)	MSC from endomyocardium	6 months improvement of 9% LVEF

Treatments using bone marrow-derived mononuclear cell derivatives (BMDMCD, Table 2) are comprised of granulocytes, hematopoietic progenitor cells, lymphocytes, plasma cells, monocytes, and macrophages. Stem cell therapies utilizing BMDMCDs was first administered in 2002, making it the most well studied system (reviewed in [170, 171]). Although it was originally thought that hematopoietic stem cells have the ability to differentiate into cardiomyocytes [172], it was quickly shown that they instead differentiate into hematopoietic fates in the ischemic myocardium[173]. Unfortunately, studies in animal models have shown that few to no implanted cells remain in the infarcted area less than a month after injection [174], suggesting that nearly all benefits are due to paracrine signaling [175] of anti-apoptotic signals. Interestingly, although the TIME trials injected cells in both the necrosis, as well as fibrosis stages, neither showed any functional benefit. Compared to other trials using BMDMCD, the TIME studies used patients with significantly lower LVEFs (37% compared to 40-50% in BOOST or TOP-CARE).

Although bone marrow-derived mesenchymal stem cells (MSC; Table 3) do not differentiate into cardiomyocytes, as was previously believed [176], they are thought to improve heart function through paracrine effects [177]. Consistent with the previous two methods, MSC have shown limited to no capability for long-term engraftment [178]. In each clinical trial mentioned, the delivery time of the therapy was well beyond the two months of developing scar tissue.

Table 2: Clinical trials utilizing bone marrow-derived mononuclear cell derivatives.

	Clinical Trials	Patients	Cells isolated and expanded from Biopsy	Result
Bone Marrow-Derived Mononuclear Cell Derivatives	BOOST [179]	60	BMMNC with < 1% CD34+	LVEF increased by 6.7% after 6 months. After 18 months, no difference between treatment and control.
	TOPCARE-AIM [180]	59 (200 for shorter study)	BMCs 7.3×10^6 CD34+/CD45+ cells	LVEF increased 9% at 4 months. Improvement persisted for 5 years.
	FOCUS-CCTRN[181]	92	100×10^6 BMMCs	1.4% improvement at 6 months.

	TIME and LateTIME: Phase II [182]	87	150 x 10 ⁶ autologous BMMNC	No functional benefit after 6 months analyzed with cardiac MRI
	SWISS-AMI [183]	200	autologous BMMNCs	no improvement in LVEF at 4 months
	BAMI Phase 3	3,000	autologous BMMNCs	Ongoing

Table 3: Mesenchymal stem cell based-therapies in clinical have reached phase II.

	Clinical Trials	Patients	Cells isolated and expanded from Biopsy	Result
Mesenchymal Stem Cells	TAC-HFT Phase I and II [37]	65	4 to 6 week expansion of autologous MSCs	No difference in LVEF
	POSEIDON Phase I and II[184]	30	20, 100, or 200 million autologous or allogenic MESs	Neither cell source stimulated significant immune response
	C-CURE [185]	47	treated autologous MESs with cytokines prior to transplantation	7% LVEF improvement

Not only has the success rate been low using these stem-cell therapies, but the findings between different studies are difficult to compare. This is partially due to the difference in the severity of patient pathologies, as well as the timing of treatment administration (Table 4). Moreover, for technical, practical, and ethical reasons, it is difficult to fully characterize the pretreated infarct area of each patient. Given the wide discrepancy of treatment start-days between trials, it is reasonable to assume they are treating vastly different microenvironments of the scarring heart. Many researchers believe that terminally differentiated cardiomyocytes derived ex vivo hold greater promise for adhering and integrating into the host tissue.

Table 4 Time points used in current clinical studies stem cell-therapy intervention [186].

Stem Cell Therapy	Time of injection after MI (days)
CDC	> 30
BMDMCD	7 - 21
MSC	> 40

hPSC CM	0-7
---------	-----

2.1.3 Human Pluripotent Stem Cells

Human embryonic stem cells (ESC) are isolated from the inner cell mass of a blastocyst five days post-fertilization [187]. They are defined by their pluripotency, or ability to differentiate into all three germ layers (ectoderm, endoderm, and mesoderm), of the developing embryo. Another essential feature is the capacity to propagate indefinitely. The immortality of the ESC can be attributed to high expression levels of telomerase, a protein that protects the ends of chromosomes during division. Together, these make the human embryonic stem cell an attractive resource for generating large cell populations. However, because deriving the original cell line involves destroying a pre-implanted embryo, their use is somewhat controversial.

Human induced pluripotent stem (iPS) cells maintain pluripotency and infinite propagation with mitigated ethical concerns surrounding human ESC. The reprogramming of mature differentiated cells into iPSCs is achieved by adding four transcription factors known to contribute to pluripotency and proliferation (Sox2, c-Myc, Klf4, and Oct4 [188], or without c-Myc [189]), or (Oct4, SOX2, NANOG, and LIN28) [190].

Adoption of iPS cells was swift, earning the scientists that discovered these genes a Nobel Prize in Physiology or Medicine in 2012. Today, there are many commercially available kits servicing the production of iPSCs [191]. The starting cell source for reprogramming has been successfully published with adult fibroblasts using a retroviral [190] and lentiviral [192] systems, and renal epithelial cells from urine using a retroviral method [193]. Additional insertion methods avoid introducing the lenti- and retro-viruses by transfecting with plasmids [194, 195], temperature sensitive Sendai viruses [196], small molecules [197, 198], and modified RNA [199]. Initially, there was concern around creating oncogenes in the generation of iPS cells – if the genes coding the transcription factor were inserted in an area of the genome that caused a frame shift, up regulation, or down regulation of proto-oncogenes. However, more recent protocols have eliminated this risk by adding the transcription factor proteins fused with cell penetrating peptide [200], or poly-arginine anchors (to assist in transport through the cell membrane), rather than inserting genes [201]. Similar techniques have been utilized for direct reprogramming of adult fibroblasts to cardiac-like cells and cardiomyocytes in mouse [202-206] and human [207].

2.1.4 Therapeutic Use of Human Pluripotent Stem Cell Derived Cardiomyocytes

The progression of hPSC-derived cell therapies into clinical trials has progressed more slowly than other stem cell types [208, 209]. One of the main challenges preventing patient use is concern regarding the hPSC's proclivity towards teratoma formation in vivo. The few hPSC-derived cell therapies with either high enough purities, delivery to immunoprotected sights, or where need outweighs the potential risks (reviewed in [210]) address the following diseases: age-related macular degeneration, Parkinson's disease, spinal cord injury, and diabetes [211, 212]. In Japan, researchers have already begin

banking stem cells, as 50 sample would be histocompatible with 90% of its population [213].

In the cardiovascular domain, a single patient has received ESC-derived Isl-1+/SSEA-1+ cardiac progenitor cells during a coronary bypass operation [214]. Although LVEF improved 10% over the course of three months, it is difficult to isolate the precise contributing factors for this improvement. In this one patient no complications involving arrhythmias, tumor formation, or immune rejection were reported. However, many researchers are quick to criticize hESC-derived CMs use in a clinical trial [215, 216], as wider studies involving non-human primates showed critical flaws (see section on “In vivo delivery of cardiomyocytes” for more details).

2.1.5 Derivation of Cardiomyocytes from Human Pluripotent Stem Cells

The most common methods for deriving cardiomyocytes (CM) from human pluripotent stem cells, both ESC and iPSCs, consist of three stages (**Figure 6**). The first stage utilizes a spontaneous differentiation phase like plating cells as a high density monolayer [217, 218], or clustering the cells into embryoid bodies using hanging drops [219], AggreWell™ plates, or microwells [220]. The culture is then guided through the biphasic WNT/ β -catenin signaling in the next two stages [221, 222]. In the second stage, mesoderm differentiation and specification is enhanced by either the addition of WNT signaling molecules activin A, BMP4, and FGF2, or by inhibiting the WNT signal inhibitor GSK3B with small molecule CHIR99021. Cardiac cell fate in the third stage is directed by blocking WNT signaling using inhibitors DKK1, IWP-2, or BMP. It should be noted that each stem cell line needs some additional optimization for cell seeding density, and timing of delivery, duration and concentration of activators or inhibitors [153], and extra cellular matrix composition [54], and period before tissue formation. Protocols with the high efficiency (characterized by the expression level of a cardiac specific marker, cardiac troponin T), around 80%, can be found in the following publications [153, 155, 156]. Up to 98% efficiency has been reported by combining activin A, bFGF, and BMP4 with multiple layers of Matrigel extracellular matrix [223].

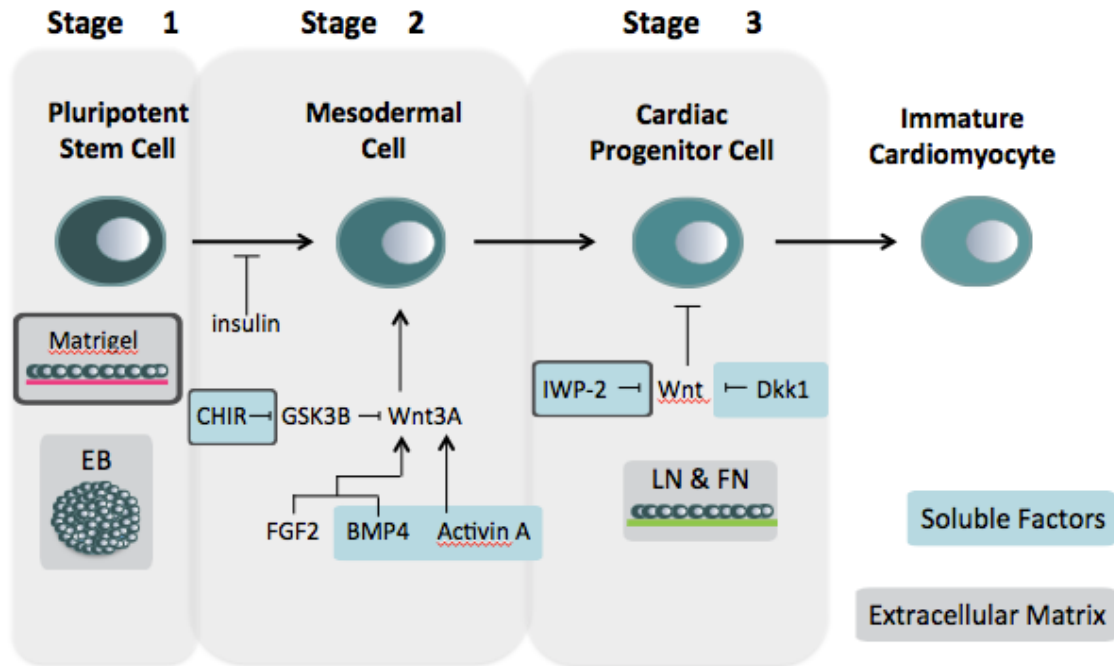


Figure 6: hPSC CM differentiation.

Human PSC CM differentiation directs cell fate by blocking or activating portions of the Wnt pathway by optimizing small molecule inhibitors CHIR and IWP-2 (outlined in grey) [156] or growth factors BMP4 and Activin A, as well as inhibitor Dkk1 (no outline) [54]. LN: laminin. FN: fibronectin. Image is adapted from Burrige et al. [224].

2.1.6 Guiding Stem Cell Differentiation Through Extracellular Interactions

In addition to soluble factors, cells are also heavily influenced by extracellular matrix (ECM) cues [225]. ECM production and degradation during development is a highly dynamic and controlled process [47, 48]. What's more, although researchers have studied the up and down regulation of ECM genes, the exact make-up of ECM at different stages in development is poorly understood [49]. Due to ethical constraints, studying the ECM composition of a developing human heart is nearly impossible. Therefore the majority of information surrounding the role of ECM proteins in heart development is gained through gene knockout studies in mice and zebrafish (reviewed by Lockhard et al. [49]).

In the initial stages of development, a looping tube of cardiomyocytes surrounding endothelial cells is supported by proteoglycans, glycoproteins, and collagens [226, 227]. As the tissue advances, fibronectin and laminin proteins seem to play a more critical role. A fibronectin knockout failed to form a heart tube, and was lethal between ED 8.5 to 10.5 of mouse development [50]. Defects to perlecan, a basement membrane protein that binds together laminin and is a major component to the cardiac jelly, caused defects in the thin myocardium phenotype, and was fatal at ED 10.5 to 12 [51].

Based off these findings, researchers have used numerous ECM components to guide hPSC fate [228]. Mouse embryonic stem cells derived on decellularized heart tissue showed

increased levels of cardiac troponin I [229]. However, the most common ECM used in initial stages of development is Matrigel (the isolated basement membrane of Engelbreth-Holm Swarm mouse sarcoma cells containing laminin, collagen IV, heparin sulfate proteoglycans, entactin/nidogen, as well as additional growth factors [230]). Human pluripotent stem cells sandwiched between two layers of Matrigel promotes promoted epithelial to mesenchymal transition, producing up to a 98% purity of cardiomyocytes [223].

In vitro studies of cardiomyocytes have repeatedly shown both laminin and fibronectin most effectively enhance cell attachment and viability [52]. Laminin was also shown to be the most effective means of cell attachment in primary human adult cardiomyocytes (obtained via patients undergoing cardiac surgery), with little variation between atrial and ventricular cardiomyocytes [53]. A laminin/fibronectin optimization for differentiating hPSC cardiac progenitor cells to CM has been shown for numerous hESC lines [54, 231].

2.1.7 Characterization of hPSC-derived CM

Thus far, the majority of hESC- and iPS cell-derived CM express immature contractions, ion channels, electrical propagation, proliferative ability, and physical characteristics (**Figure 7, Table 1**). The differences between early and late stage stem cell-derived CMs and adult CMs is reviewed by both Robertson [232], and Yang [233].

The most apparent differences between in vitro stem cell-derived CM and adult CMs are their morphology. Human stem cell-derived CMs are mononucleated, and exhibit a small circular shape with unorganized sarcomeres [156, 234]. In comparison, adult CMs are large rectangular (roughly 150µm in length) multinucleated cells with longer sarcomere structures that aligned parallel to the long access of the cell. As adult CMs hypertrophy, they often become multinucleated with substantially more mitochondria. [53] One of the most critical functional structures often lacking in the stem cell-derived CMs is the T-tubule [235]. This section of the plasma membrane, attached to the sarcoplasmic reticulum, plays a critical role in calcium transients, which may be why hPSC CMs have displayed non-uniform calcium transients across the cells. This lack of maturity is subsequently detrimental to excitation-contraction coupling in the CM-to-CM signaling [236].

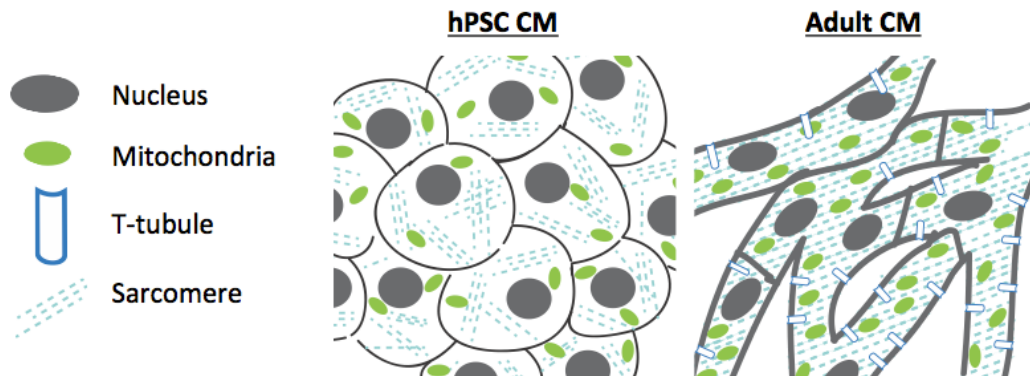


Figure 7: Human hPSC CM and adult CM phenotypic comparison.

Current hPSC CM lack key structural [237]., as well as functional properties present in mature adult cardiomyocytes. RMP: resting membrane potential. SR: sarcoplasmic reticulum.

Table 5 Differences between hPSC CM and adult CM.

Cell Shape	Circular	Long and Branching
Sarcomeres	~ 1.5 μ m Crossing	~ 2 μ m Aligned
Structure	Mononucleated No T-tubules	Multinucleated T-tubules
Mitochondria	Sporadic organization Low density	aligned with myofibrils 15-20% of cell volume
Action Potential [238]	RMP ~ -35mV to -70mV	RMP -85mV
Calcium Handling	Trans-sarcolemma Ca ²⁺ influx	Mature SR
Contractile Force	nN range/cell	μ N range/cell

2.1.8 hPSC CM Maturation

A variety of mechanisms are being explored for hPSCM maturation. Among the strategies employed include substrate stiffness, time in culture, and chemical induction [239]. In order to further mature stem cell-derived CMs, researchers are beginning to engineer stem cell microenvironments that incorporate mechanical and electrical signals, cell-to-cell contacts with previously optimized soluble growth factors [225, 240].

The use of substrate stiffness to guide differentiation began with a ground-breaking paper by Engler et al. [241]. In previous work the majority of cell culture was conducted in plastic petri dishes (10,000 kPa), while tissues in the body range from the brain (1kPa), to muscle (10kPa), and bone (100kPa). The Engler group found changing the substrate stiffness under mesenchymal stem cells to match desired tissue guided the cells towards that lineage. However, the effects of substrate stiffness on hPSC CM differentiation are producing contradictory results. Increasing the substrate stiffness (around 100kPa or > 1000kPa as apposed to the 10kPa stiffness found in muscle) has been shown to increase contractile force [242], and promote cardiac differentiation [243, 244]. Improvements to cell morphology are observed when matrix patterning is combined with softer substrate [245].

One of the most successful, yet inefficient, methods for hPSC CM maturation involves increasing the time of derived cell culture. Studies up to 100 [246], 110 [247], 231 [248], and 360 [249]. Although these studies reported improvements in electrophysiology, the cost of reagents and time are a burden for clinical application. Fortunately, the addition of cardiac developmental thyroid hormone (T3) has produced promising results (mostly

through increases or initial expression in cardiac specific markers) in as little as 30 days after differentiation [250-252].

2.1.9 Purification of hPSC-derived CM

Undifferentiated pluripotent stem cells can form teratomas if injected directly into host tissue. Even with improved methods directing tissue-specific differentiation, it will likely be necessary to purify the final hPSC-CM cell populations prior to implantation. Initially, cardiomyocytes were purified using Percoll density gradient centrifugation method. However, this method only produced a 5 to 10 fold increase in CM purity [253, 254]. CM can also be manually selected for physical characteristics like beating cells or genetically modified fluorescent structures; however, manual selection is not only susceptible to human error, but inefficient for large-scale operation. Fluorescent-activated cell sorting (FACS) has also been used as a purification method [255], but CMs exhibit only very low rates of cell survival using these methods that reduce cell cluster into single cells. In addition to fluorescent staining with genetic modification or antibodies, mitochondrial dye tetramethylrhodamine methyl ester perchlorate (TMRM) has been used [256]. TMRM exploits the fact that most immature CM do not have the high enough mitochondrial density for the dye to be detected. Another purification technique involves genetically modify the cells with an antibiotic resistance attached to the promoter of a cardiac, or cardiac progenitor cell, specific gene (i.e. Nkx2.5 [257], MYH6 [258], and ISL1 [259]). Some of these methods have been shown to achieve up to 99% CM purity [260] and are amenable to scaled-up using bioreactors [261]. However, genetically modifying cells for transplantation need extensive characterization to ensure mitigate the risks of off target effects and residual transfection agents [262].

2.1.10 Goals

While many researchers have worked towards developing and optimizing new cardiomyocyte differentiation protocols, it is unclear which method is the most efficient in time, cost, and cell purity. In this chapter, we compared two established methods for deriving cardiomyocytes from human pluripotent stem cells. The first protocol utilized the growth factors BMP4, activin A, bFGF, DKK1, and VEGF and was developed by the Keller lab [153], then later optimized with matrix signaling by the McCloskey lab [54]. The second, developed by the Palecek lab [156], used small molecule inhibitors CHIR and IWP-2.

2.2 Methods

2.2.1 Cell Source

The McCloskey lab has optimized serum-free hESC differentiation protocols for generating high purities (>70%) of CM from H7, H9 and HES2 hESC [155]. Because the study will use an iPS cell line (DF19-9-7T, WiCell) that has been transfected with puromycin resistance under α -MHC promoter (courtesy of Dr. Chiamvimonvat, UC Davis). Moreover, because our cardiac tissue substitutes will need very high cell numbers (2.5×10^6 cells per patch), we compared the efficiency, purity, and cost of generating CM using our laboratory's current protocol – based on the protocol from Gordon Keller's group

[153] - that can generate up to 70% hESC H7-derived CM [155] against another published protocol, from the Kamp and Palecek groups, that is based on modulating Wnt/beta-catenin signaling that claims to generate up to 80-98% CM [156].

2.2.2 Maintenance of human ESC cells

HES2 hESCs (fig. 2a)[263] were plated on a high density of mouse embryonic fibroblasts (MEFs). H9 hESCs were plated on Matrigel™ (Corning) coated dishes. Both cell lines were fed high glucose DMEM (gibco) supplemented with 5 ng/ml basic fibroblast growth factor (bFGF, Sigma). Once the cell colonies reached 80% confluence, cultures were passed by washing with PBS, then dissociating the colonies with Dispase for 5 min at 37°C. Cell colonies were scored with a 5mL pipette to produce small cell clusters that enhanced cell viability. Cell clusters were gently washed off the plate and into a conical vial. Cell clusters were spun at 200g for 5 min., gently resuspended to maintain uniform cell clusters, then split on MEFs at a 1:3 ratio. Media formulations remained constant and were replaced daily.

2.2.3 Maintenance of human iPS cells

DF 19-9-7T hiPSCs (WiCell) were plated on hESC qualified Matrigel™ (Corning) coated dishes, and fed mTeSR (STEMCELL Technologies, Inc.) media daily. Cultures were passed once reaching 80% confluence by washing with PBS, then dissociating the colonies for 3 min. at 37°C with Accutase (Innovative Cell Technologies). Once edges of the colonies began to lift off the dish, the culture was gently washed off the dish using mTeSR before being spun in a conical vial at 200g for 5 minutes. Cell pellets were gently resuspended in fresh mTeSR, while avoiding clusters dissociating into single cells, and were replated onto hESC-Qualified Matrigel™ that had been diluted per manufacturer specifications. Split ratios varied between 1:3 and 1:16. hiPSCs mTeSR media was replaced daily.

2.2.4 Fabrication of Honeycomb Microwells

The protocol followed was previously developed and optimized by Sa et al., 2009 [264]. A pattern of staggered wells, drawn in drafting software (AutoDesk), was printed onto biaxially prestressed PS sheets (Grafix Inc.) using a laser-jet printer (Hewlett Packard 2600N). The printed PS sheets were heated to 155°C for 5 min. Poly(dimethylsiloxane) (PDMS; Millipore Sigma) mixed using a standard protocol was poured over the mold and cured on a hot plate at 65°C overnight. Previously optimized conditions dictated the use of microwells with a final diameter of 400 µM. PDMS microwells were cut to fit within the standard 24 well tissue culture dish, and functionalized using an O₂ plasma machine (Harrick Plasma). Media was gently washed over the treated microwells surface to dislodge any air bubbles from the PDMS surface.

2.2.5 Growth Factor CM Induction Protocol

hESCs were manually picked off the MEFs and transferred to a conical vial, gently dissociated to small cell clusters (3 to 5 cells), spun down at 200g for 5 min., and resuspended in 2ml Roswell Park Memorial Institute (RPMI; Invitrogen) medium supplemented with 2% B27 (Invitrogen). EBs were then formed by transferring the hESCs

into the PDMS microwells at a seeding density of 400,000 cells/well. Gently tapping the dish on the bench ensured the cells reached the bottom of the wells. After 24 hours, uniform EBs formed in the microwells were gently moved into an ultra-low adhesion 60mm dish (Corning) with a 5mL pipette. EBs were cultured in RPMI/B27 with 25µg/mL bFGF, 50µg/mL BMP4, and 10µg/mL Activin A. After four days in culture, EBs were manually dissociated using a 1000µL pipette, and replated onto a 60mm dish coated in a 70% fibronectin (BD Bioscience), 30% laminin (BD Bioscience) blend with 5mM ROCK inhibitor (Y27632). Over the next four days, cells were cultured in RPMI/B27 with 10µg/mL DKK1, and 10µg/mL VEGF. After day 8 of differentiation, cells were fed every other day with RPMI/B27, 10µg/mL VEGF and 25µg/mL bFGF. After day 14, cells were maintained on RPMP/B27 fed every other day (**Figure 8, Table 6**).

2.2.6 Inhibitor CM Induction Protocol

The human iPS cells were first prepared by dissociating (Accutase), and plated at high density (5×10^5 cells per well of hESC-Qualified Matrigel™-coated 12-well dish) with 5 µM ROCK inhibitor (Y27632), and fed with 2mL of mTeSR™1 Medium (STEMCELL Technologies, Inc.) every day for four days (considered days -4 to -1) (**Fig. 3, Table 6**). On day 0, 12 µM of CHIR99021 (GSK-3 inhibitor) was plated with 2mL of RPMI/B27 Medium without insulin. After 24 hours, medium was replaced with 2mL of RPMI/B27mL without insulin and without GSK-3 inhibitor. On day 3, medium was made by combining 1mL of media from the dish, 1mL of fresh RPMI/B27 without insulin, and 5 mM IWP-2 (Wnt inhibitor). On day 5 of differentiation, cells were fed with RPMI/B27 without insulin. Starting on day 7, cells were fed with RPMI/B27 every other day. Cell contraction could be observed around day 12 (**Figure 8, Table 7**).

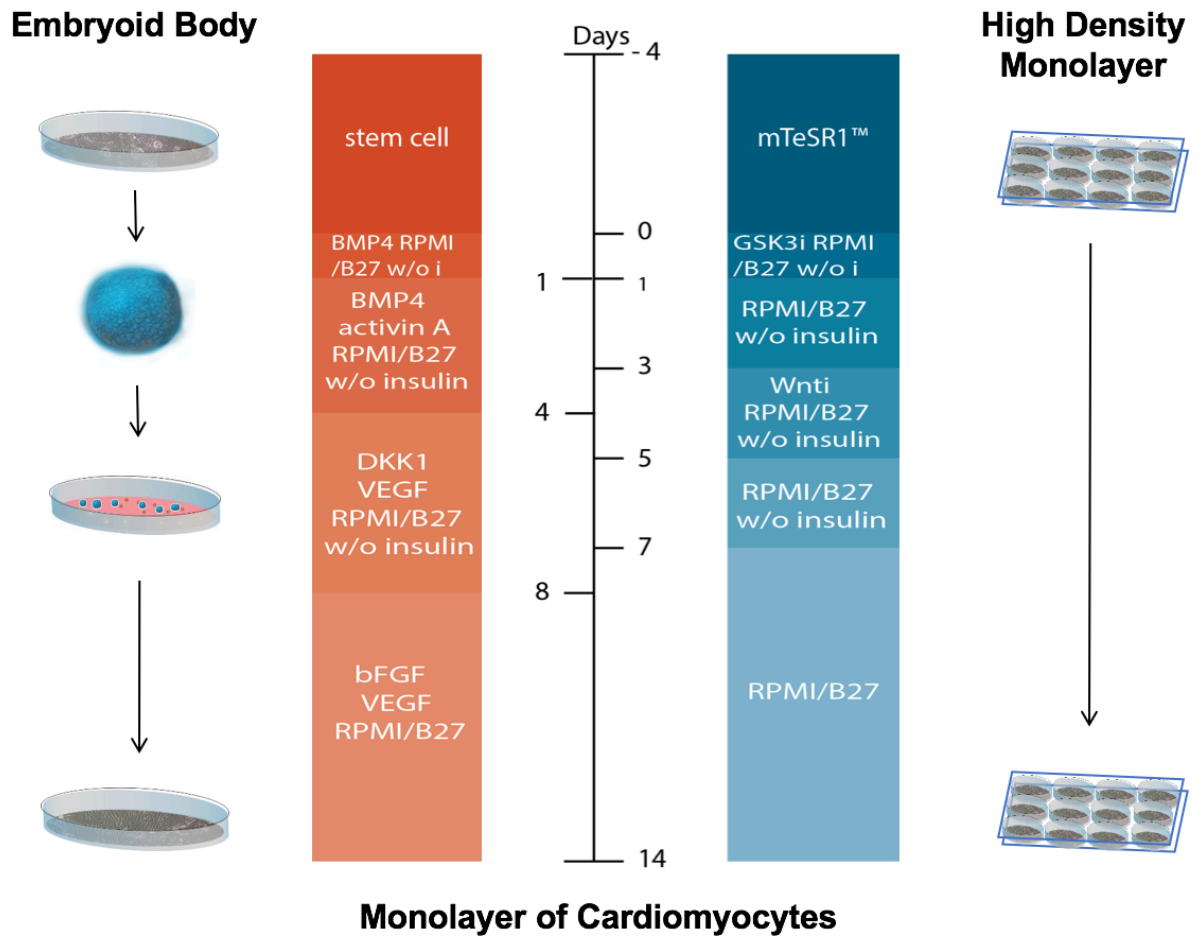


Figure 8: Embryoid body and high density monolayer human pluripotent stem cell derived cardiomyocyte differentiation protocol.

2.2.7 Purification of CM

After 21 days, the hPS-derived CMs were purified with 3.6ug/ml puromycin treatment. After for 24 hours, the cells were fed with RPMI/B27 every three days. Purified hPSC CMs were harvested between day 24 and 40.

2.2.8 Immunostaining for Fluorescence Microscopy

Cytoskeletal organization was observed under fluorescence microscopy. Between days 24 and 30, hiPSC CMs were by dissociating with .25% trypsin, and using 80% RPMI (Life Technologies), 20% FBS (Life Technologies) herein referred to as RPMI20, with 5µM Y27632 (Tocris). Cells were spun at 200g for 5 min., resuspended at a concentration of 100,000 cells/mL in RPMI20, and replating onto .1% gelatin. After two days in culture the cells were washed with PBS, fixed via 4% (vol./vol.) paraformaldehyde for 15 min. at room temperature., then washed a second time with PBS. The staining solution consisted of 5% (wt./vol) nonfat dry milk (Mountain Maid), .4% (vol./vol.) Triton X-100 and PBS, and primary antibody. Cells were incubated in the staining solution for one hour at room

temperature before undergoing three PBS washes. Secondary antibodies were added using the same base staining solution, and incubated over the cells for 20 min. at room temp. Dapi stain was added for five minutes at a concentration of 5mg/mL. Images were taken using a TE2000U Nikon microscope.

Table 6: Growth factor protocol for deriving HES2 hESC CMs

Day 0	1	2	3	4	5	6	7	8	9	10	11	12	13	14
EB					Monolayer									
Microwell	Suspension				70% fibronectin 30% laminin									
RPMI/B27 BMP4 (1µg/mL)	RPMI/B27 bFGF (25µg/mL) BMP4 (50µg/mL) Activin A (10µg/mL)				RPMI/B27 DKK1 (10µg/mL) VEGF (10µg/mL)				RPMI/B27 VEGF (10µg/mL) bFGF (25µg/mL)					

Table 7: Inhibitor protocol for deriving H9 hESC CMs and hiPSC CMs

Day -4	-3	-2	-1	0	1	2	3	4	5	6	7	8	9	10	11	12	13	14
Monolayer																		
hESC-qualified Matrigel																		
mTeSR™			RPMI/B27 w/o CHIR (12µM)	RPMI/B27 w/o insulin		1/2 media change RPMI/B27 w/o IWP-2i (5mM)		RPMI/B27										

2.2.9 Immunostaining for Fluorescence Activated Cell Sorting

Cell purities were determined using fluorescence activated cell sorting. Cells were washed with PBS, then dissociated by incubating with .25% trypsin for 5 min. at 37°C. Single cell suspension was achieved by washing each dish cell culture media. Cultures were centrifuged at 200g for 5 min., then resuspended in 1% (vol./vol.) formaldehyde and incubated for 20 min. at room temperature. Fixed cells were then centrifuged at 200g for 5 min., then fixed further in 90% (vol./vol.) cold methanol and incubated at 4°C for 15 min. Cells were counted using a hemocytometer and split to .5 million cells per. conical tube with 2mL of flow buffer containing 1% Bovine Serum Albumin in PBS. Cells were washed twice by being centrifuged at 200g for 5 min., aspirating the supernatant, then resuspending in flow buffer. Cells were stained in 100µL of flow buffer with primary antibody for one hour at room temperature, or at 4°C overnight. Cells were washed with 2mL of flow buffer, then resuspended in 100µL of flow buffer with secondary antibody and incubated for 30 min. at room temperature. Stained cells were then washed and resuspended in 2mL of flow buffer, and transferred to a round bottom flow tube. Sorting was run on BD LSR II flow cytometer.

2.2.10 Beating Cardiomyocytes

Beat rates were reported as the number of contractions per minute, or beats per minute (bpm) were determined by visually (either live or from recorded videos) counting the number of contractions each cells had over a 60 second interval using a bright field microscopy.

2.2.11 Calcium Transience

Fluo-4 AM Calcium Assay Kit (Invitrogen) was prepared per manufacturer instructions and incubated for 30 min and at room temperature for 30 min. Measurements were taken using laser scanning confocal microscopy performed on a Nikon digital eclipse C1 confocal microscope using a 20x air objective for imaging. 494nm excitation laser beams and 515 band pass emission filters were used.

2.3 Results

2.3.1 hPSC characterization

Both hESC, as well as hiPSCs were cultured at least 2 weeks before differentiating into the cardiac lineage. Both the hESC HES2 cell line and the hiPSC cell line cell types were previously transfected puromycin resistant gene under the α -myosin heavy chain gene, later be used to purify the hPSC CMs. The HES2 hESC line doubled roughly every 48 hours while the hiPSCs proliferated at a much faster rate, doubling every 24 hours. Characterization of the iPSC line is demonstrated in (**Figure 9**).

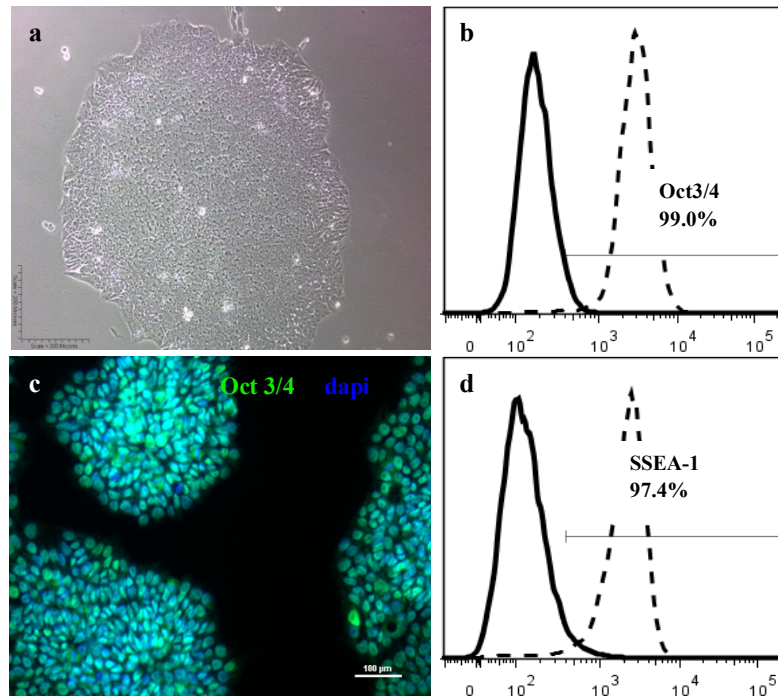


Figure 9: Characterization of the puromycin resistant α -myosin heavy chain DF19-9-7T hiPSCs.

a.) A bright field image of the stem cell colony taken at a 20x magnification (scale bar 200 μ m). Flow cytometry data collected on the LSR representing the percentage of cells positive for pluripotency markers b.) Oct3/4 and d.) SSEA-1. c.) A fluorescent microscopy image of the hiPSC colonies stained with DAPI and Oct3/4 (scale bar 100 μ m).

2.3.2 Stem Cell Derived Cardiomyocyte Differentiation Protocol Comparison

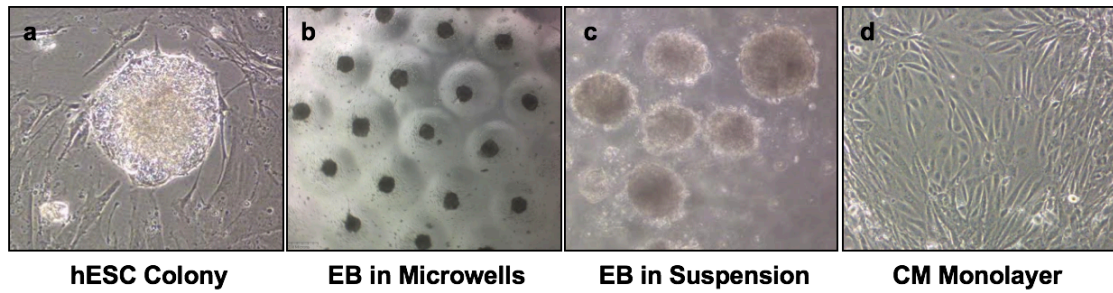
Two of the leading cardiomyocyte differentiation techniques to date include exploiting the biphasic Wnt/beta catenin pathway that drives cells towards the cardiac lineage. The first protocol uses previously optimized conditions for growth factors α -Actinin, BMP4, bFGF, DKK1 and VEGF. [155] The second protocol uses small molecules to block the inhibitory pathways that prevent cardiomyocyte development [217]. Both the growth factor, and inhibition protocols were tested for cell morphology (**Figure 10**), and cardiac-specific marker expression after puromycin purification (Table 7). The costs of differentiation, as well as time to complete the differentiation process was relatively similar between the two methods, approximately \$500 per experimental batch.

Although the size of each differentiation batch was matched to the original protocol, starting cell numbers have been set to six million cells to allow for comparison. It is also worth mentioning that in the growth factor protocol, the HES2 hESCs used required culture on a mouse fibroblast feeder layer. Separating the stem cells before induction was done manually with a glass pipette while hiPSC were cultured on Matrigel™ and did not require manual selection prior to differentiation. The ending cell number was obtained using a hemocytometer after 25 days. The percentage of cells expression cardiac-specific marker, cTnI was obtained using fluorescence activated cell sorting.

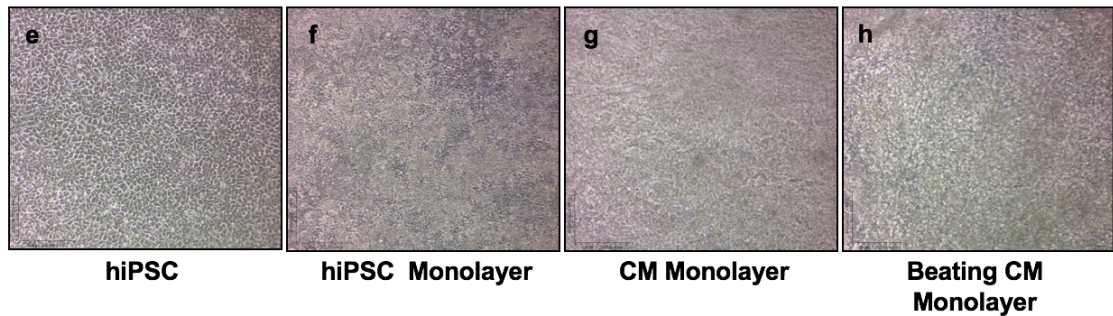
2.3.3 hiPSC CM Characterization

Using the more efficient inhibitor differentiation protocol, we analyzed cytoskeletal arrangement, the beating rates, and calcium transience of replated cardiomyocytes. Cells showed the z-band formation, but not organization (**Figure 12**), present in primary adult cardiomyocytes. The contraction rates of the cardiomyocytes suggest that although the beating rates of individual cardiomyocytes varies widely (between 30 and 130 bpm) (**Figure 12**), the majority of spontaneously contracting cells are beating around 70 or 110 bpm. No difference was observed between single cells, or clusters with five or more cells together. Furthermore, cells loaded with Fluo-4 dye show the Ca transients propagating from the center of the cell, rather than the waves seen in adult cardiomyocytes (not shown). This observation is consistent across the literature. [232]

Embryoid Body Method



High Density Monolayer Method

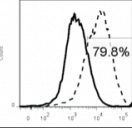
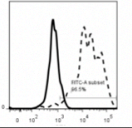
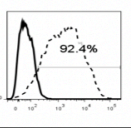


	Human Pluripotent Stem Cells	Spontaneous Differentiation	Directing to CM Cell Fate	Immature CM Proliferation
Day	-4	0	4	14

Figure 10: Morphological differences between the BMP4 Activin A hESC CMs, and the Wnt Inhibited hiPSC CMs.

a – d.) Show the stages of BMP4 Activin A differentiation. a.) This begins with a hESC colony being cultured on MEFs. b.) The cells are then lifted and transferred into micro-wells for EB formation. c.) After 24 hours, the EBs are transferred into suspension. d.) On day 5 of differentiation they are replated on a 70% laminin, 30% fibronectin substrate mixture, and cultured to day 14. e. – f.) Show the drastically different cell morphologies of the Wnt Inhibition method. e.) hiPSCs are plated onto Matrigel coated-dishes at a high density, where they undergo similar f.) spontaneous differentiation, followed by a g.) small molecule inhibition method. h.) Spontaneous beating occurs between days 12 and 17.

Table 8: Comparison of growth factor and inhibitor hPSC CM differentiation efficiency

	hESC (HES2) EB	hESC (H9) Monolayer	hiPSC Monolayer
<u>Starting Cell Number</u>	6 million cells	6 million cells (no MEFs)	6 million cells (no MEFs)
<u>Time</u>	~ 25 days	~ 25 days	~ 25 days
<u>Ending cell number</u>	~ 4 million cells	~ 20 million cells	~ 24 million cells
<u>Cardiac Troponin Expression</u>	 67.4% ± 17.5%	 79.8% ± 21.8 %	 88.7% ± 5.2%
<u>Puromycin Resistance?</u>	Yes	No	Yes
<u>Expected Cardiomyocyte Yield</u>	2.7 million CM	15.9 million CM	21.3 million CM
<u>Established EC protocol</u>	No	Yes	No

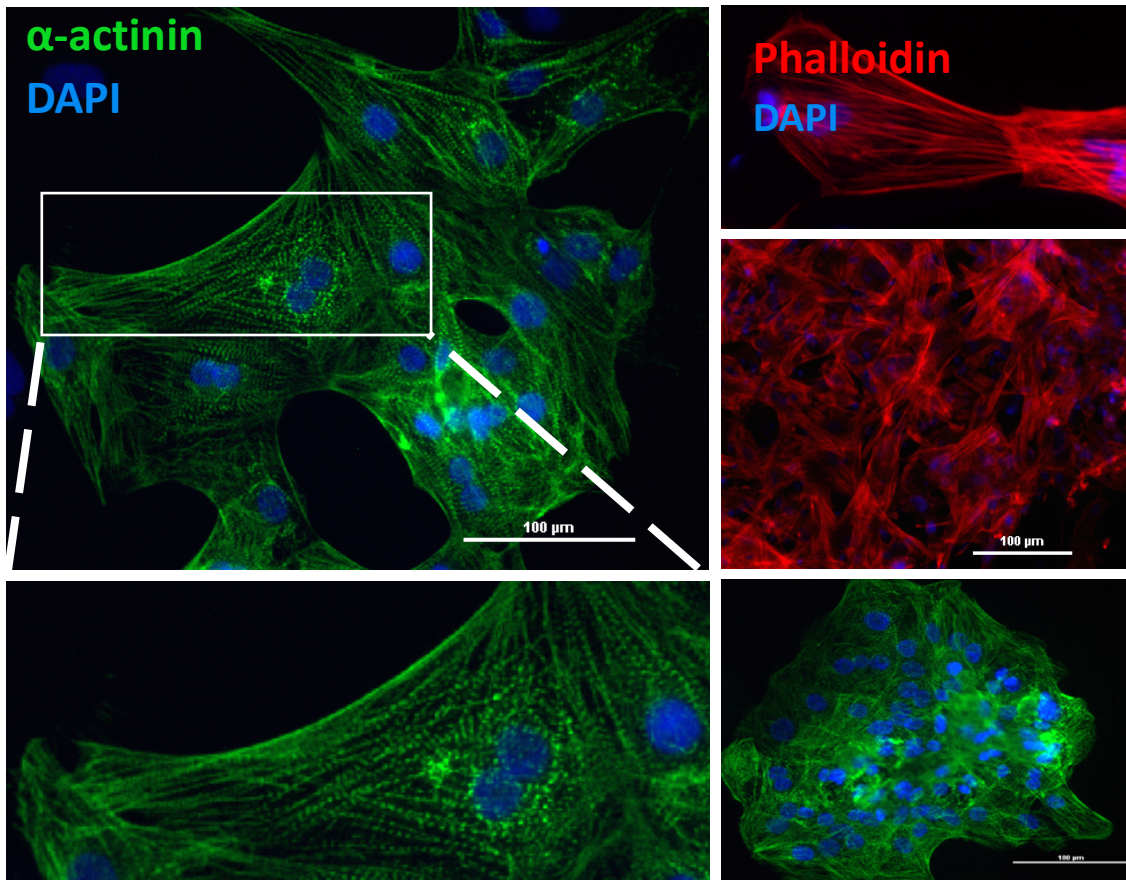


Figure 11: Replated hiPSC CMs differentiated with the inhibition method.

hiPSC CMs stained with α -actinin show the striations of z-bands in the myofibrils. Although replating hiPSC CMs causes a high rate of cell death, cytoskeletal components of the surviving replated cardiomyocytes remain relatively similar to the hiPSC CMs in the original dish.

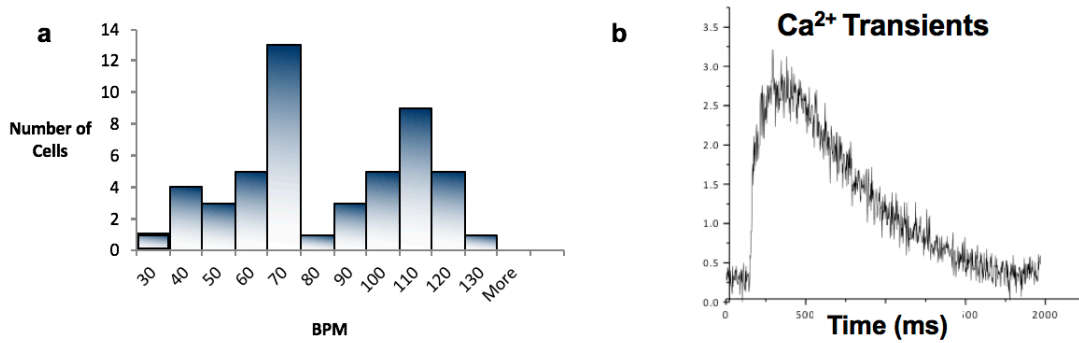


Figure 12: hiPSC CM contraction and calcium transience profile.

a.) BPM of the replated hiPSC CM were obtained by counting how many times a cell beat over 1 minute (n=50 cells). b.) Representative calcium transience graph.

2.3.4 Protocol Reproducibility

All three protocols were completed twice by two researchers. The inhibitor protocol produced a higher expression of cTnT for h9 and hiPSCs, 79.8% and 88.7% respectively, compared to the growth factor protocol, 67.4%. However, the H9 cell line did not have puromycin resistance under the α -myosin heavy chain gene. Without purification these cells had the highest standard deviation (21.8%). Therefore, the most reliable protocol was inhibitor protocol with the hiPSCs.

2.4 Discussion & Conclusion

This work reports a comparison of the two most widely cited hPSC CM differentiation protocols, using growth factors and inhibitors affecting the Wnt/beta catenin pathway, as well as, two different cell lines with very different proliferation rates. We report the efficiencies of each protocol, as well as, cardiomyocyte purity. We found the Wnt inhibition method not only produced over six times as many cardiomyocytes compared to the growth factor protocol, but the differentiation process also exhibited a greater rate of success. Sarcomere organization and calcium transience more closely matched previously reported hPSC CM immature characteristics, rather than those of adult cardiomyocytes. Interestingly, most beating rates of the hiPSC CMs included rates typical for both immature fetal cardiomyocytes (120 – 160 bpm) [265] and mature cardiomyocytes (60 – 100 bpm), with fewer (2%) falling below that physiological threshold.

Chapter 3: Fabrication of Cardiac Muscle Tissue: A Methods Comparison

3.1 Introduction

3.1.1 Cell Patterning Functional Consequence

The field of tissue engineering has inspired researchers to re-imagine, design, and construct microphysiological systems in vitro as organ models of development and disease. While drug development has historically relied on 2D cell culture and animal models, consequences of the low predictive power of these experiments on clinical outcomes is burdening the industry, with only one in ten drugs making the leap from phase I clinical trial to FDA approval [266]. What's more, the therapeutic potential of pharmaceuticals is limited in tissues that have little-to-no regenerative capabilities. As engineered 3D tissues and organ-on-a-chip technologies are better able to recapitulate human physiology with stem cells, their promise as effective tools in drug development and/or replacement tissue therapy approaches reality [267, 268]. However, the research and clinical relevance of engineered tissues is only valuable to the extent to which the cellular microenvironment and architecture mimics in vivo tissue organization. The relationship between cell structure and function has been explored extensively in systems that include the visual cortex [269], granulosa cells [270], mammary cells [271], stem cells [272], and cardiomyocytes [273]. In addition to contributing to organ-specific functions, cell structure also plays a critical role in cell growth, death, migration, and gene expression [274], as well as cell-to-cell communication and electrical propagation [115]. In a 3D context, orchestrating the cell patterning can also include more complex behaviors like angiogenesis or vasculogenesis [275], gut undulation [276], and neural circuits [277]. Recent work has expanded the field by creating techniques to pattern multiple cell types in both 2D and 3D co-culture systems [278].

3.1.2 Guiding Cell Shape in Vitro

As now well-established, cell shape and cell-to-cell connections have proven to be an indispensable component of engineered tissue. Creative solutions to guide this behavior have emerged in fabrication techniques, biomaterials, and culture platforms. In the 2D space, patterning through micro contact printing (or stamping) generates varying configurations of extracellular matrix proteins for single cells to adhere and mirror its geometry [245, 279, 280]. Longer micropatterned strips or channels can guide cell alignment and migration [281, 282]. Photolithography followed by protein patterning with serum manipulation [283] can additionally enable protease release by a serum-activated cell type. For example, the first cell degrades bovine serum albumen, the cell repellant surface, thereby prepping the space for the second cell type [284].

3.1.3 2D Surface Topography

Surface topography is another widely exploited feature for guiding cell shape. Various topological patterns can be achieved through soft lithography [285], electro-spun materials [286], as well as, using more cost effective pre-shrunk polystyrene sheets [116]. While all techniques have successfully shown to generate aligned and elongated cells, each has

distinct limitations. Photolithography requires an expensive cleaning room, patterning using serum manipulation may change with batch-to-batch variability, generating aligned fibers requires an electrospinner, and using pre-stressed polystyrene sheets to generate pattern within the material is limited to simple wells [287-289] and wrinkles [115, 290].

3.1.4 3D Technology for Cell Patterning

While 2D cell shape manipulation requires adapting the cell-to-surface interface, 3D tissue systems necessitate anchoring points through stacking monolayer cell sheets [291], natural or synthetic biomaterials [292], micro tissues surrounding posts [293, 294], or strips within microfluidic devices [59]. However, many of the deficiencies of 2D techniques remain for 3D culture as well: bioprinting [295], photolithography [296], and electrospinning [297]. What's more, many of these platforms are further enhanced by added mechanical or electrical stimuli [128]. While these supplemental set-ups improve the culture's fidelity to the dynamic cardiac environment, they also add cost and complexity. There are also several novel and creative techniques for engineering aligned cardiac tissue, what's missing is a comparison between protocols.

3.1.5 Goals

Here, we explore and compare two distinct cost-effective methods for alignment of muscle cells. These include 2D shrink-induced topographical wrinkles on PDMS [116] and polyacrylamide [157]. We also compare three distinct methods for forming 3D tissue. These are formed using either a hanging drop, sacrificial gelatin template [158], or 3D printed ring mold [159].

3.2 Methods

3.2.1 Maintenance of human iPS cells

DF 19-9-7T hiPSCs (WiCell) were plated on hESC-Qualified Matrigel™-coated dishes (Corning), and fed mTeSR Medium (STEMCELL Technologies, Inc.) daily. Cultures were passed at 80% confluence by dissociating the colonies for 3 min. with Accutase (Innovative Cell Technologies). Cell pellets were resuspended in mTeSR and replated onto hESC-Qualified Matrigel™ diluted per manufacturer specifications.

3.2.2 Cardiomyocyte differentiation

Cardiomyocytes were generated using a published protocol [156]. Briefly, human iPS cells were prepared by dissociating with Accutase (STEM CELL Technologies, Inc), plated at high density (5×10^5 cells per well in hESC-Qualified Matrigel™-coated 12-well dish), treated with 5 μ M ROCK inhibitor (Y27632; Selleckchem), and fed 2mL of mTeSR™1 Medium every day for four days (called days -4 to -1). On day 0, cells were replated in RPMI (Thermo Fisher Scientific) supplemented with 2mL of 2% B27 without insulin (Thermo Fisher Scientific) and 12 μ M of GSK-3B inhibitor (CHIR99021; Tocris). After 24 hours, medium was replaced with 2mL of this RPMI/B27 medium without insulin, but without the GSK-3 inhibitor. On day 3, conditioned medium was made and used by combining 1mL of media from the dish, 1mL of fresh RPMI/B27 without insulin, and 5 mM Wnt inhibitor (IWP-2; Tocris). On day 5 of differentiation, cells were fed with fresh

RPMI/B27 without insulin. Starting on day 7, cells were fed with RPMI/B27 with insulin every other day. After 21 days, the hPS-derived CMs were purified with 3.6ug/ml puromycin (Thermo Fisher Scientific) treatment for 24 hours, and fed with RPMI/B27 every three days. Purified hPSC CMs were harvested between day 24 and 40.

3.2.3 Fabricating Economical Wrinkles for hiPSC CM Alignment

A full description of this method, characterization of the wrinkle chips, along with its previous studies aligning rat neonatal CM and ESC-derived ECs can be found in the following publications [115, 116], and summarized in Fig. 1. Gold was sputter coated (SEM Sputter Coater; Polaron) at 0.09 torr, 30mA for two minutes to produce a coating of 30nm on pre-stained polystyrene (PS) sheets (ShinkyDinks, Inc.). In an oven set to 150 - 160°C, the Au-coated pre-stained polystyrene was exposed to temperatures above glass transition (T_g for polystyrene $\sim 105^\circ\text{C}$), causing the polystyrene to shrink and contract. Constriction at opposite ends caused buckling of the surface layer generating the wrinkled topography (Figure 13). The wrinkled chip serves as a master mold for generating subsequent PDMS cell culture microchips. A 10:1 ratio of polydimethylsiloxane (PDMS) and curing agent (Sylgard 184 Silicon Elastomer Kit, Dow Corning) is de-gassed, poured on the metal mold, and set to cure at 60°C overnight. Chips are sterilized by UV ozone cleaning, and then coated with 50 $\mu\text{g}/\text{mL}$ laminin (BD Bioscience) and seeded with 500,000 human iPSC CM/cm².

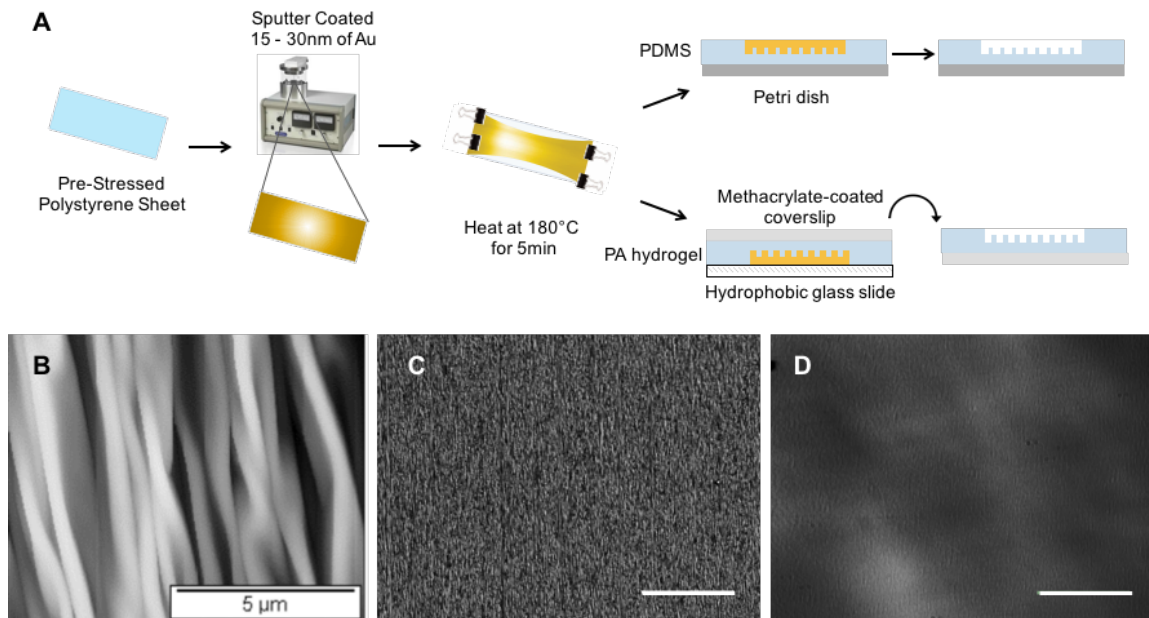


Figure 13: Wrinkle chip fabrication

A. Flowchart showing the process for producing PDMS and PA chips to promote topography-guided cell alignment. B. SEM image of the mold shows uni-directional channels. Darkfield microscopy shows the wrinkle pattern transfer into C. PDMS, and D. PA.

3.2.4 “Wrinkled” Topography on Polyacrylamide

Polyacrylamide fabrication methods are based on a protocol detailed by Tse et al [298]. A 10 kPa gel was created by degassing a solution of 25% (vol./vol.) of 40% (wt./vol.) stock acrylamide (Millipore Sigma), and 5% (vol./vol.) of 2% (wt./vol.) stock bis-acrylamide (Millipore Sigma) solution. 1% (vol./vol.) of 10% (wt./vol.) stock ammonium persulfate (APS; Millipore Sigma) initiated polymerization, while .1% (vol./vol.) N,N,N,N-tetramethyl ethlenediamine (TEMED; Millipore Sigma) accelerated the reaction at room temp. A coverslip was then activated by being submerged in a solution of .5% (vol./vol.) 3-(Trimethoxysilyl) propyl methacrylate (Millipore Sigma) and 3% (vol./vol.) of a stock 10% glacial acetic acid (Millipore Sigma) in EtOH for two hours. 25 μ L of the solution was pipetted onto the surface of a Rain-X treated wrinkle chip, and flattened using an activated glass coverslip. After 15 min. of incubation at room temp., the polyacrylamide-bound coverslip was removed from the wrinkle chip (**Fig. 13D**), submerged in PBS, and stored at 4°C. A 50 μ g/mL laminin solution was covalently bound to the surface of the polyacrylamide using 10mg/mL of the heterobifunctional linker, N-Sufosuccinimidyl-6-(‘4-Azido-2’-Nitrophenylamino)-Hexanoate (sulfo-SANPAH; CovaChem). hiPSC CM were plated onto the hydrogels at a concentration of 500,000 cells/cm².

3.2.5 Hanging Tissue Disk

Cell disks with one million hPSC CMs were formed by passing hPSC CMs were passed and suspended in RPMI with 20% FBS (Thermo Fisher Scientific). Using a multichannel pipette, 50 μ L of solution was dropped onto the lid of a 150mm cell culture dish. The lid was inverted and incubated in 37°C and 5% CO₂ for 12 hours to allow the cells to aggregate at the bottom of the droplet.

3.2.6 Microfluidic Device Fabrication

The protocol for muscle strip assembly was first developed by Neal et al. [59]. A 10:1 ratio of PDMS and curing agent was de-gassed, poured on a 3D printed mold with 0.5mm music wire inserted through the mold holes. After solidifying at 60°C for two hours, the music wire and PDMS were removed from the mold. To make individual devices, a razor blade can be used to cut through the PDMS between the hollowed-out channels. Three cavities were carved and discarded using a 6mm biopsy punch. After inserting two music wires with a diameter of 0.5mm through the device cavities, the PDMS was plasma treated and bonded to a glass coverslip.

3.2.7 Sacrificial Hydrogel-based Cardiac Tissue

Tissue forms were first created by allowing a solution of 10% wt/vol gelatin (Millipore Sigma), 1% vol/vol NaOH (Millipore Sigma), and 300 NHI units of thrombin (Millipore Sigma) form around the 0.5mm diameter wire (Fig. 2A), or 6mm o-rings. After a 45min at 4°C, the solution solidified and the wire or o-ring were removed. A solution of 5mg/mL fibrinogen (Millipore Sigma), 10% vol/vol Matrigel™, 20 million cells/mL, and RPMI with 20% FBS (Thermo Fisher Scientific) plus 1mg/mL aminocaproic acid (Millipore Sigma) was pipetted through the cavity from the displaced wire or o-ring. The microfluidic device was cultured at 37°C to allow the gelled thrombin to further diffuse into the cell-fibrinogen solution to form a fibrin-muscle strip. After 30 minutes at 37°C, the gelatin

solution was replaced with cell media treated with of 5mM ROCK inhibitor (Tocris) (Figure 14). Media was replaced daily from the center well.

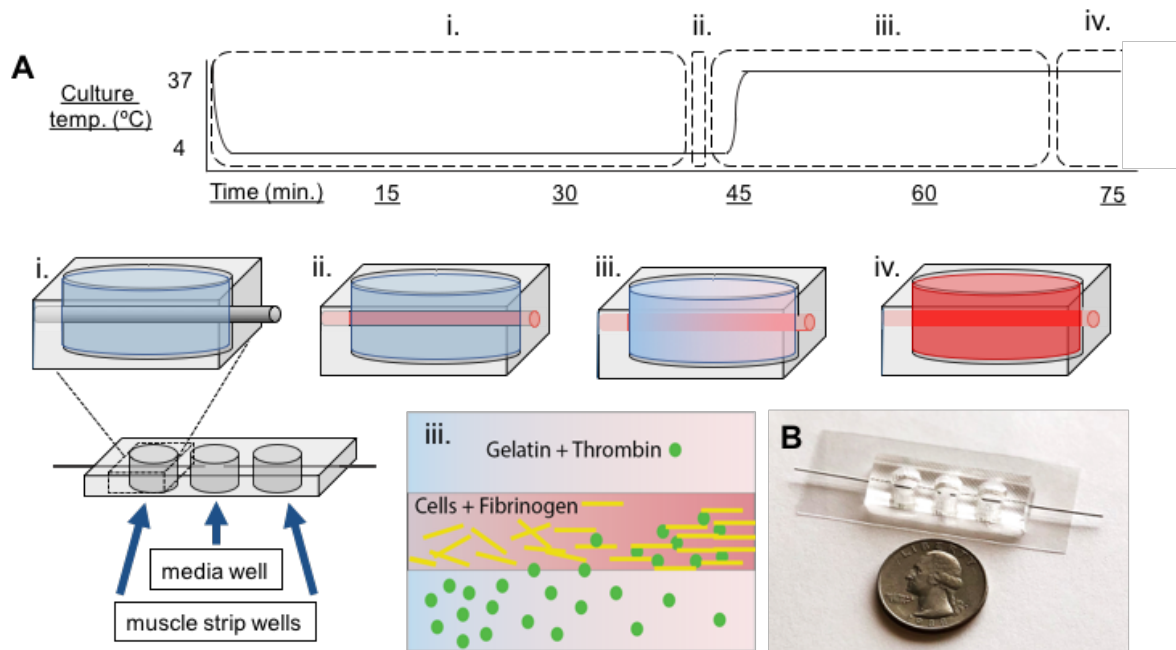


Figure 14: Muscle strip microfluidic device

Muscle strip formation starts with pipetting a solution of gelatin and thrombin over music wire in the outer wells of the microfluidic device (Ai). Once the gel solidifies, the music wire is replaced with a cell-fibrinogen solution (Aii). After placing the device into an incubator, the gelatin returns to its liquid state, allowing the thrombin to diffuse into the cell-fibrinogen solution to form fibrin (Aiii). After approximately 25 min. the liquid gelatin is replaced with media (Aiv). B. A photograph of the microfluidic device next to a quarter for scale.

3.2.8 3D Printed Ring Mold

Molds were fabricated by our collaborator, Prof. Rashid Bashir at the University of Illinois, Urbana-Champaign. Using a stereolithographic 3D printer (SLA 250/50, 3D Systems), an ultraviolet laser (325 nm) selectively polymerizes a photosensitive hydrogel resin comprised of 20% wt/vol poly (ethylene glycol) diacrylate (PEGDA;1000g/mol) with 0.5% wt/vol biocompatible photoinitiator Irgacure 2959 [299] (Figure 15). Once completed, the molds were transported in PBS, and sterilized by soaking in 70% ethanol for 30min and rinsed with sterile PBS for an additional 45 min.

3.2.9 3D Ring-based Cardiac Tissue

300 μ L of a 1% NaOH (Millipore Sigma), 200 NHI units of thrombin (Millipore Sigma), 30% vol/vol Matrigel™ (Corning), 5mg/mL fibrinogen (Millipore Sigma), and cell culture

media with 1mg/mL aminocaproic acid (Millipore Sigma) and 10 million cells/mL was pipetted into the cavity of the ring mold. After a 20min. at 37°C, the cell culture media containing 1mg/mL aminocaproic acid (Millipore Sigma) was gently added to the 35mm petri dish. Media was replaced every other day.

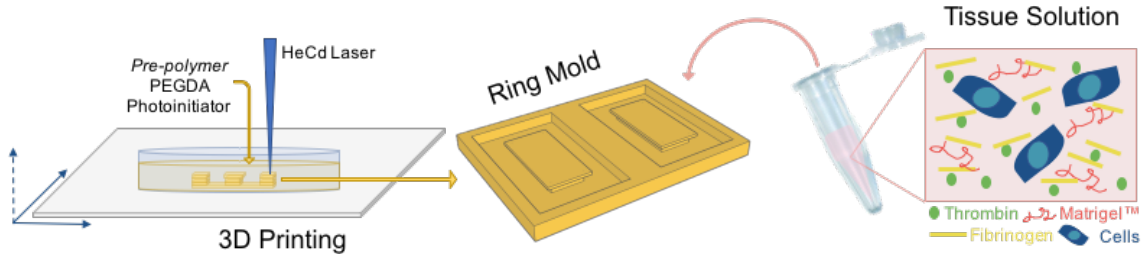


Figure 15: Muscle ring formation

Schematic representation of steriolithographic 3D printing of ring mold. The total mold is 15mm by 20mm and supports two muscle rings. A solution of thrombin, fibrinogen, Matrigel, and cells is added to the ring mold.

3.2.10 3D Quantifying Cell Alignment and Elongation

Images were processed via custom MATLAB (MathWorks, Inc) scripts. Actin labeled images were analyzed by transforming them into 8-bit images. A 2-by-2 median filtering (medfilt2) operation was carried out to ensure proper identification of edges. Image threshold values were calculated (graythresh) and used when turning the images into binary. The binary images were then dilated and eroded separately, and their difference became the cell membrane or actin skeleton. The binary outline was then analyzed for its properties (regionprops) from which the orientation was extracted. All orientations were normalized to reflect a 0° – 90° measurement and plotted on a 0° – 90° polar histogram (polarhistogram). The bin size was set to 6° when plotted. The mean angle was also calculated and displayed in text. Binary actin lengths had to be within 10 -200 pixels in size to be counted. We assumed anything smaller than 10 were greater than 200 pixels were image artifacts. The percentage of aligned cells was defined as any cell between ± 30° from the direction of the wrinkle, or ± 30° from degree average on the flat surface. The elongation factor (EF) was calculated using a ratio of each cell's maximal diameter (D_{max}), length, to the minimal diameter (D_{min}), width.

$$EF = D_{max}/D_{min}.$$

3.2.11 Immunostaining for Fluorescence Microscopy

Cytoskeletal organization was observed under fluorescence microscopy. 24 hours after cell seeding, hiPSC CMs were washed with PBS, fixed via 4% (vol./vol.) paraformaldehyde for 15 min. at room temperature. The staining solution consisted of 5% (wt./vol) nonfat dry milk, 0.4% (vol./vol.) Triton X-100 and PBS, and phalloidin (brand). Cells were incubated

in the staining solution for one hour at room temperature before undergoing three PBS washes. Dapi stain. Images were taken using a Nikon microscope.

3.2.12 3D Statistical Analysis

All comparisons for statistical significance were conducted using a student's t-test using the mean degree of alignment or EF, and the standard deviation for N= 100 cells.

3.3 Results

3.3.1 Seeding stem cell-derived CMs onto wrinkles

We first set out to optimize all previously established protocols with hiPSC CMs. While each had been used with ECs, C2C12s, and primary rat CMs, only the PDMS wrinkle condition had been previously tested on hiPSC CMs. For the wrinkled topographies, we found that replanting cells onto the patterns at earlier stages in the differentiation protocol either yielded cells that quickly became too confluent and lost alignment (spontaneous differentiation phase / day -4) or failed to adhere to the surface (mesoderm differentiation phase / day 0, and cardiac specification / day 3). Once the cells were differentiated into cardiomyocytes (> day 12), we found while plating the cells at a seeding concentration of 20,000 cells/cm² did align the cells, over five days the rate of proliferation was too high and the cells lost the elongated morphology (Figure 16). Thus, future experiments were performed by replanting hiPSC CMs onto wrinkles between days 25 and 35 at a seeding density of 50,000 cells/cm². What's more, both gelatin and laminin were tested at varying concentrations for cell adhesion. We found 50 µg/mL of laminin to be optimal for hPSC CMs adhering to both flat, as well as wrinkled surfaces.

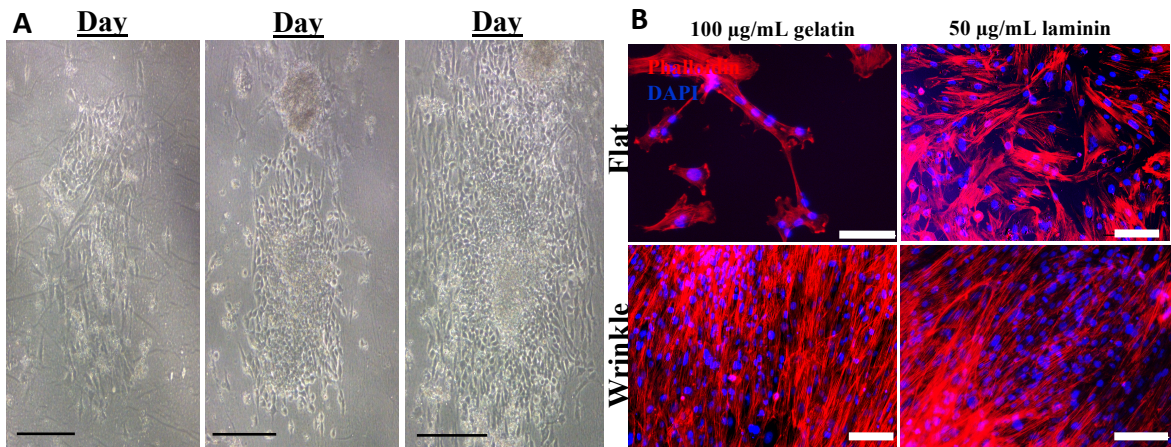


Figure 16: Early seeding of hPSC CM lose alignment on wrinkles over time

A. Images were collected at a consistent location in the dish over four days. hPSC CM plated on wrinkles at day 11 lost alignment over time as the cell concentration increased. (scale bar 100µm) B. hPSC CMs plated onto PA flat and wrinkled surfaces at day 24 preferentially adhered to the surfaces coated with laminin.

3.3.2 Alignment of cardiomyocytes on topography

hiPSC CMs were plated on PDMS or poly-acrylamide that had either a flat or shrink-induced wrinkled topography and 50 μ g/mL of laminin. The method for pattern-transfer was specifically showed distinct alignment on both the PDMS and PA wrinkled topographies, ~60% and 80% respectively, when compared to cells on their flat counterparts, ~50% and ~30% respectively (Figure 17). Elongation factors for both the PDMS and PA conditions differed significantly between the flat and wrinkled conditions. Images were collected after 24 hours due to the instability of the culture conditions.

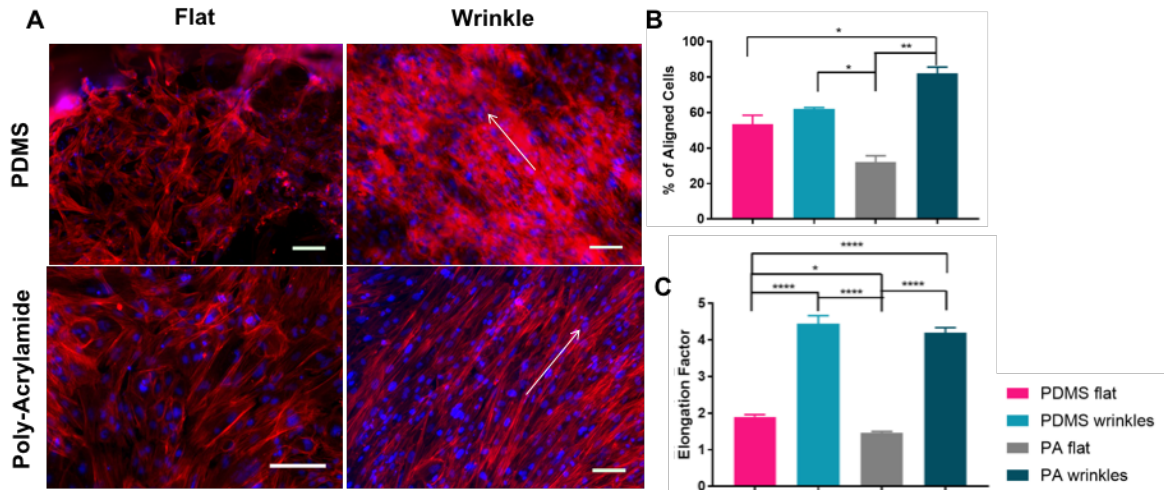


Figure 17: Topographical signals align human iPSC CM

A. Fluorescent images of hiPSC CM stained with phalloidin (red) and dapi (blue) on flat or wrinkled PDMS or PA (scale bar 100 μ m). White arrows indicate the underlying direction of the wrinkles. B. The percentage of aligned hiPSC CM on all four substrate conditions. C. The elongation factor of all four conditions.

3.3.3 Tissue engineering protocol rational

Next, we set out to compare costs of 3D cardiac construction methods. When reviewing current protocols, we focused on maintain cost efficiency and repeatability, as well as promoting cell alignment. We first layered the nanowrinkle-aligned cardiac sheets. However, the thermoresponsive polymer, poly(N-isopropylacrylamide), PNIPAM, only increased the instability of the culture conditions. Another method involved decellularizing a porcine matrix, then seeding with hiPSC CMs. However, the hiPSC CMs had difficulty adhering evenly throughout the porcine ECM as well. We then moved onto test a sacrificial hydrogel protocol originally developed by the Asada lab at MIT using C2C12 mouse myoblast cells [59]. Here, we were successfully able to culture hiPSC CM muscle strips for up to two weeks. Because the muscle strip was difficult to transfer out of the

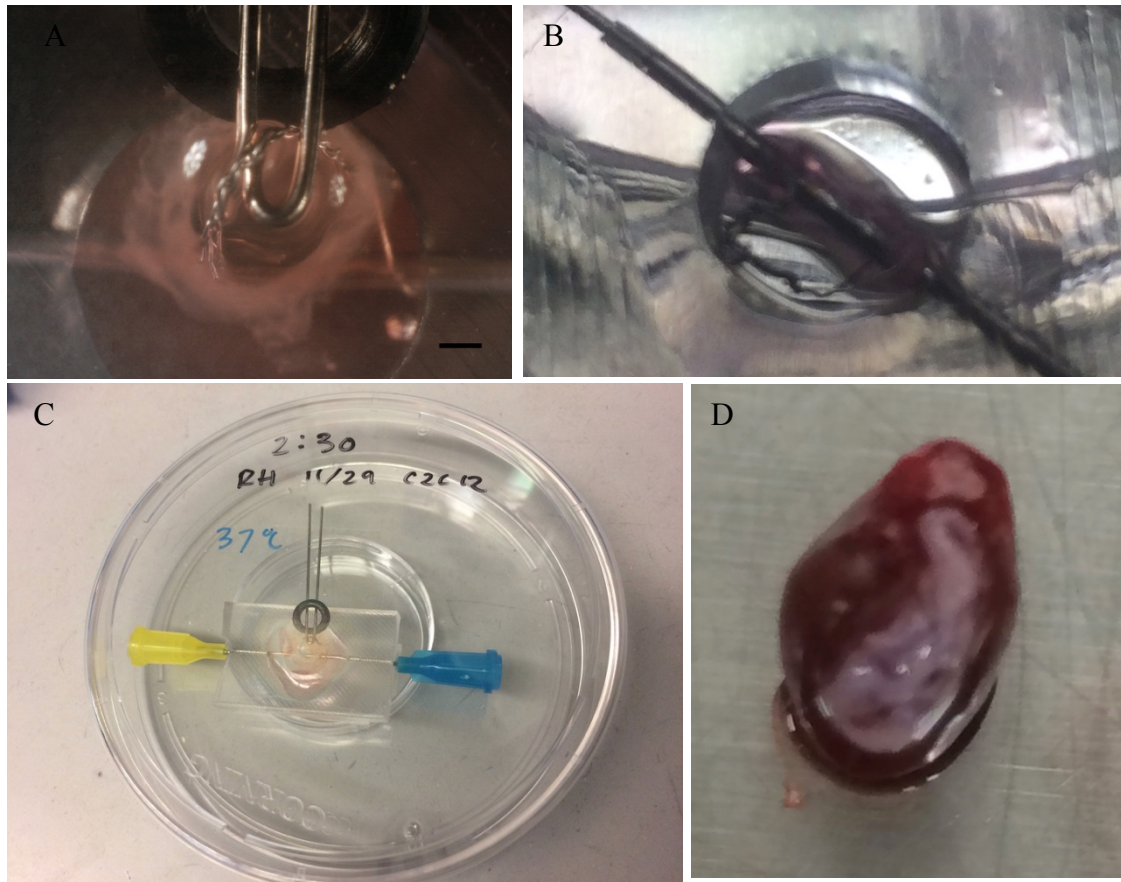


Figure 18: Sacrificial hydrogels generate ring muscle tissue

A. A rubber o-ring was placed into a gelatin and thrombin solution. After the gelatin solidified, the o-ring was removed and C2C12 mouse myoblast cells were seeded into the cavity with fibrinogen. Once the culture was placed into an incubator, the fibrinogen and thrombin crosslinked to form a fibrin gel. Media was then added to the top of the tissue (scale bar 1mm). B. Once the media was removed, two sides of the ring came together, but did not adhere into one larger tissue. C. The device could be placed within a 100cm² cell culture dish and maintained by replacing media daily. D. With a 6mm o-ring, the size of the tissue was roughly proportional to patch onto a mouse heart.

3.3.4 Alignment of cardiomyocytes in 3D culture

Once we established the optimal protocols for building a 3D tissue under tension, we then evaluated their ability to align and elongate the hiPSC CM. While all three protocols successfully produced compact hiPSC CM tissue, the percentage of aligned cells in the conditions anchored under tension was not significantly more than cells cultured in a disk. While the muscle strip did encourage cells into a more elongated morphology, elongation factor of 2.0 with approximately 55% of the cells elongated, it was still far below that of the 2D wrinkles at 4.5 elongation and 80% cell alignment (Figure 19). However, given that all of the 3D cultures consistently stable up to two weeks and developed highly contractile 3D tissue, the muscle strip protocol is considered the superior protocol.

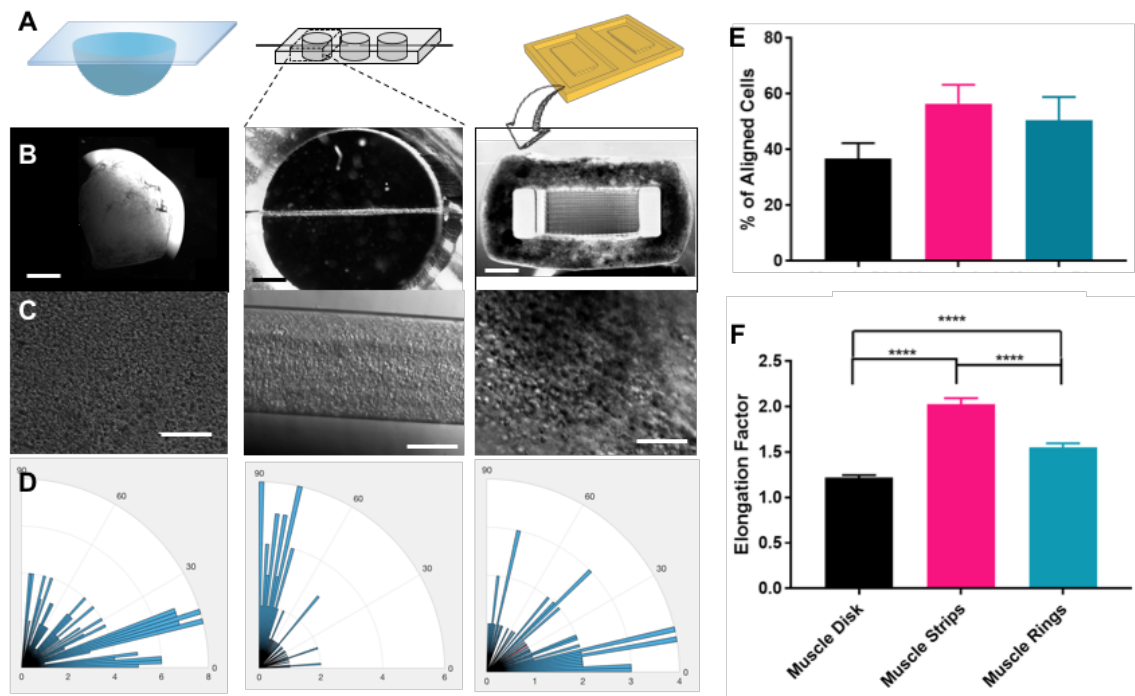


Figure 19: Tension on 3D tissue provides minimal alignment to hiPSC CM

A. Schematic representations of the hanging muscle disk, muscle strip microfluidic device, and muscle ring mold (order consistent in A-D) Stitched images taken at B. 2x (scale bar 1000 μm) and C. 10x (scale bar 100 μm) using bright field microscopy. D. Rose plots showing the orientation of each outline. E. the % of aligned hiPSC CMs in all three conditions. F. The elongation factor of the cells in all three conditions.

3.4 Discussion & Conclusion

Unlike the mouse ESC-derived ECs and neonatal mouse cardiomyocytes (NMCM) [115, 116], our lab found the hiPSC CMs plated on PDMS wrinkles early in differentiation and cultured over time did not align significantly more than the those on the flat substrate. We then tried a shrink-based wrinkle method using PE films [287] with similar average wrinkle depths (159 – 310nm). Although both studies used equivalent seeding densities, more cells/ cm^2 initially adhered to the PDMS wrinkles compared with the PE films. The decrease in CM alignment seen in the PDMS wrinkles compared to PE films may have been due to cues of cell-to-cell connections outcompeting those from the underlying topography. This finding is consistent when compared to the proliferative ECs and NMCM [115, 116]. We found that plating hPSC-derived CMs at lower concentrations increased cell death and prohibited a monolayer of adherent cells (data not shown). Interestingly, the elongation factor of the hPSC-derived CMs seeded on PDMS wrinkles after differentiation (5:1) was much closer to that of adult CMs (7:1 [245]), when compared to those on the flat substrate (2:1).

Cells on the softer PA wrinkles did align significantly more than those on the flat PA. Substrate stiffness has been found to regulate cell differentiation, proliferation, and migration [265]. For cardiomyocytes specifically, 10kPa has been shown to increase contraction force and myofibril maturity [242, 300-302]. While substrate stiffness alone has not shown to preferentially align the actin architecture, it has been shown to influence myotubule polymerization [303]. What's more, culturing rat neonatal cardiomyocytes at physiological stiffness increased CM maturation within seven days [304]. However, adhesion of hPSC CMs to both the wrinkled PDMS and PA substrates were unstable. Studies by McCain et al., showed that as cell-to-cell junctions increase, local focal adhesions to ECM decrease in rat ventricular cardiomyocytes [305]. I therefore, tried to enhance cell-ECM adhesion by covalently bonding ECM proteins to the substrate [106, 107, 306], but these methods required the use of chemicals toxic to cells if not washed thoroughly before cell seeding. and didn't significantly enhance cell-matrix adhesion.

Unlike the 2D cultures, guiding cell behavior in 3D provided stable conditions for tissue maintenance, with roughly 55% of the cells aligning under muscle strip and 50% alignment using ring tension. Although the strip and ring protocols were previously found to align C2C12s [59, 307], minimal alignment was seen in rat neonatal CM [75] for the muscle strip protocol. While the elongation factors remained low for the 3D tissues, this may be further improved by longer culture periods and the incorporation of cardiac fibroblasts [308, 309] and vasculature perfusion.

While the development of tissue engineering techniques for creating functional cardiac tissue has remained an in-demand area of research, cost effective protocols remain few and far between. By comparing two distinct methods for aligning hPSC CM, topography in 2D and tension in 3D, we hope to increase the accessibility of structurally-relevant engineered cardiovascular tissue.

Chapter 4: Microfluidic platform enables generation of multi-layered scaffold-free muscle with an endothelialized lumen

4.1 Introduction

4.1.1 Loss of Productivity in Pharmaceutical Discovery

Over the past fifty years the pharmaceutical industry's productivity in releasing new molecular entities (NME) has remained relatively constant, despite an annual compounding financial investment of 13.35% [310]. Scannell et al [311] excellently reviews speculations to the current challenges causing this decline, including the high expense of NMEs failing through clinical trials due problems concerning their efficacy and safety. What's more, similar trends persist at a global scale [312]. Through clinical trials, roughly 63% of the total cost for each NME occurs in Phases I-III, with pre-clinical trials accounting for 32% [313]. In fact, one study found the most accurate predictor of a pharmaceutical company's future success to be a high termination rate in the pre-clinical and Phase I clinical trials [314]. Reviews across major pharmaceutical companies attribute a NME's failure to reach commercialization primarily on lack of efficacy (approximately 30%), and safety (approximately 30%) [315]. Improving the efficacy of NME highlights the need for a more thorough understanding of the agent's exposure to the target site, binding kinetics, and expression of pharmacological activity once bound [316] prior to clinical trial.

Pre-clinical trials of NME use animal models, but the lack of efficacy and safety in Phases I – III of clinical trial suggest more research is necessary to elucidate accuracy of the human target marker. The diminishing efficacy of NME through clinical trial may provide further evidence against the animal model as predictive for human response (particularly when considering bioavailability) [317]. This is especially concerning when considering that in 2008, 7,900,000 animals were used in drug discovery from basic medical research, through R&D and medical safety testing, with upwards of 90% of those used for pre-clinical trials [318]. While their ability to provide valuable information regarding the complexities of immune system and whole-organ response [319], target dosing [320], and transport-associated drug toxicity [321] may never be paralleled in vitro, there is clearly a rising need for additional basic research tools [322].

4.1.2 Research and Development Bioassay Design

Current standards across pharmaceutical bioassay development departments most often rely on investigating drug-to-target interactions with molecular-based reporter assays that produce optical read-outs. The cell types are usually established cell lines with genetically modified overexpression of the drug's target. Compounding evidence suggests that these 2D experiments, performed in the typical polystyrene 96 or 384 well culture dish, are potentially missing critical differences in cell proliferation, as well as gene and protein expression associated with cells living in 3D multicellular environments[323]. However, the development of a robust high-throughput validation assays for the numerous tissue types relevant to disease remains a challenge throughout the industry.

4.1.3 Vascular Engineering in Drug Testing Applications

Although proposals for tissue engineered drug testing platforms include monolayers [324] or smaller micro tissues [58], researchers have yet to produce a robust perusable vascular model. Vascularizing engineered tissue remains a persistent challenge to producing more physiologically relevant in vitro models, as well as future regenerative medicine therapies [325]. The majority of drug delivery systems are distributed via the circulatory system, through the vascular walls, and into the target tissue(s). However, no in vitro platform to date is mimicking this physiology for drug-testing applications. The absence of this endothelial cell barrier could have implications on the NME's dosing for human tissue, and subsequently help explain the inconsistencies between pre-clinical and clinical trials. Further implications include using this platform to answer basic science questions.

4.1.5 Endothelial Cell Patterning

Using photo-lithography methods originally developed for the semi-conductor industry, endothelial cells (EC) can be patterned using SU-8-based scaffolds between collagen [326], over hepatic tissue [327], bridging fibrin [328], and encased within PDMS chambers [329]. An alternative approach involves casting the EC within a 3D hydrogel matrix with a single needle in collagen [330, 331], 3D printed degradable carbohydrate glass in fibrin [332], a calcium alginate ladder [333], or gelatin methacrylate [334]. A more rigid scaffold provides structural support to cell seeding, and most commonly uses biocompatible materials comprising alginate [335], silk [336], and/or decellularized extra cellular matrix [337]. While each of these provides a structure to guide endothelial cells, none of them promote the more complex emergence of microvascular networks.

4.1.4 Microvascular Engineering

The strategies for tissue-engineered microvasculature include: cell guidance on micro-fabricated devices and within hydrogels, injection through a pre-formed cavity within a hydrogel, surrounding a scaffold, and promoting spontaneous angio- and vasculo-genesis. The most promising strategy for generating microvascular networks uses microfluidic devices within hydrogels, but these do not yet allow integration with the primary tissue [338-340]. Vascularizing dense tissue in vitro has only reached fruition using an excision of primary vascular bed [341], murine artery and vein in situ tissues primary [342], or unpurified primary cells [343, 344] (thus not allowing for the use of a stem cell derived cell source). Commercializing this method would provide significant challenges with batch-to-batch variation, as well as scalability.

4.1.6 Promoting in Vitro Angiogenesis and Vasculogenesis

While all vascular engineering techniques mentioned above are patterning, molding, or seeding EC into a pre-formed structure, a contrasting approach provides the cells with an environment to promote spontaneous angio- or vasculo- genesis. Compared to the pre-formed EC patterns, the spontaneously aggregated EC networks more closely mimic the processes of vasculature in development and wound healing. Within these microfluidic devices, cell culture media runs along the adjacent side channels past a center channel containing hydrogel (usually collagen [345] or fibrin [346]) to promote anastomosis of nutrients across parallel channels. ECs are suspended in

the middle gel channel and self-assemble via vasculogenesis, and along the sides of the media chamber to invade the gel, imitating angiogenesis. As the field has progressed, additional accessory cells, i.e. pericytes and fibroblasts, aid in stabilizing the vessels over a two week period [347]. High throughput devices provide many segments of these spontaneously formed networks for larger studies [348].

4.1.7 Goals

In this chapter, a novel microfluidic device was designed and developed to facilitate the formation of an endothelialized lumen through muscle tissue. This protocol was tested for endothelial cell adhesion, perfusability, and tube uniformity. Lastly, we also tested the addition of an electrospun silk scaffold for tissue stability.

4.2 Methods

4.2.1 Device Fabrication

A plastic mold was first 3D printed with .5mm diameter holes spaced 10mm apart over a 4mm deep trough. Polydimethylsiloxane (PDMS), Sylgard® Silicone Elastomer, was made per manufacturer instructions at a 1:10 cross linker to polymer ratio. The mixed and de-gassed PDMS was then poured over a 3D-printed mold with 0.5mm music wire set through a 20G needle shaft (**Figure 20**). After solidifying at 60°C for two hours, the music wire and PDMS were removed from the mold. To make individual devices, a razor blade cut the PDMS along the hollowed out channels. The center insert was made using a 4mm and 6mm biopsy punch after removing an 8mm (diameter) hole from the center of the device. One side of the semi-circle insert was cut off before suspending the tissue-holder inside the 8mm well via a 20 gauge needle. After inserting a 25 gauge needle to the other end of the channel, devices were plasma treated and bonded to a glass coverslip. Dimensions of the 3D-printed mold and completed microfluidic device are in **Figure 21**.

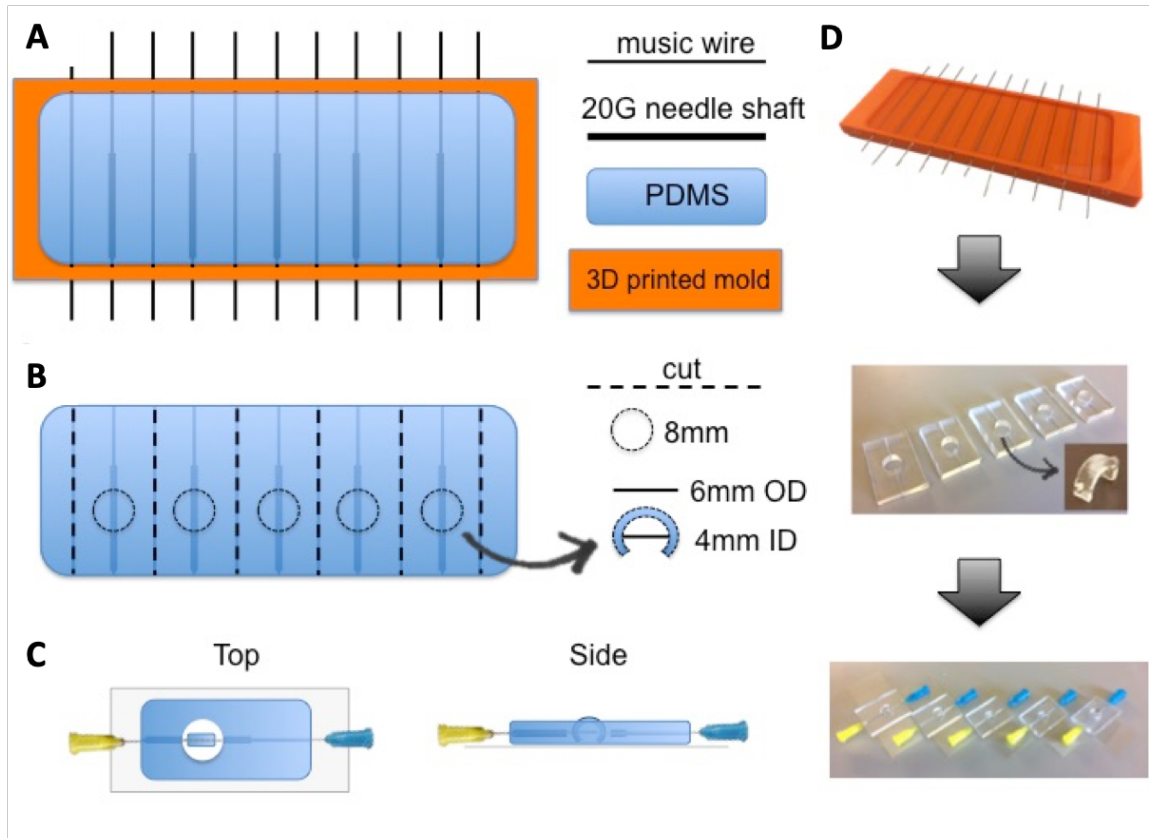


Figure 20: PDMS device fabrication

A. PDMS is poured surrounding a 20G needle shaft over music wire into a 3D-printed mold. B. Once the PDMS has cured, the music wire is removed from the mold. PDMS is then extracted, the needle shaft is removed, and each of the five devices is separated. An 8mm biopsy punch is used to form a well in each of the devices. C. An illustration of top and side views of the microfluidic device. D. Photographs of the devices in the mold, cut, then completed.

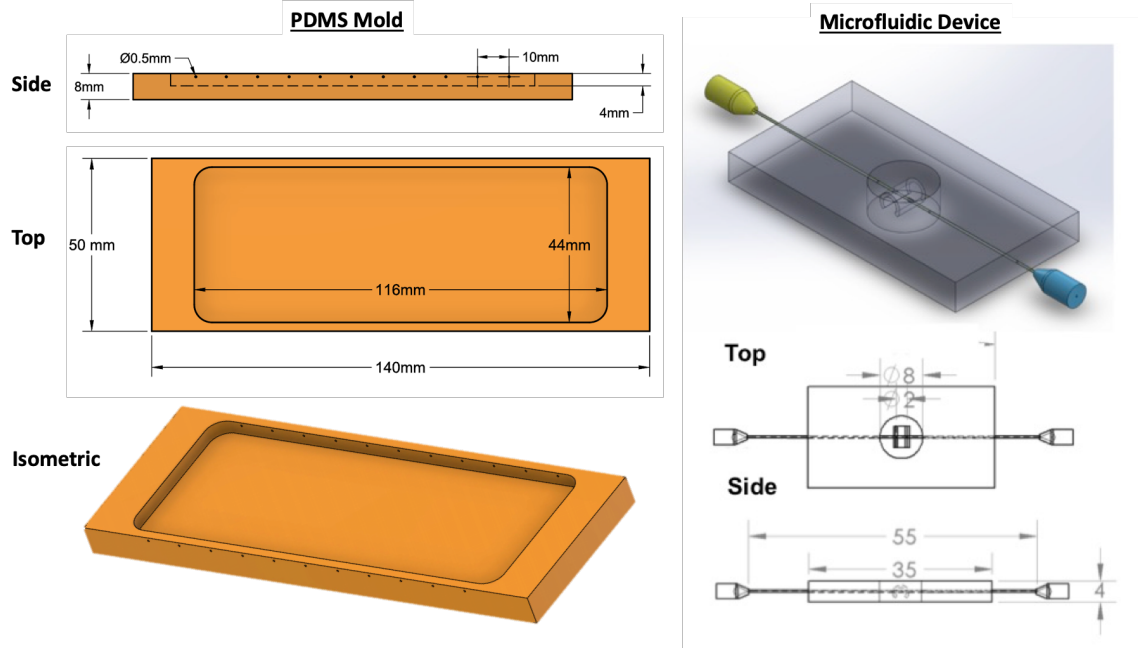


Figure 21: Dimensions for the 3D-printed mold and completed microfluidic device

3.2.1 Maintenance of human iPS cells

DF 19-9-7T hiPSCs (WiCell) were plated on hESC-Qualified Matrigel™-coated dishes (Corning), and fed mTeSR Medium (STEMCELL Technologies, Inc.) daily. Cultures were passed at 80% confluence by dissociating the colonies for 3 min. with Accutase (Innovative Cell Technologies). Cell pellets were resuspended in mTeSR and replated onto hESC-Qualified Matrigel™ diluted per manufacturer specifications.

3.2.2 Cardiomyocyte differentiation

Cardiomyocytes were generated using a published protocol [156]. Briefly, human iPS cells were prepared by dissociating with Accutase (STEM CELL Technologies, Inc), plated at high density (5×10^5 cells per well in hESC-Qualified Matrigel™-coated 12-well dish), treated with 5 μ M ROCK inhibitor (Y27632; Selleckchem), and fed 2mL of mTeSR™1 Medium every day for four days (called days -4 to -1). On day 0, cells were replated in RPMI (Thermo Fisher Scientific) supplemented with 2mL of 2% B27 without insulin (Thermo Fisher Scientific) and 12 μ M of GSK-3B inhibitor (CHIR99021; Tocris). After 24 hours, medium was replaced with 2mL of this RPMI/B27 medium without insulin, but without the GSK-3 inhibitor. On day 3, conditioned medium was made and used by combining 1mL of media from the dish, 1mL of fresh RPMI/B27 without insulin, and 5 mM Wnt inhibitor (IWP-2; Tocris). On day 5 of differentiation, cells were fed with fresh RPMI/B27 without insulin. Starting on day 7, cells were fed with RPMI/B27 with insulin every other day. After 21 days, the hPS-derived CMs were purified with 3.6 μ g/ml puromycin (Thermo Fisher Scientific) treatment for 24 hours, and fed with RPMI/B27 every three days. Purified hPSC CMs were harvested between day 24 and 40.

4.2.3 Cell line maintenance

Murine C2C12 myoblast cells were cultured on in medium containing: 88% High Glucose DMEM, 10% FBS, 1% L-glutamine, and 1% penicillin-streptomycin. C2C12s were used in experiments between passes 23 and 33. Human umbilical vein endothelial cell (HUVEC; Life Technologies) were cultured in Endothelial Cell Growth Medium (EGMTM-2 with BulletKitTM; Lonza) on fibronectin coated plates (10 $\mu\text{g}/\text{mL}$; Corning) and used in experiments between passages 3-6. Both cells were passed using .25% trypsin (Corning) at concentrations between 10,000 cells/ cm^2 to 30,000 cells/ cm^2 . In the muscle strip device, both C2C12 and HUVEC were injected at a concentration of 20×10^6 cells/mL.

4.2.3 Scaffold-free tissue construction

Although the bulk tissue can theoretically consist of many different cell types, initial progress was established using C2C12 mouse myoblast cells, or human induced stem cell derived cardiomyocytes (using a protocol developed by Lian et al. [217]). The process of tissue assembly takes two days (**Figure 22**) with “bulk tissue” and “endothelial tube” phases. Both tissue assembly protocols are modified from the sacrificial hydrogel procedure developed by Neal et al. [59]. In short, 250 μL of a solution consisting of 1% NaOH, 10% gelatin, 30 NIH units/mL thrombin, in RPMI with 20% fetal bovine serum and 1% aminocaproic acid (RPMI20+) is pipetted into the well of the microfluidic device. While the solution solidifies at 4°C, cells in the bulk tissue are suspended at a concentration of 20 million cells/mL into a solution with 10% Matrigel, 5mg/mL fibrinogen, and RPMI20+. The cell solution is then extruded through the 17G needle into the solidified gelatin solution. The microfluidic device is then placed into an incubator. As the gelatin transitions from a solid to a liquid state the thrombin diffuses into the cell solution, forming a fibrin hydrogel. The next day, this process is repeated using endothelial cells through the 20G needle. Five minutes after adding the endothelial cell solution, the inner 25G needle is removed generating a perfusable channel through the center.

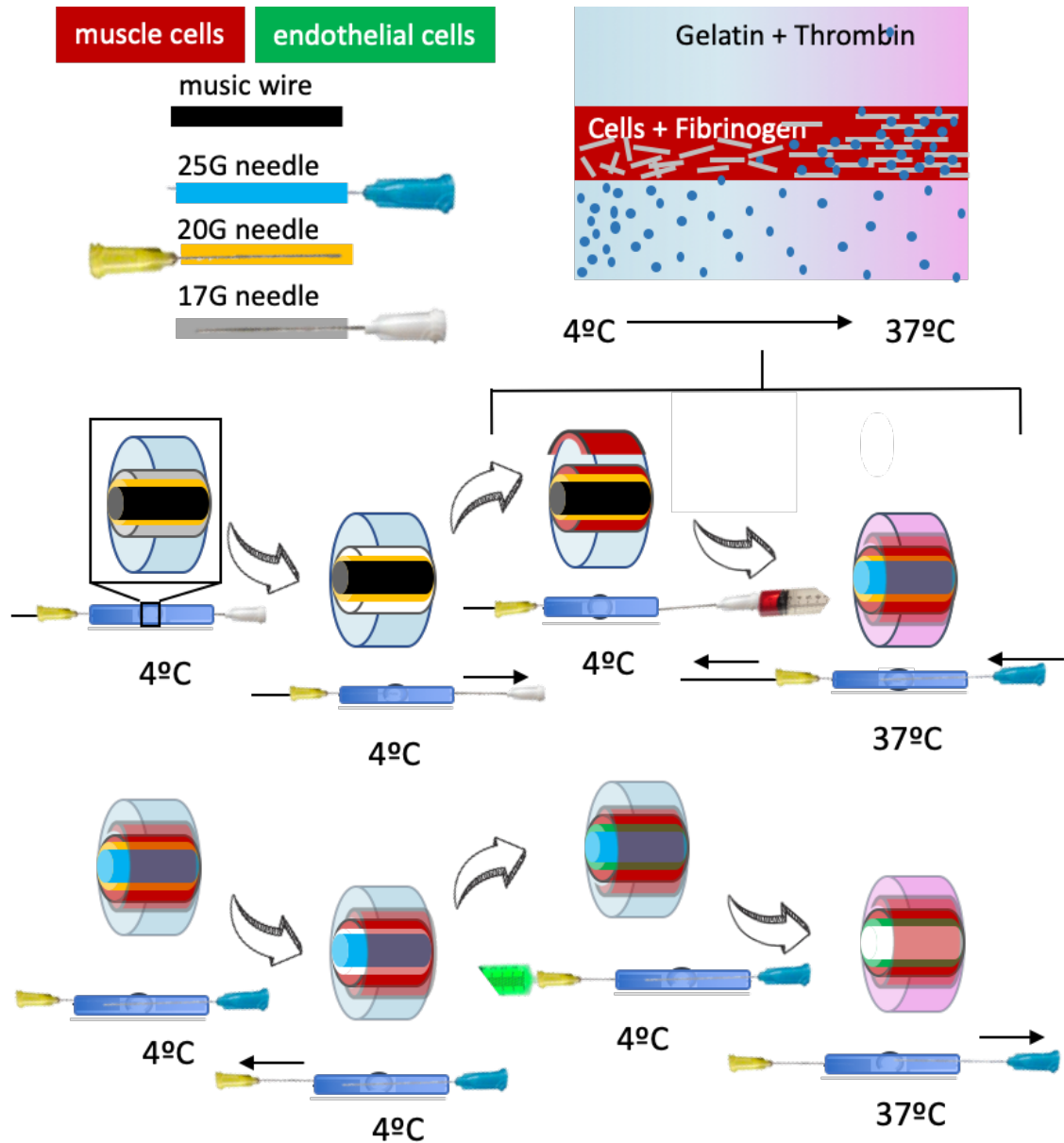


Figure 22: Endothelialized muscle tissue construction

The process for seeding the microfluidic device with cells involves sequentially removing concentric needles from the center cavity within the gelatin, and replacing the space with a solution of cells. After the gelatin-thrombin solution has solidified at 4°C, the 17G needle (grey) is removed from the center cavity of the device, and the muscle cell-fibrinogen solution (red) is added to the cavity via the 17G needle. Additional cells may be added to the top of the device to further increase the volume of muscle tissue. Once the fibrin solution has cross-linked, the 17G needle is replaced with a 25G needle (blue), and thread through the center of the 20G needle (yellow). At this point, the music wire (black) in the center of the 20G needle that prevented muscle cells from flowing through the media

channel is removed. After 24 hours in culture, media within the center well is replaced with another gelatin-thrombin solution. Once the gel solidifies at 4°C, the 20G needle is removed from the center of the cavity, and an endothelial-fibrinogen solution (green) is added through the 20G needle. After 5 min. at 37°C, the 25G needle is removed from the center of the cavity, leaving a lumen through the tissue. For extended time in culture, parafilm was wrapped around the needle hubs to prevent media from leaking.

4.2.3 Silk processing

Bombyx mori cocoons were processed following the methods published by Jin, H. [349] (illustrated in **Figure 23 A**). First, cocoons were boiled in 0.3 M sodium carbonate for 30 minutes, then rinsed with distilled water to remove the pro-inflammatory sericin protein. After boiling, the silk was dissolved in 9.3 M lithium bromide for 30 minutes and dialyzed for 48 hours. The electrospinning solution was prepared by dissolving 2.5% w/v of polyethylene oxide (PEO) into 5% silk solution, and placed on a rotator overnight.

4.2.3 Electrospinning

A syringe pump set at 5 $\mu\text{L}/\text{min}$ was connected to tubing filled with 10 mL of silk/PEO solution. A 23G dispensing tip was used and connected to a positive charge of 5 kV. The distance from ground was set to 9 cm. The silk scaffolds were submerged in 90/10 (v/v) methanol/water for sterilization and induction of β -sheet formation for 20 minutes and desiccated overnight.

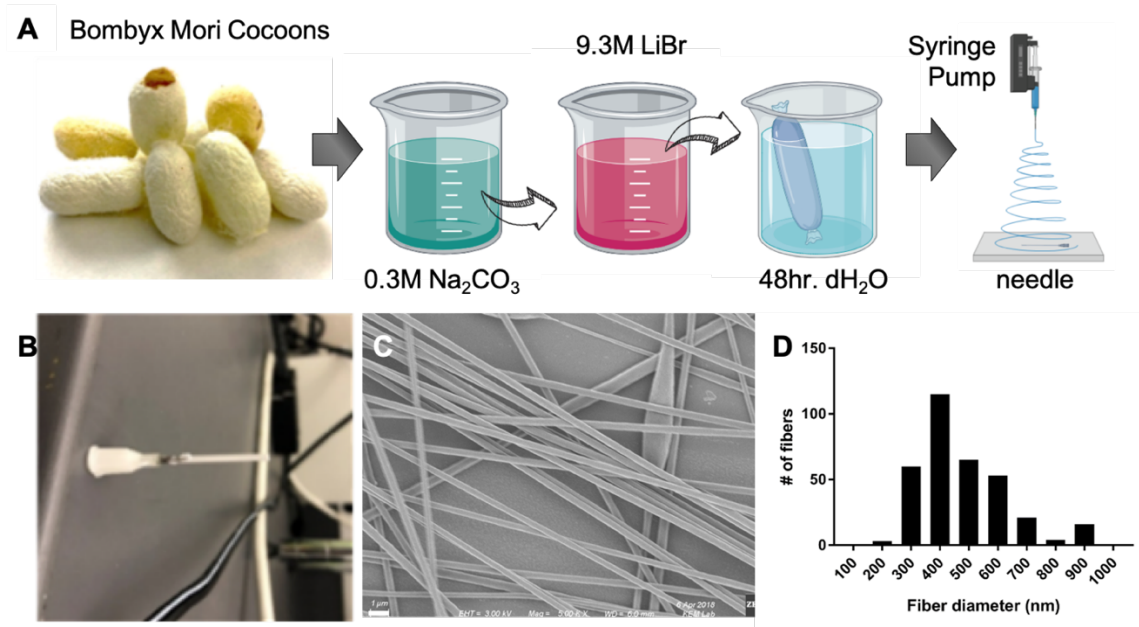


Figure 23: Silk processing and fiber diameter

A. *Bombyx mori* cocoons were processed to remove pro-inflammatory sericin proteins, dissolved, then dialyzed. A solution of 2.5% PEO and 5% silk was electro spun onto a 17G needle (B) to create elongated fibers. C. SEM imaging on a Zeiss Gemini 500 (scale bar

1 μ m) was used to measure fiber diameter (D) with ImageJ software. The average diameter of the silk fibers was 470 ± 150 nm.

4.2.4 Culture Conditions under Flow

Once the tissue in the microfluidic device had set for over one hour, the remaining needles were connected with luer locks to a Mini-pump variable flow (Fisher Scientific) peristaltic pump to test for perfusability. Flowrates were visualized using FluoSpheres™ Polystyrene Microspheres (Invitrogen) beads.

4.2.5 Cell Staining

Spatial organization of muscle and endothelial cells were visualized by staining muscle cells with CellTracker Red, or endothelial cells with Cell Tracker Green CMTPX (Invitrogen) dye. Cells were stained <24 hours prior to being injected into the device. Images were taken on either a confocal (Nikon Eclipse C1) or fluorescent (TE2000U Nikon) microscope.

4.3 Results

4.3.1 Design Criteria and Iterations

Our goal was to design a method for the fabrication and subsequent culture of engineered muscle tissue (using protocols compared in chapter 3) surrounding a perfusable endothelialized lumen. Additional design criteria included the following: cost of production, physiologically relevant size of the endothelial lumen, and a modular design. Because the design included only commercially available components and no additional technical expertise (such custom wafers or clean room photolithography), the cost could be brought down to under \$1/device without the need for large-scale manufacturing. Thus far, many engineered vascular designs to date have focused on larger arteries and veins (up to 25mm in diameter) and smaller capillaries (down to 8 μ m in diameter) (Figure 24). Focusing on a simpler design for arteriole-sized vessels (around 500 μ m) may have both the benefits of controlled cell-to-cell interactions in the larger tissues, as well as the smaller scale needed for mid-throughput studies.

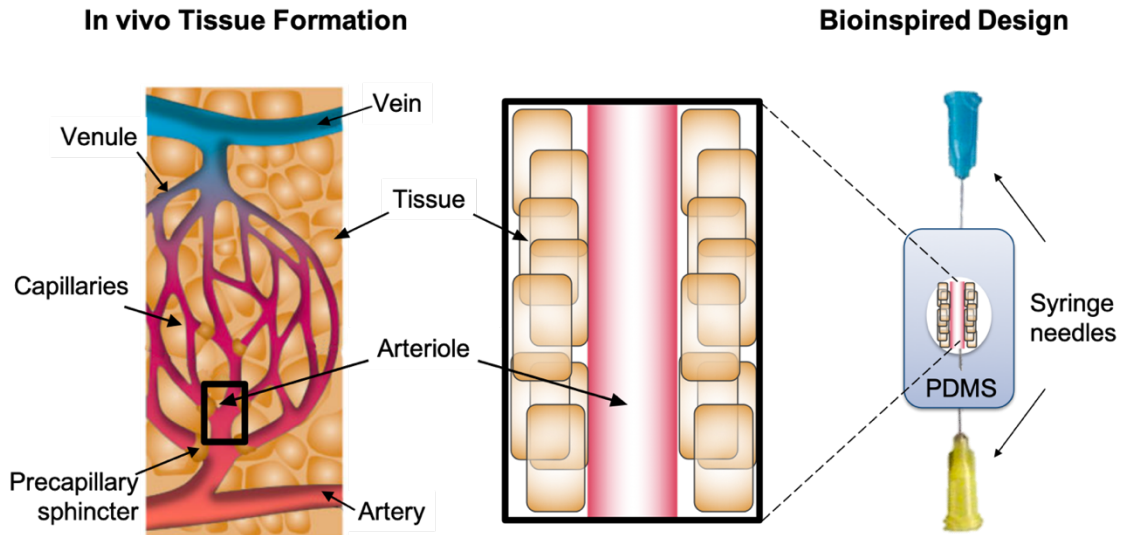


Figure 24: Biology-inspired tissue assembly device design

The biggest challenges included balancing the time of tissue curing needed for adequate structural support and preventing media from leaking through from the perimeter of the device. When the fibrinogen-thrombin solution began forming at 37°C, there was a precise time window in which the inner needle could be slowly removed. In <1 min. the cells would not have formed adequate connections with the polymerizing fibrin, and the middle of the lumen would be collapsed with cells. If the needle was removed >5 min. after polymerization had begun, the cells would stick to the inner needle, and removing the inner needle would pull the cells out with it. To enhance hydrophobicity, the needles were also coated in rainx, then washed with diH₂O.

The second biggest challenge was preventing media from leaking from the outer areas where tissue or needle met with PDMS. We were able to prevent media from leaking out of the well by leaving <2mm of each needle in the center of the well for the cells to grip. We also prevented media from leaking through the inner most needle when the outer muscle was being injected by filling the 20G needle with music wire. Another challenge was when the 17G needle was replaced with the 25G needle, the space in the PDMS allowed for media to escape. This was solved by inserting just the needle portion of the 17G needle into the device to surround the fully in-tact 25G needle.

4.3.2 Muscle and endothelial cells form tubes using the concentric needle protocol

In order to test if the concentric needle method could successfully generate tissues with perfusable lumens, we first set out to make a single tube (**Figure 25**). A muscle tube was first generated using the 20G needle as the outer guide for the tissue, and the 25G needle for the inner diameter, dimensions in (*Table 9: Needle dimensions provided by Sigma.*). Based on the average size of the muscle tubes, the tissue seems to form around the inner needle, then compact slightly further once the needle is removed. If the cells were

preferentially adhering to the gelatin mold, the expected outer diameters would be closer to 900 μ m.

Table 9: Needle dimensions provided by Sigma.

Needle size	Outer diameter (μ m)	Inner diameter (μ m)
25G	514 \pm 0.000064	260 \pm 0.00019
20G	908 \pm 0.000064	603 \pm 0.00019
17G	1473 \pm 0.00013	1067 \pm 0.00038

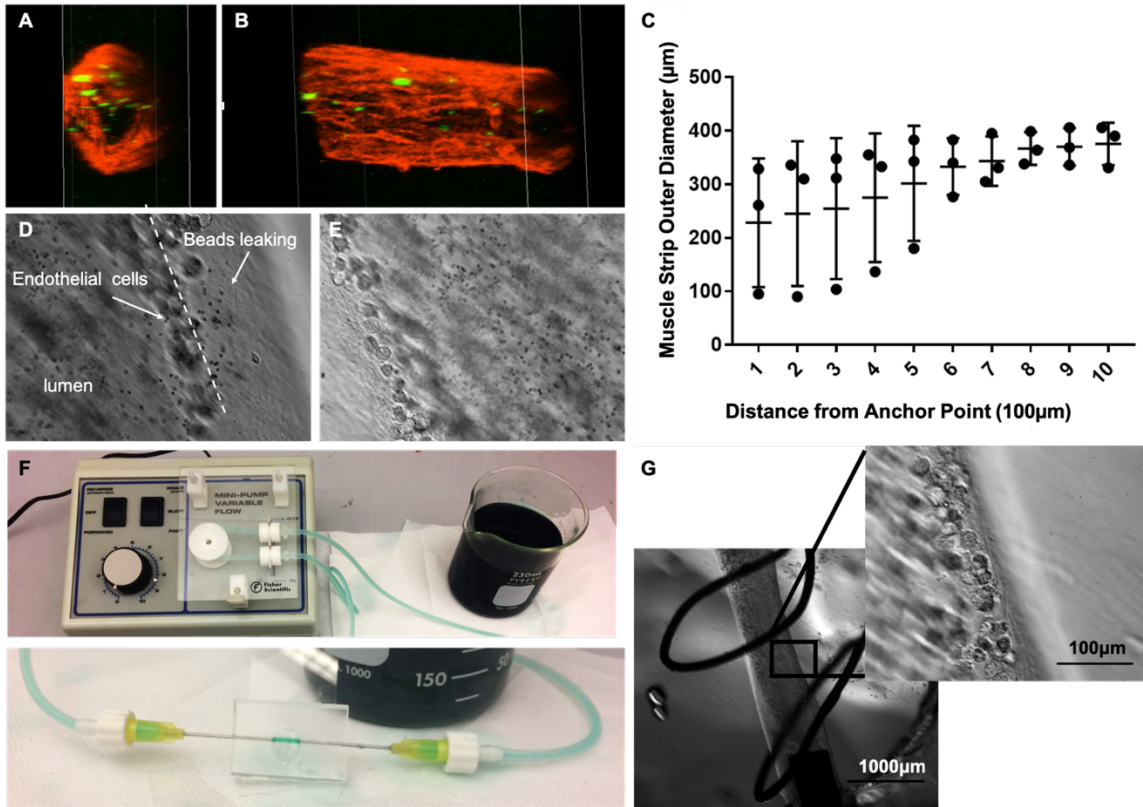


Figure 25: Single layer perfusable tissue tube

Confocal microscopy (Nicon Eclipse C1) was used to image a C2C12 muscle ring dyed with cell tracker red, images taken on day 3. This showed the cells were capable of holding a lumen (A) as well as elongating (B). In contrast, the endothelial cells (green) introduced as a mix with the single lumen did not show any patterning. Tubes also displayed more consistent lumen diameters, between 300 and 400 μ m, 600 μ m from the connection with the needles on day 3. However, towards the edge of the device, the tube diameter dropped as low as 100 μ m (n=3) (C). Endothelial cells-only protocols also generated perfusable tubes. Although some beads surpassed the EC wall barrier, the fibrin prevented the beads from escaping to the outer media (D). In most instances, the beads all stayed within the EC

lumen (E). Perfusion was achieved using a peristaltic pump, here with green dye for lumen visualization (F). (G) shows an EC tube at 2x and 10x magnification in brightfield.

4.3.2 Formation of the endothelialized lumen through muscle tissue

While a majority of muscle tissue was generated using less expensive C2C12 skeletal myoblast cells (Figure 26) hiPSC CMs derived using the optimal protocol described in Chapter 2. [217] were also capable of forming a perfusable lumen through a bulk muscle tissue. However, compared with C2C12 skeletal myoblasts, the hiPSC CMs alone did not adequately compact around the EC lumen. This was solved by adding ECs into the hiPSC CM/fibrinogen mixture at a ratio of 1:10 (while keeping the overall cell concentration at 20 million cells/mL) (Figure 26 A & B).

After silk was electrospun and added to a 17G needle, the silk-laden needle was added to the device through vertical slits cut above the channels, rather than horizontally through the pre-formed channels in the PDMS. The protocol for seeding cells then became consistent with the scaffold-free protocol. However, when muscle cells were injected into the outer tube of the device, it proceeded to push the silk scaffolding free from the EC layer. Although, a portion of the muscle cells still adhered to the ECs rather than the unwound silk scaffolding. Co-cultures were carried out for five days. It should be noted that both the silk-bound EC portion of the EC tube (left), as well as the unwound portion of the tube (right) compacts over the five day period. The change in muscle decreasing from 1.2 mm at day 0 to 617 μ m at day 5, and EC decreasing from \sim 812 μ m at day 0 to 413 μ m at day 5. Unlike the single layered tubes, differences in diameter between the center and anchor-points appeared minimal.

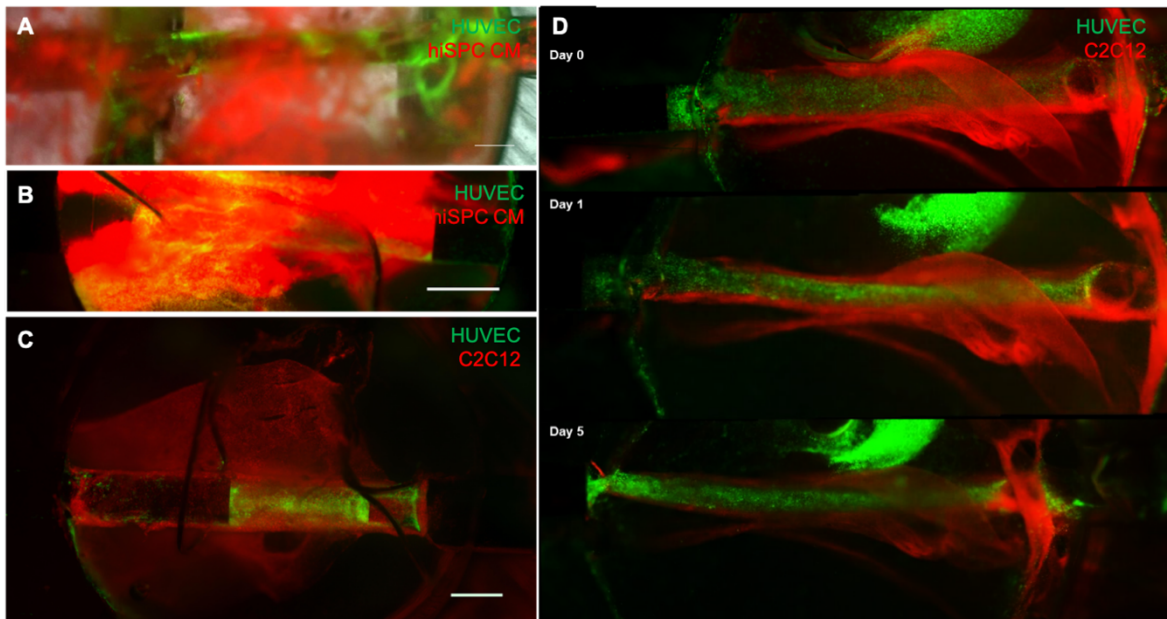


Figure 26: Endothelial tubes within muscle tissue

HUVECS successfully formed perfusable tubes within hiPSC CMs (A), however, the hiPSC CMs were unable to form a high enough concentration within the fibrin to compact around the EC tube. The assembly of hiPSC CM muscle tissue surrounding an EC lumen could only be achieved when EC:hiPSC CM ratio of 1:10 was added into the muscle layer. C2C12s were able to both hold a tube around the EC layer, as well as surround the tissue with the bulk muscle tissue layer (C). Scale bars were 1000 μ m. When C2C12s were seeded through electrospun silk surrounding the 17G needle, the force of cell seeding pushed the muscle tissue off a half of the EC layer (D).

4.4 DISCUSSION/CONCLUSION

In this chapter, we constructed a fabrication and culture method for engineering endothelialized muscle tissue. The design criteria included i) ease of protocol reproducibility, ii) perfusability, iii) both scaffold or scaffold-free iterations, iv) and cell source flexibility.

To increase reproducibility between researchers, we designed the device to be easily automated by common laboratory equipment. By adding cell solutions using concentric medical needles, tissue-construction discrepancies between scientists can be decreased by replacing manual cell loading via pipette with a syringe pump. What's more, physiological shear stress can be achieved using a standard laboratory peristaltic pump, rather than a specialized flow control system. The system also negates the need for expensive clean room-generated wafers.

The initial goal of the project was to design a scaffold-free tissue to improve cell-to-cell adhesion and communication. However, similarly to previously reported results with muscle strips [75], the tissue was found to compact over time. We therefore incorporated silk into the tissue with the goal of increasing its structural integrity and consistency for longer culture periods. Silk fibroin is a natural polymer popular for its ability to incorporate various ECM proteins and growth factors [350]. While silk can be processed into gels, films, or freeze-dried sponges [351], electrospun silk has been shown to have similar elastic modulus and ultimate tensile strength when compared to native rat aorta [352]. What's more, the fiber diameter was verified with SEM to be an average of 470 ± 150 nm, a comparable width to the wrinkles found to align EC and CM in aim 2. We found that while C2C12 cells did adhere to both the electrospun silk, as well as surrounding the EC tube, the silk-C2C12 bulk tissue unraveled away from the EC tube. So while the device can be constructed with biomaterials, the rigidity of a scaffold may be pushed away from the tube when injecting muscle cells.

Vascular shear stresses, blood pressures, and blood flow rates vary greatly depending on the shape (diameter, branch points, curvature) of the tube, fitness and activity of the individual, as well as vascular diseases (wall stiffening, plaques, injury) [353]. Using the peristaltic pump, a max flowrate of 0.137 mL/s produced a shear stress of 5.161 dynes/cm². This falls on the low end of shear stress experienced in capillaries (2.8 - 95.5 dynes/cm²) [128]. Future work could use a high speed camera to verify the burst point of the endothelial

cell tube by gradually increasing the flowrate using a syringe pump, as a higher shear stress may be more valuable when using the device to study vascular disease. While we did not observe any EC sprouting off the center tube, future work will optimize external signals such as growth factors, oxygen levels, and endothelial sub-phenotype to encourage angiogenesis.

Chapter 5: Conclusion

Preventing congestive heart failure following a myocardial infarction (MI) requires daily medications, a pacemaker, and/or surgery; however, none of these strategies will repair the damaged cardiac cells. Cell therapy can lead to moderate improvement in global heart function [1], but the elapsed time between MI and treatment has been a major source of discrepancy between stem cell therapy strategies. Moreover, improvement is limited to 5% increase in ejection fraction if using mesenchymal stem cells (MSC) [2] and even less from bone marrow cell (BMC) [2-4]. No study to date has proven that injected cells can remain viable long term and electromechanically integrate with damaged myocardium. Moreover, the resident cardiac cells do not proliferate to any extent that could lead to repair. Although some minimal expansion potential was claimed, this is currently controversial and initial publications have since been retracted and subject to concern [168, 354]. Therefore, many researchers believe that engineered cardiac tissue is expected to be required for true heart repair. A myriad of obstacles remain before this ambitious goal enters clinical practice. The goal of this thesis was to advance three of the predominant challenges facing cardiovascular tissue engineering: generating a pure cardiac cell source, organizing cardiomyocytes to mimic native heart tissue, and introducing endothelial cells for future vascularization.

The optimal cell source for engineering cardiac tissue is currently thought to be human iPS cell-derived CM. These cells can be generated from the patients' own tissue, potentially providing enough autologous CM; however, current reprogramming methods followed by CM differentiation, expansion and cell purification takes over 1.5 months of customized labor and the final quality control to test for cell maturation and purity may easily take another two weeks. By this time, a severely compromised infarcted heart has a well-established scar tissue. While many researchers work towards generating new hPSC CM protocols, no one had compared which method was the most efficient in time, cost, and cell purity. We discovered this need after first following one of the predominant CM differentiation protocols. This method was developed by the Keller lab [153], then later optimized with matrix signaling by the McCloskey lab [54], and utilized the growth factors BMP4, activin A, bFGF, DKK1, and VEGF. It required the cells to form an EB for the initial spontaneous differentiation phase, then return to a monolayer for an induction down the mesodermal cell lineage. Through this transition, we found many of the cells were dying and we were unable to efficiently generate enough cells to explore future cardiac patch designs. We therefore transitioned to using small molecule inhibitors, CHIR and IWP-2 (a protocol developed by the Palecek lab [156]). Our first observation was the drastically different morphologies produced by both protocols produced cells that spontaneously beat, the growth factor protocol generated elongated and heterogeneously shaped cells, while the inhibitor protocol produced densely packed small cells without a distinguished morphology. When re-plated onto gelatin, the α -actinin staining showed that cardiomyocytes generated by the inhibitor protocol were capable of a more expanded morphology with z-band formation. What's more, the inhibitor method not only produced a higher percentage of cardiac troponin positive cells (~ 80-89% compared to 67%), it also produced six times as many cardiomyocytes. While the field still needs to determine conclusively whether the benefits of generating patient-specific cells outweigh

an off-the-shelf developed cell bank, our results indicate that the inhibitor method exceeded the growth factor method in both cell purity, as well as final cell yield for both hiPSC and hESCs.

Once we established the preferred hPSC CM differentiation method, we next set out to compare methods for patterning cardiomyocytes. Efforts to implant cardiomyocytes into animal models have shown underwhelming cell retention rates. Our theory was that pre-aligning cardiomyocytes in vitro would improve the engineered tissue's ability to electrically and mechanically couple when implanted. Here, we set out to analyze the ability for varying cell patterning platforms to align and elongate hPSC CMs. We first tried a method for generating nano-wrinkles developed by our collaborator, Prof. Khine. Although the technology had been previously used to pattern mouse embryonic stem cell derived endothelial cells and rat neonatal cardiomyocytes, we set out to determine if this would translate to hPSC CMs. Our initial plan to differentiate the cells on the wrinkles proved unsuccessful. Cells passed onto the wrinkles at the spontaneous differentiation or mesoderm phase failed to adhere. While the cells could align on the wrinkles as soon as day 12, the proliferation rates at that time meant the cells quickly became too confluent and lost alignment and elongation. Cells that were transferred after day 24 aligned and elongated significantly compared to the flat controls on both PDMS, as well as PA. However, we were never able to maintain a stable culture, as the cell sheets would dissociate from the wrinkles and ball-up to form spheres. Cells cultured on the flat controls of these conditions were able to be maintained as expected. While efforts were made to covalently bond extra cellular matrix proteins to both the PDMS and PA surfaces, these methods were ultimately too toxic to the cells, despite repeated washing. Thus, we transitioned to test 3D cell patterning methods.

For the 3D platform, we worked to adapt a sacrificial gel-based microfluidic device, originally designed by Prof. Hara Asada for skeletal muscle, to develop hiPSC CM muscle strips. We showed the muscle strip was capable of aligning 55% of the hiPSC CMs, with an elongation factor significantly higher than the hanging cell disk control. While these results looked comparable to muscle strips made with rat neonatal cardiomyocytes, we thought increasing the tension on the tissue may improve the cell morphology. We then attempted to use the same sacrificial hydrogel protocol within an o-ring as the mold, rather than a rod-shaped channel. Interestingly, this method failed to mimic the compact tissue formed by the muscle strip method. We next tried to form the muscle ring using a mold printed by Prof. Rashi Bashir's lab at UIUC. In this method, both fibrinogen and thrombin components were added to the bulk of the tissue, rather than diffusing together as the sacrificial mold melted. Adding all components at once proved to be lower throughput, as the crosslinking time began during the handling period. This method succeeded in generating the desired compact engineered ring tissue. The ring tissue was then removed from the mold, and stretched around metal posts. While this method did not succeed in improving hiPSC CM alignment and elongation, the cell morphology was improved from the hanging disk control. This method could also more efficiently incorporate an increased number of cells (6 million cells/ring) compared to either the muscle strip protocol (200,000 cells/strip), or layering cell sheets using a thermoresponsive polymer (10,000 cells/layer).

After determining the most efficient protocols for generating and patterning hPSC CMs, we next moved on to vascularizing the pre-patterned tissue. Inspired by the muscle strip protocol, I designed a novel microfluidic device that incorporated the sacrificial gel method over multiple layers. Additional design criteria considered the ease of tissue construction reproducibility, the option for both scaffold and scaffold free iterations, and cell source flexibility. The initial plan was to create an endothelial-lined lumen by placing a placeholder wire in the center of an endothelial strip. Bulk tissue would be generated by surrounding the tissue with a muscle ring. However, we found that the endothelial cell tube was not strong enough to encapsulate the perfused liquid longer than one day. I then designed a concentric needle system that would consist of a muscle strip surrounding an endothelial tube using concentric needles. After the initial idea conceptualization, parameters that required optimizing included the preventing following: the fibrinogen and cell solution from adhering to the inner needle, cell solution from flowing through rather than around the inner needle, and leaking from the outer channels of the device. We also tested different gauge needle combinations, time for thrombin diffusion, and rates of perfusion. Once the design and protocol were finalized, we then moved onto testing the device with and without a scaffold, and on multiple cell types.

When making the endothelial lumen through a muscle tube, we found that the diameter varied depending on its proximity to the needle. We then tried to replicate the protocol using silk scaffolding to provide structural support. The addition of scaffolding to the device also made it more versatile. While a scaffold-free tissue increases space for cell-to-cell communication, scaffolds can be useful tools for drug delivery or growth factor incorporation. We therefore added electro spun silk around the center needle, and followed the tissue construction protocol as previously demonstrated. The tissue continued to compact over five days, indicating that the cells were still adhering to needles to form tension throughout the muscle bundle.

References

1. Murphy, S.L., J. Xu, and K.D. Kochanek, *Deaths: final data for 2010*. Natl Vital Stat Rep, 2013. **61**(4): p. 1-117.
2. Finegold, J.A., P. Asaria, and D.P. Francis, *Mortality from ischaemic heart disease by country, region, and age: statistics from World Health Organisation and United Nations*. Int J Cardiol, 2013. **168**(2): p. 934-45.
3. *WHO publishes definitive atlas on global heart disease and stroke epidemic*. Indian J Med Sci, 2004. **58**(9): p. 405-6.
4. Go, A.S., et al., *Heart disease and stroke statistics--2014 update: a report from the American Heart Association*. Circulation, 2014. **129**(3): p. e28-e292.
5. Ovbiagele, B., et al., *Forecasting the future of stroke in the United States: a policy statement from the American Heart Association and American Stroke Association*. Stroke, 2013. **44**(8): p. 2361-75.
6. Griffin, B.P., *Manual of cardiovascular medicine*. 4th ed. 2013, Philadelphia: Wolters Kluwer Health/Lippincott Williams & Wilkins. xx, 1171 p.
7. Klabunde, R.E., *Cardiovascular physiology concepts*. 2nd ed. 2012, Philadelphia, PA: Lippincott Williams & Wilkins/Wolters Kluwer. xi, 243 p.
8. Braunwald, E., *The treatment of acute myocardial infarction: the Past, the Present, and the Future*. Eur Heart J Acute Cardiovasc Care, 2012. **1**(1): p. 9-12.
9. Fleming, R.R., *A short history of cardiology*. Clio Med, 1997. **40**: p. ix-xviii, 1-229.
10. Bishop, J.E., et al., *Enhanced deposition of predominantly type I collagen in myocardial disease*. J Mol Cell Cardiol, 1990. **22**(10): p. 1157-65.
11. Holmes, J.W., T.K. Borg, and J.W. Covell, *Structure and mechanics of healing myocardial infarcts*. Annu Rev Biomed Eng, 2005. **7**: p. 223-53.
12. Sun, Y. and K.T. Weber, *Infarct scar: a dynamic tissue*. Cardiovasc Res, 2000. **46**(2): p. 250-6.
13. Wei, S., et al., *Left and right ventricular collagen type I/III ratios and remodeling post-myocardial infarction*. J Card Fail, 1999. **5**(2): p. 117-26.
14. Whittaker, P., D.R. Boughner, and R.A. Kloner, *Analysis of healing after myocardial infarction using polarized light microscopy*. Am J Pathol, 1989. **134**(4): p. 879-93.
15. Takahashi, S., A.C. Barry, and S.M. Factor, *Collagen degradation in ischaemic rat hearts*. Biochem J, 1990. **265**(1): p. 233-41.
16. Sato, S., et al., *Connective tissue changes in early ischemia of porcine myocardium: an ultrastructural study*. J Mol Cell Cardiol, 1983. **15**(4): p. 261-75.
17. Whittaker, P., D.R. Boughner, and R.A. Kloner, *Role of collagen in acute myocardial infarct expansion*. Circulation, 1991. **84**(5): p. 2123-34.
18. Cleutjens, J.P., et al., *Regulation of collagen degradation in the rat myocardium after infarction*. J Mol Cell Cardiol, 1995. **27**(6): p. 1281-92.
19. Carlyle, W.C., et al., *Delayed reperfusion alters matrix metalloproteinase activity and fibronectin mRNA expression in the infarct zone of the ligated rat heart*. J Mol Cell Cardiol, 1997. **29**(9): p. 2451-63.

20. Murry, C.E., H. Reinecke, and L.M. Pabon, *Regeneration gaps: observations on stem cells and cardiac repair*. J Am Coll Cardiol, 2006. **47**(9): p. 1777-85.
21. Whelan, R.S., V. Kaplinskiy, and R.N. Kitsis, *Cell death in the pathogenesis of heart disease: mechanisms and significance*. Annu Rev Physiol, 2010. **72**: p. 19-44.
22. Olivetti, G., et al., *Cardiomyopathy of the aging human heart. Myocyte loss and reactive cellular hypertrophy*. Circ Res, 1991. **68**(6): p. 1560-8.
23. Bergmann, O., et al., *Evidence for cardiomyocyte renewal in humans*. Science, 2009. **324**(5923): p. 98-102.
24. Thygesen, K., et al., *Third universal definition of myocardial infarction*. J Am Coll Cardiol, 2012. **60**(16): p. 1581-98.
25. Braunwald, E., *Myocardial reperfusion, limitation of infarct size, reduction of left ventricular dysfunction, and improved survival. Should the paradigm be expanded?* Circulation, 1989. **79**(2): p. 441-4.
26. Gruntzig, A.R., A. Senning, and W.E. Siegenthaler, *Nonoperative dilatation of coronary-artery stenosis: percutaneous transluminal coronary angioplasty*. N Engl J Med, 1979. **301**(2): p. 61-8.
27. Zarrabi, A., et al., *The open-artery hypothesis revisited*. Tex Heart Inst J, 2006. **33**(3): p. 345-52.
28. Fraser, K.H., et al., *The use of computational fluid dynamics in the development of ventricular assist devices*. Med Eng Phys, 2011. **33**(3): p. 263-80.
29. Enomoto, Y., et al., *Early ventricular restraint after myocardial infarction: extent of the wrap determines the outcome of remodeling*. Ann Thorac Surg, 2005. **79**(3): p. 881-7; discussion 881-7.
30. Blom, A.S., et al., *Ventricular restraint prevents infarct expansion and improves borderzone function after myocardial infarction: a study using magnetic resonance imaging, three-dimensional surface modeling, and myocardial tagging*. Ann Thorac Surg, 2007. **84**(6): p. 2004-10.
31. Klodell, C.T., Jr., et al., *Worldwide surgical experience with the Paracor HeartNet cardiac restraint device*. J Thorac Cardiovasc Surg, 2008. **135**(1): p. 188-95.
32. George, I., et al., *Effect of passive cardiac containment on ventricular synchrony and cardiac function in awake dogs*. Eur J Cardiothorac Surg, 2007. **31**(1): p. 55-64.
33. Magovern, J.A., et al., *Effect of a flexible ventricular restraint device on cardiac remodeling after acute myocardial infarction*. ASAIO J, 2006. **52**(2): p. 196-200.
34. Kjekshus, J.K., *Factors influencing infarct size following coronary artery occlusion*. J Oslo City Hosp, 1974. **24**(11-12): p. 155-75.
35. Frishman, W.H., *Cardiology patient page. Beta-adrenergic blockers*. Circulation, 2003. **107**(18): p. e117-9.
36. Clifford, D.M., et al., *Stem cell treatment for acute myocardial infarction*. The Cochrane database of systematic reviews, 2012. **2**: p. CD006536.
37. Heldman, A.W., et al., *Transendocardial mesenchymal stem cells and mononuclear bone marrow cells for ischemic cardiomyopathy: the TAC-HFT randomized trial*. JAMA, 2014. **311**(1): p. 62-73.

38. Afzal, M.R., et al., *Adult Bone Marrow Cell Therapy for Ischemic Heart Disease: Evidence and Insights From Randomized Controlled Trials*. *Circulation research*, 2015. **117**(6): p. 558-75.
39. Jeevanantham, V., et al., *Adult bone marrow cell therapy improves survival and induces long-term improvement in cardiac parameters: a systematic review and meta-analysis*. *Circulation*, 2012. **126**(5): p. 551-68.
40. Forrester, J.S., et al., *New paradigms of myocardial regeneration post-infarction: tissue preservation, cell environment, and pluripotent cell sources*. *JACC Cardiovasc Interv*, 2009. **2**(1): p. 1-8.
41. Hirt, M.N., A. Hansen, and T. Eschenhagen, *Cardiac tissue engineering: state of the art*. *Circ Res*, 2014. **114**(2): p. 354-67.
42. Moscona, A.A., *Tissues from dissociated cells*. *Sci Am*, 1959. **200**(5): p. 132-4 passim.
43. Hasan, A., et al., *Injectable Hydrogels for Cardiac Tissue Repair after Myocardial Infarction*. *Advanced Science*, 2015. **2**(11): p. n/a-n/a.
44. Kelly, D.J., et al., *Increased myocyte content and mechanical function within a tissue-engineered myocardial patch following implantation*. *Tissue Eng Part A*, 2009. **15**(8): p. 2189-201.
45. Robinson, K.A., et al., *Extracellular matrix scaffold for cardiac repair*. *Circulation*, 2005. **112**(9 Suppl): p. I135-43.
46. Turner, W.S., et al., *Cardiac tissue development for delivery of embryonic stem cell-derived endothelial and cardiac cells in natural matrices*. *J Biomed Mater Res B Appl Biomater*, 2012. **100**(8): p. 2060-72.
47. Bowers, S.L., I. Banerjee, and T.A. Baudino, *The extracellular matrix: at the center of it all*. *J Mol Cell Cardiol*, 2010. **48**(3): p. 474-82.
48. Daley, W.P., S.B. Peters, and M. Larsen, *Extracellular matrix dynamics in development and regenerative medicine*. *J Cell Sci*, 2008. **121**(Pt 3): p. 255-64.
49. Lockhart, M., et al., *Extracellular matrix and heart development*. *Birth Defects Res A Clin Mol Teratol*, 2011. **91**(6): p. 535-50.
50. Georges-Labouesse, E.N., et al., *Mesodermal development in mouse embryos mutant for fibronectin*. *Dev Dyn*, 1996. **207**(2): p. 145-56.
51. Costell, M., et al., *Hyperplastic conotruncal endocardial cushions and transposition of great arteries in perlecan-null mice*. *Circ Res*, 2002. **91**(2): p. 158-64.
52. Choi, S., et al., *Effects of various extracellular matrix proteins on the growth of HL-1 cardiomyocytes*. *Cells Tissues Organs*, 2013. **198**(5): p. 349-56.
53. Bird, S.D., et al., *The human adult cardiomyocyte phenotype*. *Cardiovasc Res*, 2003. **58**(2): p. 423-34.
54. Sa, S., L. Wong, and K.E. McCloskey, *Combinatorial fibronectin and laminin signaling promote highly efficient cardiac differentiation of human embryonic stem cells*. *Biores Open Access*, 2014. **3**(4): p. 150-61.
55. Leor, J., et al., *Bioengineered cardiac grafts: A new approach to repair the infarcted myocardium?* *Circulation*, 2000. **102**(19 Suppl 3): p. III56-61.
56. Zimmermann, W.H., et al., *Three-dimensional engineered heart tissue from neonatal rat cardiac myocytes*. *Biotechnol Bioeng*, 2000. **68**(1): p. 106-14.

57. Tulloch, N.L., et al., *Growth of engineered human myocardium with mechanical loading and vascular coculture*. *Circ Res*, 2011. **109**(1): p. 47-59.
58. Hansen, A., et al., *Development of a drug screening platform based on engineered heart tissue*. *Circ Res*, 2010. **107**(1): p. 35-44.
59. Neal, D., et al., *Formation of elongated fascicle-inspired 3D tissues consisting of high-density, aligned cells using sacrificial outer molding*. *Lab Chip*, 2014. **14**(11): p. 1907-16.
60. Xiong, Q., et al., *A fibrin patch-based enhanced delivery of human embryonic stem cell-derived vascular cell transplantation in a porcine model of postinfarction left ventricular remodeling*. *Stem Cells*, 2011. **29**(2): p. 367-75.
61. Landa, N., et al., *Effect of injectable alginate implant on cardiac remodeling and function after recent and old infarcts in rat*. *Circulation*, 2008. **117**(11): p. 1388-96.
62. Li, R.K., et al., *Survival and function of bioengineered cardiac grafts*. *Circulation*, 1999. **100**(19 Suppl): p. II63-9.
63. Radisic, M., et al., *Functional assembly of engineered myocardium by electrical stimulation of cardiac myocytes cultured on scaffolds*. *Proc Natl Acad Sci U S A*, 2004. **101**(52): p. 18129-34.
64. Dvir, T., et al., *Prevascularization of cardiac patch on the omentum improves its therapeutic outcome*. *Proc Natl Acad Sci U S A*, 2009. **106**(35): p. 14990-5.
65. Patra, C., et al., *Silk protein fibroin from *Antheraea mylitta* for cardiac tissue engineering*. *Biomaterials*, 2012. **33**(9): p. 2673-80.
66. Hata, H., et al., *Engineering a novel three-dimensional contractile myocardial patch with cell sheets and decellularised matrix*. *Eur J Cardiothorac Surg*, 2010. **38**(4): p. 450-5.
67. Ott, H.C., et al., *Perfusion-decellularized matrix: using nature's platform to engineer a bioartificial heart*. *Nat Med*, 2008. **14**(2): p. 213-21.
68. Godier-Furnemont, A.F., et al., *Composite scaffold provides a cell delivery platform for cardiovascular repair*. *Proc Natl Acad Sci U S A*, 2011. **108**(19): p. 7974-9.
69. Davis, M.E., et al., *Custom design of the cardiac microenvironment with biomaterials*. *Circ Res*, 2005. **97**(1): p. 8-15.
70. Malafaya, P.B., G.A. Silva, and R.L. Reis, *Natural-origin polymers as carriers and scaffolds for biomolecules and cell delivery in tissue engineering applications*. *Adv Drug Deliv Rev*, 2007. **59**(4-5): p. 207-33.
71. Hubbell, J.A., *Materials as morphogenetic guides in tissue engineering*. *Current Opinion in Biotechnology*, 2003. **14**(5): p. 551-558.
72. Chen, Q.-Z., et al., *Biomaterials in cardiac tissue engineering: Ten years of research survey*. *Materials Science and Engineering: R: Reports*, 2008. **59**(1-6): p. 1-37.
73. Kaiser, N.J. and K.L. Coulombe, *Physiologically inspired cardiac scaffolds for tailored in vivo function and heart regeneration*. *Biomed Mater*, 2015. **10**(3): p. 034003.
74. Golden, A.P. and J. Tien, *Fabrication of microfluidic hydrogels using molded gelatin as a sacrificial element*. *Lab Chip*, 2007. **7**(6): p. 720-5.

75. Chan, V., et al., *Fabrication and characterization of optogenetic, multi-strip cardiac muscles*. Lab Chip, 2015. **15**(10): p. 2258-68.
76. Grover, C.N., R.E. Cameron, and S.M. Best, *Investigating the morphological, mechanical and degradation properties of scaffolds comprising collagen, gelatin and elastin for use in soft tissue engineering*. J Mech Behav Biomed Mater, 2012. **10**: p. 62-74.
77. Storm, C., et al., *Nonlinear elasticity in biological gels*. Nature, 2005. **435**(7039): p. 191-4.
78. Hubbell, J.A., *Materials as morphogenetic guides in tissue engineering*. Curr Opin Biotechnol, 2003. **14**(5): p. 551-8.
79. Weisel, J.W., *Fibrinogen and fibrin*. Adv Protein Chem, 2005. **70**: p. 247-99.
80. Janmey, P.A., J.P. Winer, and J.W. Weisel, *Fibrin gels and their clinical and bioengineering applications*. J R Soc Interface, 2009. **6**(30): p. 1-10.
81. El-Sherbiny, I.M. and M.H. Yacoub, *Hydrogel scaffolds for tissue engineering: Progress and challenges*. Glob Cardiol Sci Pract, 2013. **2013**(3): p. 316-42.
82. George, M. and T.E. Abraham, *Polyionic hydrocolloids for the intestinal delivery of protein drugs: alginate and chitosan--a review*. J Control Release, 2006. **114**(1): p. 1-14.
83. Sun, J. and H. Tan, *Alginate-Based Biomaterials for Regenerative Medicine Applications*. Materials, 2013. **6**(4): p. 1285.
84. Kong, H.J., et al., *Controlling rigidity and degradation of alginate hydrogels via molecular weight distribution*. Biomacromolecules, 2004. **5**(5): p. 1720-7.
85. Shachar, M., et al., *The effect of immobilized RGD peptide in alginate scaffolds on cardiac tissue engineering*. Acta Biomater, 2011. **7**(1): p. 152-62.
86. Altman, G.H., et al., *Silk-based biomaterials*. Biomaterials, 2003. **24**(3): p. 401-16.
87. Horan, R.L., et al., *In vitro degradation of silk fibroin*. Biomaterials, 2005. **26**(17): p. 3385-93.
88. Sofia, S., et al., *Functionalized silk-based biomaterials for bone formation*. J Biomed Mater Res, 2001. **54**(1): p. 139-48.
89. Fuchs, S., et al., *Outgrowth endothelial cells isolated and expanded from human peripheral blood progenitor cells as a potential source of autologous cells for endothelialization of silk fibroin biomaterials*. Biomaterials, 2006. **27**(31): p. 5399-408.
90. Unger, R.E., et al., *Endothelialization of a non-woven silk fibroin net for use in tissue engineering: growth and gene regulation of human endothelial cells*. Biomaterials, 2004. **25**(21): p. 5137-46.
91. Gilbert, T.W., T.L. Sellaro, and S.F. Badylak, *Decellularization of tissues and organs*. Biomaterials, 2006. **27**(19): p. 3675-83.
92. Brown, B.N. and S.F. Badylak, *Extracellular matrix as an inductive scaffold for functional tissue reconstruction*. Transl Res, 2014. **163**(4): p. 268-85.
93. Skrzypiec-Spring, M., et al., *Isolated heart perfusion according to Langendorff---still viable in the new millennium*. J Pharmacol Toxicol Methods, 2007. **55**(2): p. 113-26.
94. Brown, B.N., et al., *Surface characterization of extracellular matrix scaffolds*. Biomaterials, 2010. **31**(3): p. 428-37.

95. Bursac, N., et al., *Cultivation in rotating bioreactors promotes maintenance of cardiac myocyte electrophysiology and molecular properties*. Tissue Eng, 2003. **9**(6): p. 1243-53.
96. Zong, X., et al., *Electrospun fine-textured scaffolds for heart tissue constructs*. Biomaterials, 2005. **26**(26): p. 5330-8.
97. Rai, R., et al., *Synthesis, properties and biomedical applications of poly (glycerol sebacate)(PGS): a review*. Progress in Polymer Science, 2012. **37**(8): p. 1051-1078.
98. Ye, X., et al., *Scalable units for building cardiac tissue*. Adv Mater, 2014. **26**(42): p. 7202-8.
99. Bursac, N., et al., *Novel anisotropic engineered cardiac tissues: studies of electrical propagation*. Biochem Biophys Res Commun, 2007. **361**(4): p. 847-53.
100. Dvir, T., et al., *Nanowired three-dimensional cardiac patches*. Nat Nanotechnol, 2011. **6**(11): p. 720-5.
101. Dykman, L.A. and N.G. Khlebtsov, *Gold nanoparticles in biology and medicine: recent advances and prospects*. Acta Naturae, 2011. **3**(2): p. 34-55.
102. Giljohann, D.A., et al., *Gold nanoparticles for biology and medicine*. Angew Chem Int Ed Engl, 2010. **49**(19): p. 3280-94.
103. Witzenburg, C., et al., *Mechanical changes in the rat right ventricle with decellularization*. J Biomech, 2012. **45**(5): p. 842-9.
104. Mohan, G. and N.D. Gallant, *Surface chemistry gradients on silicone elastomers for high-throughput modulation of cell-adhesive interfaces*. J Biomed Mater Res A, 2015. **103**(6): p. 2066-76.
105. Tallawi, M., et al., *Strategies for the chemical and biological functionalization of scaffolds for cardiac tissue engineering: a review*. J R Soc Interface, 2015. **12**(108): p. 20150254.
106. Kuddannaya, S., et al., *Surface chemical modification of poly(dimethylsiloxane) for the enhanced adhesion and proliferation of mesenchymal stem cells*. ACS Appl Mater Interfaces, 2013. **5**(19): p. 9777-84.
107. Ribeiro, A.J., et al., *Stable, covalent attachment of laminin to microposts improves the contractility of mouse neonatal cardiomyocytes*. ACS Appl Mater Interfaces, 2014. **6**(17): p. 15516-26.
108. Vandenberg, E.T. and U.J. Krull, *The prevention of adsorption of interferents to radiolabelled protein by Tween 20*. J Biochem Biophys Methods, 1991. **22**(4): p. 269-77.
109. Yuan, H., W.M. Mullett, and J. Pawliszyn, *Biological sample analysis with immunoaffinity solid-phase microextraction*. Analyst, 2001. **126**(8): p. 1456-61.
110. Wang, Z.H. and G. Jin, *Covalent immobilization of proteins for the biosensor based on imaging ellipsometry*. J Immunol Methods, 2004. **285**(2): p. 237-43.
111. Gupta, V. and K.J. Grande-Allen, *Effects of static and cyclic loading in regulating extracellular matrix synthesis by cardiovascular cells*. Cardiovasc Res, 2006. **72**(3): p. 375-83.
112. Shimizu, T., et al., *Fabrication of pulsatile cardiac tissue grafts using a novel 3-dimensional cell sheet manipulation technique and temperature-responsive cell culture surfaces*. Circ Res, 2002. **90**(3): p. e40.

113. Shimizu, T., et al., *Long-term survival and growth of pulsatile myocardial tissue grafts engineered by the layering of cardiomyocyte sheets*. *Tissue Eng*, 2006. **12**(3): p. 499-507.
114. Kubo, H., et al., *Development of automated 3-dimensional tissue fabrication system Tissue Factory - Automated cell isolation from tissue for regenerative medicine*. *Conf Proc IEEE Eng Med Biol Soc*, 2013. **2013**: p. 358-61.
115. Luna, J.I., et al., *Multiscale biomimetic topography for the alignment of neonatal and embryonic stem cell-derived heart cells*. *Tissue Eng Part C Methods*, 2011. **17**(5): p. 579-88.
116. Hatano, R., et al., *Endothelial cells derived from embryonic stem cells respond to cues from topographical surface patterns*. *J Biol Eng*, 2013. **7**: p. 18.
117. Carson, D., et al., *Nanotopography-Induced Structural Anisotropy and Sarcomere Development in Human Cardiomyocytes Derived from Induced Pluripotent Stem Cells*. *ACS Appl Mater Interfaces*, 2016.
118. Jung, G., et al., *Time-dependent evolution of functional vs. remodeling signaling in induced pluripotent stem cell-derived cardiomyocytes and induced maturation with biomechanical stimulation*. *FASEB J*, 2015.
119. Rao, C., et al., *The effect of microgrooved culture substrates on calcium cycling of cardiac myocytes derived from human induced pluripotent stem cells*. *Biomaterials*, 2013. **34**(10): p. 2399-411.
120. Feinberg, A.W., et al., *Controlling the contractile strength of engineered cardiac muscle by hierarchal tissue architecture*. *Biomaterials*, 2012. **33**(23): p. 5732-41.
121. Yin, L., H. Bien, and E. Entcheva, *Scaffold topography alters intracellular calcium dynamics in cultured cardiomyocyte networks*. *Am J Physiol Heart Circ Physiol*, 2004. **287**(3): p. H1276-85.
122. Voorhees, A.P. and H.C. Han, *A model to determine the effect of collagen fiber alignment on heart function post myocardial infarction*. *Theor Biol Med Model*, 2014. **11**: p. 6.
123. Kira, Y., et al., *Effect of long-term cyclic mechanical load on protein synthesis and morphological changes in cultured myocardial cells from neonatal rat*. *Cardiovasc Drugs Ther*, 1994. **8**(2): p. 251-62.
124. Fink, C., et al., *Chronic stretch of engineered heart tissue induces hypertrophy and functional improvement*. *FASEB J*, 2000. **14**(5): p. 669-79.
125. Zimmermann, W.H., et al., *Engineered heart tissue grafts improve systolic and diastolic function in infarcted rat hearts*. *Nat Med*, 2006. **12**(4): p. 452-8.
126. Garot, J., et al., *Fast determination of regional myocardial strain fields from tagged cardiac images using harmonic phase MRI*. *Circulation*, 2000. **101**(9): p. 981-8.
127. Gorcsan, J., 3rd and H. Tanaka, *Echocardiographic assessment of myocardial strain*. *J Am Coll Cardiol*, 2011. **58**(14): p. 1401-13.
128. Simmons, C.S., B.C. Petzold, and B.L. Pruitt, *Microsystems for biomimetic stimulation of cardiac cells*. *Lab Chip*, 2012. **12**(18): p. 3235-48.
129. Murry, C.E. and G. Keller, *Differentiation of embryonic stem cells to clinically relevant populations: lessons from embryonic development*. *Cell*, 2008. **132**(4): p. 661-80.

130. Montgomery, M.O., et al., *Alterations in sheep fetal right ventricular tissue with induced hemodynamic pressure overload*. Basic Res Cardiol, 1998. **93**(3): p. 192-200.
131. Dupont, E., et al., *Altered connexin expression in human congestive heart failure*. J Mol Cell Cardiol, 2001. **33**(2): p. 359-71.
132. Clark, E.B., et al., *Effect of increased pressure on ventricular growth in stage 21 chick embryos*. Am J Physiol, 1989. **257**(1 Pt 2): p. H55-61.
133. Sedmera, D., et al., *Remodeling of chick embryonic ventricular myoarchitecture under experimentally changed loading conditions*. Anat Rec, 1999. **254**(2): p. 238-52.
134. Sedmera, D., R.P. Thompson, and F. Kolar, *Effect of increased pressure loading on heart growth in neonatal rats*. J Mol Cell Cardiol, 2003. **35**(3): p. 301-9.
135. Gavard, J., et al., *Lamellipodium extension and cadherin adhesion: two cell responses to cadherin activation relying on distinct signalling pathways*. J Cell Sci, 2004. **117**(Pt 2): p. 257-70.
136. Kresh, J.Y. and A. Chopra, *Intercellular and extracellular mechanotransduction in cardiac myocytes*. Pflugers Arch, 2011. **462**(1): p. 75-87.
137. Hatta, K. and M. Takeichi, *Expression of N-cadherin adhesion molecules associated with early morphogenetic events in chick development*. Nature, 1986. **320**(6061): p. 447-9.
138. Radice, G.L., et al., *Developmental defects in mouse embryos lacking N-cadherin*. Dev Biol, 1997. **181**(1): p. 64-78.
139. Gwak, S.J., et al., *The effect of cyclic strain on embryonic stem cell-derived cardiomyocytes*. Biomaterials, 2008. **29**(7): p. 844-56.
140. Shimko, V.F. and W.C. Claycomb, *Effect of mechanical loading on three-dimensional cultures of embryonic stem cell-derived cardiomyocytes*. Tissue Eng Part A, 2008. **14**(1): p. 49-58.
141. Vishal Gupta, K.J.G.-A., *Effects of static and cyclic loading in regulating extracellular matrix synthesis by cardiovascular cells* Cardiovasc Res, 2006: p. 375-83.
142. Ono S., W.L.K., Yamashita H., Covell J.W., Ross J. Jr. , *Effect of coronary artery reperfusion on transmural myocardial remodeling in dogs* Circulation, 1995. **91**: p. 1143 - 53.
143. Lee A.A., M.A.D., *Multiaxial myocardial mechanics and extracellular matrix remodeling: mechanochemical regulation of cardiac fibroblast function* Adv Exp Med Biol 1997. **430**: p. 227 - 40.
144. Brown, T.D., *Techniques for mechanical stimulation of cells in vitro: a review* Journal of Biomechanics 2000. **33**(1): p. 3 - 14.
145. Chelsey S. Simmons, B.C.P.a.B.L.P., *Microsystems for biomimetic stimulation of cardiac cells* Lab Chip 2012. **12**: p. 3235 - 48.
146. Peloso, A., et al., *Current achievements and future perspectives in whole-organ bioengineering*. Stem Cell Res Ther, 2015. **6**: p. 107.
147. Akhyari, P., et al., *The quest for an optimized protocol for whole-heart decellularization: a comparison of three popular and a novel decellularization*

- technique and their diverse effects on crucial extracellular matrix qualities. Tissue Eng Part C Methods, 2011. 17(9): p. 915-26.*
148. Momtahan, N., et al., *Strategies and processes to decellularize and recellularize hearts to generate functional organs and reduce the risk of thrombosis. Tissue Eng Part B Rev, 2015. 21(1): p. 115-32.*
 149. Lu, T.Y., et al., *Repopulation of decellularized mouse heart with human induced pluripotent stem cell-derived cardiovascular progenitor cells. Nat Commun, 2013. 4: p. 2307.*
 150. Guyette, J.P., et al., *Bioengineering Human Myocardium on Native Extracellular Matrix. Circ Res, 2016. 118(1): p. 56-72.*
 151. Wainwright, J.M., et al., *Preparation of cardiac extracellular matrix from an intact porcine heart. Tissue Eng Part C Methods, 2010. 16(3): p. 525-32.*
 152. Remlinger, N.T., P.D. Wearden, and T.W. Gilbert, *Procedure for decellularization of porcine heart by retrograde coronary perfusion. J Vis Exp, 2012(70): p. e50059.*
 153. Kattman, S.J., et al., *Stage-specific optimization of activin/nodal and BMP signaling promotes cardiac differentiation of mouse and human pluripotent stem cell lines. Cell Stem Cell, 2011. 8(2): p. 228-40.*
 154. Sa, S. and K. McCloskey, *Activin A and BMP4 Signaling for Efficient Cardiac Differentiation of H7 and H9 Human Embryonic Stem Cells. J Stem Cells Regen Med, 2012. 8(3): p. 198-202.*
 155. Sa, S. and K.E. McCloskey, *Stage-specific cardiomyocyte differentiation method for H7 and H9 human embryonic stem cells. Stem Cell Rev, 2012. 8(4): p. 1120-8.*
 156. Lian, X., et al., *Directed cardiomyocyte differentiation from human pluripotent stem cells by modulating Wnt/beta-catenin signaling under fully defined conditions. Nat Protoc, 2013. 8(1): p. 162-75.*
 157. Lu, D., et al., *Differential regulation of morphology and stemness of mouse embryonic stem cells by substrate stiffness and topography. Biomaterials, 2014. 35(13): p. 3945-55.*
 158. Neal, D.M., et al., *Mechanical Characterization and Shape Optimization of Fascicle-Like 3D Skeletal Muscle Tissues Contracted with Electrical and Optical Stimuli. Tissue Eng Part A, 2015.*
 159. Raman, R., et al., *Optogenetic skeletal muscle-powered adaptive biological machines. Proc Natl Acad Sci U S A, 2016. 113(13): p. 3497-502.*
 160. Gerbin, K.A. and C.E. Murry, *The winding road to regenerating the human heart. Cardiovasc Pathol, 2015. 24(3): p. 133-140.*
 161. Beltrami, A.P., et al., *Adult cardiac stem cells are multipotent and support myocardial regeneration. Cell, 2003. 114(6): p. 763-76.*
 162. Oh, H., et al., *Cardiac muscle plasticity in adult and embryo by heart-derived progenitor cells. Ann N Y Acad Sci, 2004. 1015: p. 182-9.*
 163. Kubo, H., et al., *Increased cardiac myocyte progenitors in failing human hearts. Circulation, 2008. 118(6): p. 649-57.*
 164. Bolli, R., et al., *Cardiac stem cells in patients with ischaemic cardiomyopathy (SCIPIO): initial results of a randomised phase 1 trial. Lancet, 2011. 378(9806): p. 1847-57.*

165. Malliaras, K., et al., *Intracoronary cardiosphere-derived cells after myocardial infarction: evidence of therapeutic regeneration in the final 1-year results of the CADUCEUS trial (Cardiosphere-Derived autologous stem Cells to reverse ventricular dysfunction)*. J Am Coll Cardiol, 2014. **63**(2): p. 110-22.
166. Nakata, M., et al., *The ALCADIA (AutoLogous Human CARDiac--Derived Stem Cell To Treat Ischemic cARDiomyopathy) Trial*. 2012.
167. Yacoub, M.H. and J. Terrovitis, *CADUCEUS, SCIPIO, ALCADIA: Cell therapy trials using cardiac-derived cells for patients with post myocardial infarction LV dysfunction, still evolving*. Glob Cardiol Sci Pract, 2013. **2013**(1): p. 5-8.
168. The Lancet, E., *Expression of concern: the SCIPIO trial*. Lancet, 2014. **383**(9925): p. 1279.
169. Patella, V., et al., *Stem cell factor in mast cells and increased mast cell density in idiopathic and ischemic cardiomyopathy*. Circulation, 1998. **97**(10): p. 971-8.
170. Simari, R.D., et al., *Bone marrow mononuclear cell therapy for acute myocardial infarction: a perspective from the cardiovascular cell therapy research network*. Circ Res, 2014. **114**(10): p. 1564-8.
171. Clifford, D.M., et al., *Stem cell treatment for acute myocardial infarction*. Cochrane Database Syst Rev, 2012. **2**: p. CD006536.
172. Orlic, D., et al., *Bone marrow cells regenerate infarcted myocardium*. Nature, 2001. **410**(6829): p. 701-5.
173. Balsam, L.B., et al., *Haematopoietic stem cells adopt mature haematopoietic fates in ischaemic myocardium*. Nature, 2004. **428**(6983): p. 668-73.
174. Agbulut, O., et al., *Comparison of human skeletal myoblasts and bone marrow-derived CD133+ progenitors for the repair of infarcted myocardium*. J Am Coll Cardiol, 2004. **44**(2): p. 458-63.
175. Laflamme, M.A. and C.E. Murry, *Heart regeneration*. Nature, 2011. **473**(7347): p. 326-35.
176. Toma, C., et al., *Human mesenchymal stem cells differentiate to a cardiomyocyte phenotype in the adult murine heart*. Circulation, 2002. **105**(1): p. 93-8.
177. Mirosou, M., et al., *Secreted frizzled related protein 2 (Sfrp2) is the key Akt-mesenchymal stem cell-released paracrine factor mediating myocardial survival and repair*. Proc Natl Acad Sci U S A, 2007. **104**(5): p. 1643-8.
178. Noiseux, N., et al., *Mesenchymal stem cells overexpressing Akt dramatically repair infarcted myocardium and improve cardiac function despite infrequent cellular fusion or differentiation*. Mol Ther, 2006. **14**(6): p. 840-50.
179. Meyer, G.P., et al., *Intracoronary bone marrow cell transfer after myocardial infarction: eighteen months' follow-up data from the randomized, controlled BOOST (BOne marrOw transfer to enhance ST-elevation infarct regeneration) trial*. Circulation, 2006. **113**(10): p. 1287-94.
180. Leistner, D.M., et al., *Transplantation of progenitor cells and regeneration enhancement in acute myocardial infarction (TOPCARE-AMI): final 5-year results suggest long-term safety and efficacy*. Clin Res Cardiol, 2011. **100**(10): p. 925-34.
181. Perin, E.C., et al., *Effect of transendocardial delivery of autologous bone marrow mononuclear cells on functional capacity, left ventricular function, and perfusion*

- in chronic heart failure: the FOCUS-CCTRN trial.* JAMA, 2012. **307**(16): p. 1717-26.
182. Traverse, J.H., et al., *Effect of the use and timing of bone marrow mononuclear cell delivery on left ventricular function after acute myocardial infarction: the TIME randomized trial.* JAMA, 2012. **308**(22): p. 2380-9.
 183. Surder, D., et al., *Intracoronary injection of bone marrow-derived mononuclear cells early or late after acute myocardial infarction: effects on global left ventricular function.* Circulation, 2013. **127**(19): p. 1968-79.
 184. Hare, J.M., et al., *Comparison of allogeneic vs autologous bone marrow-derived mesenchymal stem cells delivered by transendocardial injection in patients with ischemic cardiomyopathy: the POSEIDON randomized trial.* JAMA, 2012. **308**(22): p. 2369-79.
 185. Bartunek, J., et al., *Cardiopoietic stem cell therapy in heart failure: the C-CURE (Cardiopoietic stem Cell therapy in heart failURE) multicenter randomized trial with lineage-specified biologics.* J Am Coll Cardiol, 2013. **61**(23): p. 2329-38.
 186. Maher, K.O. and C. Xu, *Marching towards regenerative cardiac therapy with human pluripotent stem cells.* Discov Med, 2013. **15**(85): p. 349-56.
 187. Thomson, J.A., et al., *Embryonic stem cell lines derived from human blastocysts.* Science, 1998. **282**(5391): p. 1145-7.
 188. Takahashi, K. and S. Yamanaka, *Induction of pluripotent stem cells from mouse embryonic and adult fibroblast cultures by defined factors.* Cell, 2006. **126**(4): p. 663-76.
 189. Nakagawa, M., et al., *Generation of induced pluripotent stem cells without Myc from mouse and human fibroblasts.* Nat Biotechnol, 2008. **26**(1): p. 101-6.
 190. Yu, J., et al., *Induced pluripotent stem cell lines derived from human somatic cells.* Science, 2007. **318**(5858): p. 1917-20.
 191. Eisenstein, M., *IPSCs: One cell to rule them all?* Nat Meth, 2010. **7**(1): p. 81-85.
 192. Takahashi, K., et al., *Induction of Pluripotent Stem Cells from Adult Human Fibroblasts by Defined Factors.* Cell, 2007. **131**(5): p. 861-872.
 193. Zhou, T., et al., *Generation of human induced pluripotent stem cells from urine samples.* Nat Protoc, 2012. **7**(12): p. 2080-9.
 194. Junying Yu, K.H., Kim Smuga-Otto, Shulan Tian, Ron Stewart, Igor I. Slukvin, James A. Thomson, *Human induced pluripotent stem cells free of vector and transgene sequences* Science 2009. **324**: p. 797 - 801.
 195. Okita K, N.M., Hyenjong H, Ichisaka T, and Yamanaka S, *Generation of mouse induced pluripotent stem cells without viral vectors* Science, 2008. **322**: p. 949-53.
 196. *Global burden of disease: Cause of death* W.H. Organization, Editor. 2004. p. 2 - 26.
 197. Shi Y, D.C., et al. , *Induction of pluripotent stem cells from mouse embryonic fibroblasts by Oct4 and Klf4 with small-molecule compounds.* Cell Stem Cell, 2008. **3**: p. 568-74.
 198. Huangfu D, M.R., Guo W et al. , *Induction of pluripotent stem cells by defined factors is greatly improved by small-molecule compounds.* Nat Biotechnol, 2008. **26**(7): p. 795 - 97.

199. Warren L, M.P., Ahfeldt T et al. , *Highly efficient reprogramming to pluripotency and directed differentiation of human cells with synthetic modified mRNA*. Cell Stem Cell, 2010. **7**(5): p. 618 - 30.
200. Kim, D., et al., *Generation of human induced pluripotent stem cells by direct delivery of reprogramming proteins*. Cell Stem Cell, 2009. **4**(6): p. 472-6.
201. Zhou, H., et al., *Generation of Induced Pluripotent Stem Cells Using Recombinant Proteins*. Cell Stem Cell, 2009. **4**(5): p. 381-384.
202. Efe, J.A., et al., *Conversion of mouse fibroblasts into cardiomyocytes using a direct reprogramming strategy*. Nat Cell Biol, 2011. **13**(3): p. 215-22.
203. Qian, L., et al., *Reprogramming of mouse fibroblasts into cardiomyocyte-like cells in vitro*. Nat Protoc, 2013. **8**(6): p. 1204-15.
204. Jayawardena, T.M., et al., *MicroRNA-mediated in vitro and in vivo direct reprogramming of cardiac fibroblasts to cardiomyocytes*. Circ Res, 2012. **110**(11): p. 1465-73.
205. Ieda, M., et al., *Direct reprogramming of fibroblasts into functional cardiomyocytes by defined factors*. Cell, 2010. **142**(3): p. 375-86.
206. Fu, J.D. and D. Srivastava, *Direct reprogramming of fibroblasts into cardiomyocytes for cardiac regenerative medicine*. Circ J, 2015. **79**(2): p. 245-54.
207. Fu, J.D., et al., *Direct reprogramming of human fibroblasts toward a cardiomyocyte-like state*. Stem Cell Reports, 2013. **1**(3): p. 235-47.
208. Sanganalmath, S.K. and R. Bolli, *Cell therapy for heart failure: a comprehensive overview of experimental and clinical studies, current challenges, and future directions*. Circ Res, 2013. **113**(6): p. 810-34.
209. Loughran, J.H., et al., *Stem cell therapy: promising treatment in heart failure?* Curr Heart Fail Rep, 2013. **10**(1): p. 73-80.
210. Heslop, J.A., et al., *Concise review: workshop review: understanding and assessing the risks of stem cell-based therapies*. Stem Cells Transl Med, 2015. **4**(4): p. 389-400.
211. Trounson, A. and N.D. DeWitt, *Pluripotent stem cells progressing to the clinic*. Nat Rev Mol Cell Biol, 2016. **17**(3): p. 194-200.
212. Thies, R.S. and C.E. Murry, *The advancement of human pluripotent stem cell-derived therapies into the clinic*. Development, 2015. **142**(20): p. 3614.
213. Hayden, E.C., *California ponders cell-banking venture*. Nature, 2011. **472**(7344): p. 403.
214. Menasche, P., et al., *Human embryonic stem cell-derived cardiac progenitors for severe heart failure treatment: first clinical case report*. Eur Heart J, 2015. **36**(30): p. 2011-7.
215. Anderson, M.E., et al., *Embryonic stem cell-derived cardiac myocytes are not ready for human trials*. Circ Res, 2014. **115**(3): p. 335-8.
216. Murry, C.E., J.J. Chong, and M.A. Laflamme, *Letter by Murry et al regarding article, "Embryonic stem cell-derived cardiac myocytes are not ready for human trials"*. Circ Res, 2014. **115**(10): p. e28-9.
217. Lian, X., et al., *Robust cardiomyocyte differentiation from human pluripotent stem cells via temporal modulation of canonical Wnt signaling*. Proc Natl Acad Sci U S A, 2012. **109**(27): p. E1848-57.

218. Laflamme, M.A., et al., *Cardiomyocytes derived from human embryonic stem cells in pro-survival factors enhance function of infarcted rat hearts*. Nat Biotechnol, 2007. **25**(9): p. 1015-24.
219. Itskovitz-Eldor, J., et al., *Differentiation of human embryonic stem cells into embryoid bodies compromising the three embryonic germ layers*. Mol Med, 2000. **6**(2): p. 88-95.
220. Sa, S., et al., *Round-bottomed honeycomb microwells: embryoid body shape correlates with stem cell fate*. 2012.
221. Naito, A.T., et al., *Developmental stage-specific biphasic roles of Wnt/beta-catenin signaling in cardiomyogenesis and hematopoiesis*. Proc Natl Acad Sci U S A, 2006. **103**(52): p. 19812-7.
222. Ueno, S., et al., *Biphasic role for Wnt/beta-catenin signaling in cardiac specification in zebrafish and embryonic stem cells*. Proc Natl Acad Sci U S A, 2007. **104**(23): p. 9685-90.
223. Zhang, J., et al., *Extracellular matrix promotes highly efficient cardiac differentiation of human pluripotent stem cells: the matrix sandwich method*. Circ Res, 2012. **111**(9): p. 1125-36.
224. BurrIDGE, P.W., et al., *Production of de novo cardiomyocytes: human pluripotent stem cell differentiation and direct reprogramming*. Cell Stem Cell, 2012. **10**(1): p. 16-28.
225. Ghafar-Zadeh, E., J.R. Waldeisen, and L.P. Lee, *Engineered approaches to the stem cell microenvironment for cardiac tissue regeneration*. Lab Chip, 2011. **11**(18): p. 3031-48.
226. Markwald, R.R., et al., eds. *Use of collagen gel cultures to study heart development: Preteoglycan and glycoprotein interactions during formation of endocardial cushion tissue*. ed. R.L. Trelstad. 1984, Alan R. Liss: New York, NY. 323-350.
227. Kitten, G.T., R.R. Markwald, and D.L. Bolender, *Distribution of basement membrane antigens in cryopreserved early embryonic hearts*. Anat Rec, 1987. **217**(4): p. 379-90.
228. Wang, H., X. Luo, and J. Leighton, *Extracellular Matrix and Integrins in Embryonic Stem Cell Differentiation*. Biochem Insights, 2015. **8**(Suppl 2): p. 15-21.
229. Higuchi, S., et al., *Heart extracellular matrix supports cardiomyocyte differentiation of mouse embryonic stem cells*. J Biosci Bioeng, 2013. **115**(3): p. 320-5.
230. Kleinman, H.K., et al., *Isolation and characterization of type IV procollagen, laminin, and heparan sulfate proteoglycan from the EHS sarcoma*. Biochemistry, 1982. **21**(24): p. 6188-93.
231. Baharvand, H., et al., *The effect of extracellular matrix on embryonic stem cell-derived cardiomyocytes*. J Mol Cell Cardiol, 2005. **38**(3): p. 495-503.
232. Robertson, C., D.D. Tran, and S.C. George, *Concise review: maturation phases of human pluripotent stem cell-derived cardiomyocytes*. Stem Cells, 2013. **31**(5): p. 829-37.

233. Yang, X., L. Pabon, and C.E. Murry, *Engineering adolescence: maturation of human pluripotent stem cell-derived cardiomyocytes*. *Circ Res*, 2014. **114**(3): p. 511-23.
234. Zhang, J., et al., *Functional cardiomyocytes derived from human induced pluripotent stem cells*. *Circ Res*, 2009. **104**(4): p. e30-41.
235. Snir, M., et al., *Assessment of the ultrastructural and proliferative properties of human embryonic stem cell-derived cardiomyocytes*. *Am J Physiol Heart Circ Physiol*, 2003. **285**(6): p. H2355-63.
236. Ziman, A.P., et al., *Excitation-contraction coupling changes during postnatal cardiac development*. *J Mol Cell Cardiol*, 2010. **48**(2): p. 379-86.
237. Gherghiceanu, M., et al., *Cardiomyocytes derived from human embryonic and induced pluripotent stem cells: comparative ultrastructure*. *J Cell Mol Med*, 2011. **15**(11): p. 2539-51.
238. Keung, W., K.R. Boheler, and R.A. Li, *Developmental cues for the maturation of metabolic, electrophysiological and calcium handling properties of human pluripotent stem cell-derived cardiomyocytes*. *Stem Cell Res Ther*, 2014. **5**(1): p. 17.
239. Veerman, C., et al., *Immaturity of human stem-cell derived cardiomyocytes in culture: fatal flaw or soluble problem?* *Stem Cells Dev*, 2015.
240. Parker, K.K. and D.E. Ingber, *Extracellular matrix, mechanotransduction and structural hierarchies in heart tissue engineering*. *Philos Trans R Soc Lond B Biol Sci*, 2007. **362**(1484): p. 1267-79.
241. Engler, A.J., et al., *Matrix elasticity directs stem cell lineage specification*. *Cell*, 2006. **126**(4): p. 677-89.
242. Hazeltine, L.B., et al., *Effects of substrate mechanics on contractility of cardiomyocytes generated from human pluripotent stem cells*. *Int J Cell Biol*, 2012. **2012**: p. 508294.
243. Arshi, A., et al., *Rigid microenvironments promote cardiac differentiation of mouse and human embryonic stem cells*. *Sci Technol Adv Mater*, 2013. **14**(2).
244. Young, J.L. and A.J. Engler, *Hydrogels with time-dependent material properties enhance cardiomyocyte differentiation in vitro*. *Biomaterials*, 2011. **32**(4): p. 1002-9.
245. Ribeiro, A.J., et al., *Contractility of single cardiomyocytes differentiated from pluripotent stem cells depends on physiological shape and substrate stiffness*. *Proc Natl Acad Sci U S A*, 2015. **112**(41): p. 12705-10.
246. Lundy, S.D., et al., *Structural and functional maturation of cardiomyocytes derived from human pluripotent stem cells*. *Stem Cells Dev*, 2013. **22**(14): p. 1991-2002.
247. Sartiani, L., et al., *Developmental changes in cardiomyocytes differentiated from human embryonic stem cells: a molecular and electrophysiological approach*. *Stem Cells*, 2007. **25**(5): p. 1136-44.
248. Otsuji, T.G., et al., *Progressive maturation in contracting cardiomyocytes derived from human embryonic stem cells: Qualitative effects on electrophysiological responses to drugs*. *Stem Cell Res*, 2010. **4**(3): p. 201-13.

249. Kamakura, T., et al., *Ultrastructural maturation of human-induced pluripotent stem cell-derived cardiomyocytes in a long-term culture*. *Circ J*, 2013. **77**(5): p. 1307-14.
250. Ribeiro, M.C., et al., *Functional maturation of human pluripotent stem cell derived cardiomyocytes in vitro--correlation between contraction force and electrophysiology*. *Biomaterials*, 2015. **51**: p. 138-50.
251. Lee, Y.K., et al., *Triiodothyronine promotes cardiac differentiation and maturation of embryonic stem cells via the classical genomic pathway*. *Mol Endocrinol*, 2010. **24**(9): p. 1728-36.
252. Yang, X., et al., *Tri-iodo-l-thyronine promotes the maturation of human cardiomyocytes-derived from induced pluripotent stem cells*. *J Mol Cell Cardiol*, 2014. **72**: p. 296-304.
253. Laflamme, M.A., et al., *Formation of human myocardium in the rat heart from human embryonic stem cells*. *Am J Pathol*, 2005. **167**(3): p. 663-71.
254. Xu, C., et al., *Characterization and enrichment of cardiomyocytes derived from human embryonic stem cells*. *Circ Res*, 2002. **91**(6): p. 501-8.
255. Dubois, N.C., et al., *SIRPA is a specific cell-surface marker for isolating cardiomyocytes derived from human pluripotent stem cells*. *Nat Biotechnol*, 2011. **29**(11): p. 1011-8.
256. Hattori, F., et al., *Nongenetic method for purifying stem cell-derived cardiomyocytes*. *Nat Methods*, 2010. **7**(1): p. 61-6.
257. Elliott, D.A., et al., *NKX2-5(eGFP/w) hESCs for isolation of human cardiac progenitors and cardiomyocytes*. *Nat Methods*, 2011. **8**(12): p. 1037-40.
258. Anderson, D., et al., *Transgenic enrichment of cardiomyocytes from human embryonic stem cells*. *Mol Ther*, 2007. **15**(11): p. 2027-36.
259. Bu, L., et al., *Human ISL1 heart progenitors generate diverse multipotent cardiovascular cell lineages*. *Nature*, 2009. **460**(7251): p. 113-7.
260. Klug, M.G., et al., *Genetically selected cardiomyocytes from differentiating embryonic stem cells form stable intracardiac grafts*. *J Clin Invest*, 1996. **98**(1): p. 216-24.
261. Zandstra, P.W., et al., *Scalable production of embryonic stem cell-derived cardiomyocytes*. *Tissue Eng*, 2003. **9**(4): p. 767-78.
262. Levine, B.L., et al., *Global Manufacturing of CAR T Cell Therapy*. *Mol Ther Methods Clin Dev*, 2017. **4**: p. 92-101.
263. Xu, C., et al., *Feeder-free growth of undifferentiated human embryonic stem cells*. *Nat Biotechnol*, 2001. **19**(10): p. 971-4.
264. Nguyen, D., et al., *Tunable shrink-induced honeycomb microwell arrays for uniform embryoid bodies*. *Lab Chip*, 2009. **9**(23): p. 3338-44.
265. Pildner von Steinburg, S., et al., *What is the "normal" fetal heart rate?* *PeerJ*, 2013. **1**: p. e82.
266. Hay, M., et al., *Clinical development success rates for investigational drugs*. *Nat Biotechnol*, 2014. **32**(1): p. 40-51.
267. Ronaldson-Bouchard, K. and G. Vunjak-Novakovic, *Organs-on-a-Chip: A Fast Track for Engineered Human Tissues in Drug Development*. *Cell Stem Cell*, 2018. **22**(3): p. 310-324.

268. Shi, Y., et al., *Induced pluripotent stem cell technology: a decade of progress*. Nat Rev Drug Discov, 2017. **16**(2): p. 115-130.
269. Van Essen, D. and J. Kelly, *Correlation of cell shape and function in the visual cortex of the cat*. Nature, 1973. **241**(5389): p. 403-5.
270. Huet, C., et al., *Extracellular matrix regulates ovine granulosa cell survival, proliferation and steroidogenesis: relationships between cell shape and function*. J Endocrinol, 2001. **169**(2): p. 347-60.
271. Haeuptle, M.T., et al., *Effect of cell shape change on the function and differentiation of rabbit mammary cells in culture*. J Cell Biol, 1983. **96**(5): p. 1425-34.
272. Kumar, G., et al., *The determination of stem cell fate by 3D scaffold structures through the control of cell shape*. Biomaterials, 2011. **32**(35): p. 9188-96.
273. Kuo, P.L., et al., *Myocyte shape regulates lateral registry of sarcomeres and contractility*. Am J Pathol, 2012. **181**(6): p. 2030-7.
274. Huang, S. and D.E. Ingber, *Shape-dependent control of cell growth, differentiation, and apoptosis: switching between attractors in cell regulatory networks*. Exp Cell Res, 2000. **261**(1): p. 91-103.
275. Chung, S., et al., *Microfluidic platforms for studies of angiogenesis, cell migration, and cell-cell interactions. Sixth International Bio-Fluid Mechanics Symposium and Workshop March 28-30, 2008 Pasadena, California*. Ann Biomed Eng, 2010. **38**(3): p. 1164-77.
276. Jalili-Firoozinezhad, S., et al., *Modeling radiation injury-induced cell death and countermeasure drug responses in a human Gut-on-a-Chip*. Cell Death Dis, 2018. **9**(2): p. 223.
277. Ma, W., et al., *CNS stem and progenitor cell differentiation into functional neuronal circuits in three-dimensional collagen gels*. Exp Neurol, 2004. **190**(2): p. 276-88.
278. Goubko, C.A. and X. Cao, *Patterning multiple cell types in co-cultures: A review*. Materials Science and Engineering: C, 2009. **29**(6): p. 1855-1868.
279. Brock, A., et al., *Geometric determinants of directional cell motility revealed using microcontact printing*. Langmuir, 2003. **19**(5): p. 1611-7.
280. Moeller, J., et al., *Controlling cell shape on hydrogels using lift-off protein patterning*. PLoS One, 2018. **13**(1): p. e0189901.
281. Mrksich, M., et al., *Using microcontact printing to pattern the attachment of mammalian cells to self-assembled monolayers of alkanethiolates on transparent films of gold and silver*. Exp Cell Res, 1997. **235**(2): p. 305-13.
282. Bettinger, C.J., R. Langer, and J.T. Borenstein, *Engineering substrate topography at the micro- and nanoscale to control cell function*. Angew Chem Int Ed Engl, 2009. **48**(30): p. 5406-15.
283. Bhatia, S.N., M.L. Yarmush, and M. Toner, *Controlling cell interactions by micropatterning in co-cultures: hepatocytes and 3T3 fibroblasts*. J Biomed Mater Res, 1997. **34**(2): p. 189-99.
284. Nelson, C.M., et al., *Degradation of micropatterned surfaces by cell-dependent and -independent processes*. Langmuir, 2003. **19**(5): p. 1493-1499.
285. Yim, E.K., et al., *Nanopattern-induced changes in morphology and motility of smooth muscle cells*. Biomaterials, 2005. **26**(26): p. 5405-13.

286. Wang, W., et al., *Effects of Schwann cell alignment along the oriented electrospun chitosan nanofibers on nerve regeneration*. J Biomed Mater Res A, 2009. **91**(4): p. 994-1005.
287. Chen, A., et al., *Shrink-film configurable multiscale wrinkles for functional alignment of human embryonic stem cells and their cardiac derivatives*. Adv Mater, 2011. **23**(48): p. 5785-91.
288. Chen, C.S., et al., *Shrinky-Dink microfluidics: 3D polystyrene chips*. Lab Chip, 2008. **8**(4): p. 622-4.
289. Chen, C.S., et al., *Shrinky-dink hanging drops: a simple way to form and culture embryoid bodies*. J Vis Exp, 2008(13).
290. Hatano, R., et al., *Endothelial cells derived from embryonic stem cells respond to cues from topographical surface patterns*. J Biol Eng, 2013. **7**(1): p. 18.
291. Shimizu, T., et al., *Cell sheet engineering for myocardial tissue reconstruction*. Biomaterials, 2003. **24**(13): p. 2309-16.
292. Aubin, H., et al., *Directed 3D cell alignment and elongation in microengineered hydrogels*. Biomaterials, 2010. **31**(27): p. 6941-6951.
293. Thavandiran, N., et al., *Design and formulation of functional pluripotent stem cell-derived cardiac microtissues*. Proc Natl Acad Sci U S A, 2013. **110**(49): p. E4698-707.
294. Legant, W.R., et al., *Microfabricated tissue gauges to measure and manipulate forces from 3D microtissues*. Proc Natl Acad Sci U S A, 2009. **106**(25): p. 10097-102.
295. Zhang, Y.S., et al., *Bioprinting 3D microfibrinous scaffolds for engineering endothelialized myocardium and heart-on-a-chip*. Biomaterials, 2016. **110**: p. 45-59.
296. Bian, W., et al., *Mesoscopic hydrogel molding to control the 3D geometry of bioartificial muscle tissues*. Nat Protoc, 2009. **4**(10): p. 1522-34.
297. Kenar, H., G.T. Kose, and V. Hasirci, *Design of a 3D aligned myocardial tissue construct from biodegradable polyesters*. J Mater Sci Mater Med, 2010. **21**(3): p. 989-97.
298. Tse, J.R. and A.J. Engler, *Preparation of hydrogel substrates with tunable mechanical properties*. Curr Protoc Cell Biol, 2010. **Chapter 10**: p. Unit 10 16.
299. Cvetkovic, C., et al., *Three-dimensionally printed biological machines powered by skeletal muscle*. Proc Natl Acad Sci U S A, 2014. **111**(28): p. 10125-30.
300. Hersch, N., et al., *The constant beat: cardiomyocytes adapt their forces by equal contraction upon environmental stiffening*. Biol Open, 2013. **2**(3): p. 351-61.
301. Rodriguez, A.G., et al., *Substrate stiffness increases twitch power of neonatal cardiomyocytes in correlation with changes in myofibril structure and intracellular calcium*. Biophys J, 2011. **101**(10): p. 2455-64.
302. Engler, A.J., et al., *Embryonic cardiomyocytes beat best on a matrix with heart-like elasticity: scar-like rigidity inhibits beating*. J Cell Sci, 2008. **121**(Pt 22): p. 3794-802.
303. McCain, M.L., et al., *Matrix elasticity regulates the optimal cardiac myocyte shape for contractility*. Am J Physiol Heart Circ Physiol, 2014. **306**(11): p. H1525-39.

304. Jacot, J.G., A.D. McCulloch, and J.H. Omens, *Substrate stiffness affects the functional maturation of neonatal rat ventricular myocytes*. Biophys J, 2008. **95**(7): p. 3479-87.
305. McCain, M.L., et al., *Cooperative coupling of cell-matrix and cell-cell adhesions in cardiac muscle*. Proc Natl Acad Sci U S A, 2012. **109**(25): p. 9881-6.
306. Wipff, P.J., et al., *The covalent attachment of adhesion molecules to silicone membranes for cell stretching applications*. Biomaterials, 2009. **30**(9): p. 1781-9.
307. Raman, R., C. Cvetkovic, and R. Bashir, *A modular approach to the design, fabrication, and characterization of muscle-powered biological machines*. Nat Protoc, 2017. **12**(3): p. 519-533.
308. Li, Y., H. Asfour, and N. Bursac, *Age-dependent functional crosstalk between cardiac fibroblasts and cardiomyocytes in a 3D engineered cardiac tissue*. Acta Biomater, 2017. **55**: p. 120-130.
309. Zhang, D., et al., *Tissue-engineered cardiac patch for advanced functional maturation of human ESC-derived cardiomyocytes*. Biomaterials, 2013. **34**(23): p. 5813-20.
310. Munos, B., *Lessons from 60 years of pharmaceutical innovation*. Nat Rev Drug Discov, 2009. **8**(12): p. 959-68.
311. Scannell, J.W., et al., *Diagnosing the decline in pharmaceutical R&D efficiency*. Nat Rev Drug Discov, 2012. **11**(3): p. 191-200.
312. Pammolli, F., L. Magazzini, and M. Riccaboni, *The productivity crisis in pharmaceutical R&D*. Nat Rev Drug Discov, 2011. **10**(6): p. 428-38.
313. Paul, S.M., et al., *How to improve R&D productivity: the pharmaceutical industry's grand challenge*. Nat Rev Drug Discov, 2010. **9**(3): p. 203-14.
314. Ringel, M., et al., *Does size matter in R&D productivity? If not, what does?* Nat Rev Drug Discov, 2013. **12**(12): p. 901-2.
315. Kola, I. and J. Landis, *Can the pharmaceutical industry reduce attrition rates?* Nat Rev Drug Discov, 2004. **3**(8): p. 711-5.
316. Morgan, P., et al., *Can the flow of medicines be improved? Fundamental pharmacokinetic and pharmacological principles toward improving Phase II survival*. Drug Discov Today, 2012. **17**(9-10): p. 419-24.
317. Shanks, N., R. Greek, and J. Greek, *Are animal models predictive for humans?* Philos Ethics Humanit Med, 2009. **4**: p. 2.
318. Tralau, T. and A. Luch, *Drug-mediated toxicity: illuminating the 'bad' in the test tube by means of cellular assays?* Trends Pharmacol Sci, 2012. **33**(7): p. 353-64.
319. Trosko, J.E. and C.C. Chang, *Factors to consider in the use of stem cells for pharmaceutical drug development and for chemical safety assessment*. Toxicology, 2010. **270**(1): p. 18-34.
320. Snyder, R.D., *Possible structural and functional determinants contributing to the clastogenicity of pharmaceuticals*. Environ Mol Mutagen, 2010. **51**(8-9): p. 800-14.
321. Zolk, O. and M.F. Fromm, *Transporter-mediated drug uptake and efflux: important determinants of adverse drug reactions*. Clin Pharmacol Ther, 2011. **89**(6): p. 798-805.

322. Hartung, T. and G. Daston, *Are in vitro tests suitable for regulatory use?* Toxicol Sci, 2009. **111**(2): p. 233-7.
323. Edmondson, R., et al., *Three-dimensional cell culture systems and their applications in drug discovery and cell-based biosensors.* Assay Drug Dev Technol, 2014. **12**(4): p. 207-18.
324. Chen, A., et al., *Integrated platform for functional monitoring of biomimetic heart sheets derived from human pluripotent stem cells.* Biomaterials, 2014. **35**(2): p. 675-83.
325. Abbott, R.D. and D.L. Kaplan, *Strategies for improving the physiological relevance of human engineered tissues.* Trends Biotechnol, 2015. **33**(7): p. 401-7.
326. Liu, Y., et al., *Microfabricated scaffold-guided endothelial morphogenesis in three-dimensional culture.* Biomed Microdevices, 2011. **13**(5): p. 837-46.
327. Baranski, J.D., et al., *Geometric control of vascular networks to enhance engineered tissue integration and function.* Proc Natl Acad Sci U S A, 2013. **110**(19): p. 7586-91.
328. Yeon, J.H., et al., *In vitro formation and characterization of a perfusable three-dimensional tubular capillary network in microfluidic devices.* Lab Chip, 2012. **12**(16): p. 2815-22.
329. Zhang, B., et al., *A standalone perfusion platform for drug testing and target validation in micro-vessel networks.* Biomicrofluidics, 2013. **7**(4): p. 44125.
330. Chrobak, K.M., D.R. Potter, and J. Tien, *Formation of perfused, functional microvascular tubes in vitro.* Microvasc Res, 2006. **71**(3): p. 185-96.
331. Price, G.M., K.M. Chrobak, and J. Tien, *Effect of cyclic AMP on barrier function of human lymphatic microvascular tubes.* Microvasc Res, 2008. **76**(1): p. 46-51.
332. Miller, J.S., et al., *Rapid casting of patterned vascular networks for perfusable engineered three-dimensional tissues.* Nat Mater, 2012. **11**(9): p. 768-74.
333. Zheng, Y., et al., *In vitro microvessels for the study of angiogenesis and thrombosis.* Proc Natl Acad Sci U S A, 2012. **109**(24): p. 9342-7.
334. Sadr, N., et al., *SAM-based cell transfer to photopatterned hydrogels for microengineering vascular-like structures.* Biomaterials, 2011. **32**(30): p. 7479-90.
335. Gandhi, J.K., E.C. Opara, and E.M. Brey, *Alginate-based strategies for therapeutic vascularization.* Ther Deliv, 2013. **4**(3): p. 327-41.
336. Konwarh, R., P. Gupta, and B.B. Mandal, *Silk-microfluidics for advanced biotechnological applications: A progressive review.* Biotechnol Adv, 2016. **34**(5): p. 845-58.
337. Serbo, J.V. and S. Gerecht, *Vascular tissue engineering: biodegradable scaffold platforms to promote angiogenesis.* Stem Cell Res Ther, 2013. **4**(1): p. 8.
338. Uzel, S.G., A. Pavesi, and R.D. Kamm, *Microfabrication and microfluidics for muscle tissue models.* Prog Biophys Mol Biol, 2014. **115**(2-3): p. 279-93.
339. Hasan, A., et al., *Microfluidic techniques for development of 3D vascularized tissue.* Biomaterials, 2014. **35**(26): p. 7308-25.
340. Smith, Q. and S. Gerecht, *Going with the flow: microfluidic platforms in vascular tissue engineering.* Curr Opin Chem Eng, 2014. **3**: p. 42-50.
341. Sakaguchi, K., T. Shimizu, and T. Okano, *Construction of three-dimensional vascularized cardiac tissue with cell sheet engineering.* J Control Release, 2014.

342. Chiu, L.L., et al., *Perfusable branching microvessel bed for vascularization of engineered tissues*. Proc Natl Acad Sci U S A, 2012. **109**(50): p. E3414-23.
343. Vollert, I., et al., *In vitro perfusion of engineered heart tissue through endothelialized channels*. Tissue Eng Part A, 2014. **20**(3-4): p. 854-63.
344. Vandenburg, H., et al., *Drug-screening platform based on the contractility of tissue-engineered muscle*. Muscle Nerve, 2008. **37**(4): p. 438-47.
345. Song, J.W., D. Bazou, and L.L. Munn, *Anastomosis of endothelial sprouts forms new vessels in a tissue analogue of angiogenesis*. Integr Biol (Camb), 2012. **4**(8): p. 857-62.
346. Kim, S., et al., *Engineering of functional, perfusable 3D microvascular networks on a chip*. Lab Chip, 2013. **13**(8): p. 1489-500.
347. Whisler, J.A., M.B. Chen, and R.D. Kamm, *Control of perfusable microvascular network morphology using a multiculture microfluidic system*. Tissue Eng Part C Methods, 2014. **20**(7): p. 543-52.
348. Moya, M.L., et al., *In vitro perfused human capillary networks*. Tissue Eng Part C Methods, 2013. **19**(9): p. 730-7.
349. Jin, H.J., et al., *Electrospinning Bombyx mori silk with poly(ethylene oxide)*. Biomacromolecules, 2002. **3**(6): p. 1233-9.
350. Kasoju, N. and U. Bora, *Silk fibroin in tissue engineering*. Adv Healthc Mater, 2012. **1**(4): p. 393-412.
351. Vepari, C. and D.L. Kaplan, *Silk as a Biomaterial*. Prog Polym Sci, 2007. **32**(8-9): p. 991-1007.
352. Lovett, M., et al., *Tubular silk scaffolds for small diameter vascular grafts*. Organogenesis, 2010. **6**(4): p. 217-24.
353. Samady, H., et al., *Coronary artery wall shear stress is associated with progression and transformation of atherosclerotic plaque and arterial remodeling in patients with coronary artery disease*. Circulation, 2011. **124**(7): p. 779-88.
354. Kajstura, J., et al., *Cardiomyogenesis in the aging and failing human heart*. Circulation, 2012. **126**(15): p. 1869-81.